STUDIES ON SUPPORTED ZIEGLER CATALYSTS.

by

Douglas A. Keir, B.Sc.

Thesis submitted to the University of Nottingham
for the degree of Doctor of Philosophy,

October 1974.

To Eric and Jean.

ACKNOWLEDGEMENTS

The author wishes to thank his supervisors Professor D. D. Eley and Dr. R. Rudham for their constant encouragement during this work and for the inculcation of the practical and theoretical fundamentals of scientific research. He is indebted to Dr. C. H. Rochester for his help and advice during the course of the infrared studies. For the construction and maintenance of the apparatus the author extends his gratitude to the technical staff of the Department, and in particular to Mr. A. Buckland for his skill and patience in developing the vacuum microbalance. Gratitude is expressed to Dr. A. Roper and his colleagues of the now defunct Carrington Plastics Laboratory, Shell Research LTD. for several helpful discussions during the course of this work. Finally the author thanks Shell Research LTD. for financial support during the tenure of this research.

ABSTRACT

The work reported in this thesis is a series of investigations designed to elucidate the nature of the olefin polymerisation reaction catalysed by a Ziegler-type system supported on magnesia and on rutile. All activation and polymerisation reactions were studied by direct vapour/solid or gas/solid interactions. Infrared spectroscopy was employed to present a qualitative picture of all stages of catalyst activation and to identify polymeric species formed when the catalyst was exposed to ethylene and propylene monomers. A quantitative investigation of catalyst activation on the magnesia support was undertaken using gravimetric and analytical techniques. In the light of these results a reaction scheme has been proposed for the production of active sites on the magnesia surface. An essentially similar scheme is proposed for activation of the rutile support. Polymerisation of ethylene and propylene monomers by the magnesia based catalyst was followed gravimetrically. A study of the process variables such as temperature, monomer pressure and the effects of feedstock impurities was undertaken in order to formulate a kinetic model for the system. Strong kinetic evidence is presented for mass transfer control of the polymerisation rate. Such a model was supported by studies of the nature of the polymer formed, which appeared as a coherent encapsulating film on the catalyst surface.

In a further series of experiments the permeation properties of ethylene and propylene monomers in their corresponding polymers were investigated. It is proposed that the permeation parameters derived from these studies find parallels in the olefin polymerisation reaction and this is interpreted as further evidence for diffusion control of the polymerisation reaction.

CONTENTS

PREFACE

The object of this investigation was to study the kinetic features of gas-phase olefin polymerisations using a supported Ziegler catalyst system. Initial studies using microgravimetric and infrared spectroscopic techniques revealed features characteristic of a diffusion controlled reaction. Accordingly the diffusion properties of the olefins concerned in their respective polyolefins were investigated.

CHAPTER ONE

INTRODUCTION

PART A Olefin Polymerisation by Ziegler-Natta Catalysts.

1A.1) Development of olefin polymerisation.

Although the existence of ethylene polymers had been recognised as early as 1898[1], a commercial process for their production was not developed until 1937[2]. I.C.I. patented a process to produce low-density polyethylene from ethylene gas under conditions of high temperature and pressure, using trace amounts of oxygen as catalyst. A modification of this conventional high-pressure process was introduced in 1956[3], producing a more commercially important high-density polyethylene. The early fifties saw the development of new systems for the production of high-density polyolefins. Ziegler, working at the Max Planck Institute in Germany, discovered that the combination of $TiCl_4$ with an aluminium alkyl produced a catalyst capable of polymerising ethylene monomer at sub-atmospheric pressures[4,5,6]. Subsequent work on this system by Natta led to the development of stereospecific catalysts for α-olefin polymerisation[7]. Phillips Petroleum[8] and the Standard Oil Company[9] (Indiana) introduced low-pressure polymerisation catalysts based on chromium oxides and molybdenum oxides respectively. Today, olefin polymers and co-polymers are produced mainly from low-pressure catalyst systems based on transition metal compounds.

1A.2) The Ziegler-Natta catalyst system.

i) Definition - It is generally recognised that Ziegler-type catalysts are formed by combining, under an inert atmosphere, a metal alkyl or hydride with a transition metal salt. This chemical definition is taken to include the metal alkyls or hydrides of groups one to three and the transition metal salts of groups four to eight of the periodic table of elements. The term 'Ziegler-Natta catalyst' is applied to those combinations, within the above definition, which exhibit a stereo-regulating capacity for α-olefin polymerisation. The number of such combinations is obviously vast, but the choice of a particular catalyst system and the experimental conditions used are dictated by the structure of the monomer to be polymerised and by the required stereoregularity of the resultant polymer. Thus we find that not only the chemical properties of the catalyst components, but also the physical state of the catalyst combination, are important parameters.

ii) Stereoregular Polyolefins - Before the development of the Ziegler-Natta catalysts, high polymers were classified as wholly amorphous, or partly crystalline, on the basis of their X-ray diffraction patterns[10]. Natta realised that the physical properties of polymers (density, melting point, tensile strength etc.) could be directly related to the steric configurations of the individual polymer molecules[11,12]. Subsequently, he was able to define three classes of polyolefins, according to the degree of order in the molecules:-

a) Atactic polymer - those olefin polymers in which the assymetric carbon atoms display completely random order of D- and L- configurations:

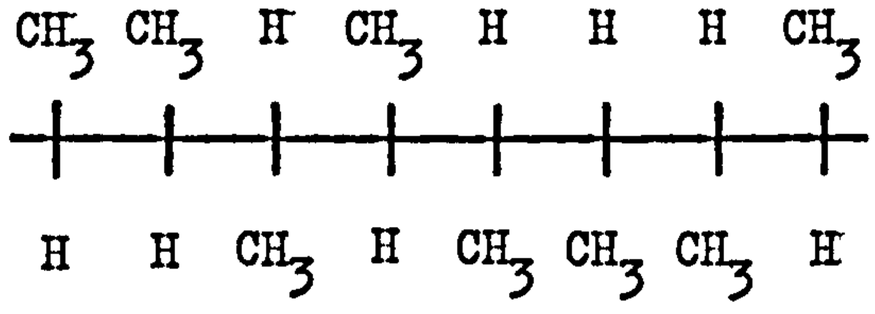

b) Isotactic polymer - those linear, crystallisable polymers of α-olefins, of head-to-tail structure, in which, over a certain chain length, the assymetric carbon atoms display the same steric configuration:

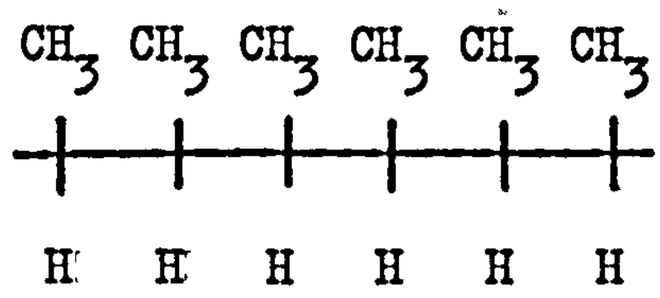

c) Syndictactic polymer - those linear cyrstallisable polymers of α-olefins in which, over a certain chain length, the assymetric carbon atoms are alternatively D- and L- configuration along the chain:

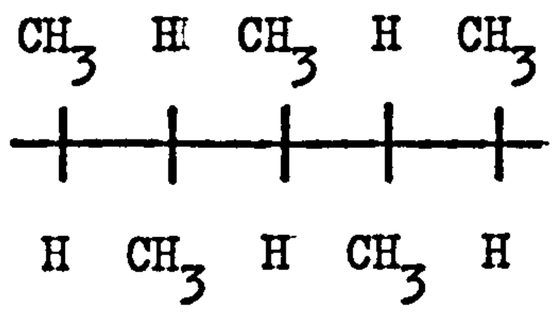

This terminology cannot of course be applied to polyethylenes, which are generally classified according to their degree of crystallinity. Several methods of estimating the degree of crystallinity have been developed[13]. One method defines atactic polymer as that fraction of a polymer sample which is soluble in boiling hexane. An infrared spectroscopic method is based on the relative intensities of bands characteristic of crystalline and amorphous polymer respectively.

X-ray diffraction and density measurements have also been used. Since each method gives a slightly different result for the crystalline content, it is often misleading to compare data determined by the different methods.

iii) Heterogeneous Ziegler-Natta catalysts. The heterogeneous catalyst consists of a soluble metal alkyl and an insoluble transition metal salt, suspended in a hydrocarbon slurry (generally n-heptane or hexane). Following Ziegler's discovery, much work centred around the system $Al(C_2H_5)_3/TiCl_3$, although the use of $Al(C_2H_5)_2Cl$ instead of $Al(C_2H_5)_3$ has occasioned much interest, due to the greater stability of this system under polymerisation conditions[14]. The versatility of the heterogeneous system is evidenced by the voluminous literature on the subject[15,16,17]. Much of the earlier work is covered in the patent literature and is pre-occupied with catalysts based on titanium or vanadium halides in conjunction with aluminium or zinc alkyls. More recently there have appeared many publications[13,18,19,20,21]. concerning the use of the halides of Sc, Co, Cr, Fe, Mn, Hf and Zr together with the alkyls of such metals as B, Sn and Pb. For the sake of clarity and continuity, subsequent discussion will be confined, as far as possible, to systems based on titanium halides and aluminium alkyls, except where useful contrast or comparison with other systems is considered relevant. One consequence of the very large number of catalysts is that it is now possible to produce polyolefins of pre-specified properties. The $Al(C_2H_5)_3/\alpha\text{-}TiCl_3$ system, for example, will polymerise propylene gas to 80-90% isotactic polymer, while $Zn(C_2H_5)_2/\alpha\text{-}TiCl_3$

yields only 30-40% isotactic material[22]. This discovery, that the polymer isotacticity fell with increasing ionic radius of the metal atom of the alkyl, suggested that the metal alkyl was intimately connected with the active site. The stereospecificity of the $Al(C_2H_5)_2Cl/TiCl_3$ catalyst also depends upon the crystalline modification of the $TiCl_3$ used[23]. Reduction of $TiCl_4$ with hydrogen at 800°C produces highly crystalline, purple α-$TiCl_3$. Polymerisation using this material leads to a highly stereo-regular polymer. In situ reduction of $TiCl_4$ using the metal alkyl as reducing agent results in a mixture of products, certainly containing some β-$TiCl_3$. This procedure leads to a polymer product of lower stereoregularity. These studies led Natta to conclude that the active sites were produced on the crystal surfaces of $TiCl_3$ when the two catalyst components were mixed, and that the isotactic stereoregulation process was closely dependent upon the nature of the crystal surface of the solid component of the catalyst[24].

iv) Homogeneous Ziegler-Natta catalysts. In 1955, Natta reported that the soluble complex (1) formed by reaction of bis-cyclopentadienyl titanium dichloride ($Cp_2.TiCl_2$) with an aluminium alkyl in hydrocarbon medium, was an active catalyst for ethylene polymerisation[25]:

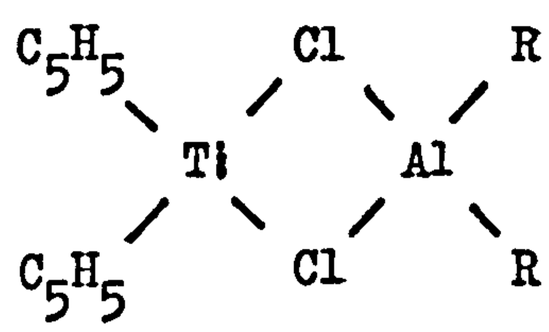

(1)

Further work revealed several similar, soluble Ziegler systems[15]. The

negligible stereospecificity of such catalysts was taken as evidence in support of Natta's theory that stereospecificity was a function of the crystal surface surrounding the active site[26]. However in 1962, Natta discovered that highly syndiotactic polypropylene could be produced using the soluble catalyst system ($VCl_4/Al(C_2H_5)_2Cl$/anisole) at temperatures below 233K[27]. These stereospecific soluble catalysts are now well documented[28]. Since they yield only syndiotactic polymer, in contrast to the heterogeneous catalysts which give isotactic material, it has been suggested that the fundamental stereoregulating mechanisms are of a different nature. Nevertheless, the soluble catalysts are more amenable to kinetic investigations and have often been employed in mechanistic studies.

v) Solid phase studies on Ziegler-Natta catalysts. Careful studies of heterogeneous Ziegler-Natta catalysts are often complicated by solvent-catalyst[29] or solvent-monomer[30] interactions. Accordingly investigations have been made of the interaction of gaseous olefin monomers with solid-phase Ziegler-Natta catalysts, in the absence of a hydrocarbon medium. In an extended series of papers, Rodriguez et al[31] made a careful study of the reaction between α-$TiCl_3$ and AlR_3 vapour ($R = CH_3$, C_2H_5). The ensuing complex was an active polymerisation catalyst for ethylene gas. Lipman and Norrish[32] polymerised ethylene using the solid produced when the vapours of $TiCl_4$ and $Al(CH_3)_3$ were reacted together. A detailed electron microscopy study of ethylene polymerisation on $TiCl_3/Al(C_2H_5)_3$ has recently been reported[33]. Such studies have contributed much to the mechanistic understanding and will be discussed in detail at a later stage (section A.4).

vi) Studies on supported Ziegler-Natta catalysts. The objective of such an approach is to react the catalyst components together on the surface of an inert support. Most of the published work in this field has appeared in patent form[34], and some of the claims are conflicting. British Patent 1,024,336, for example, claims that $Mg(OH)_2$ yields an inactive supported catalyst, while South African Patent 687,223 specifically names $Mg(OH)_2$ as the basis for an active system. Much of the work concerns the use of oxides, carbonates, hydroxides and hydroxychlorides of the group two metals, especially Mg and Ca. Refluxing one of these powders with pure $TiCl_4$ liquid, followed by treatment with a hydrocarbon solution of a metal alkyl, produces a catalyst which is active for olefin polymerisation. A recent patent[34,k] claims that the system ($MgCl_2.6H_2O/Al(C_2H_5)_3/TiCl_4$) can produce 74000 gm. polyethylene per gm. Ti, an activity which exceeds that of many conventional Ziegler catalysts. Tung and McInnich[35], in 1960, studied the effect of metal oxide additives on olefin polymerisation with the system $TiCl_4/Al(C_2H_5)_3$ in n-heptane solution. They were able to correlate the degree of rate enhancement with the basicity of the oxide - Na_2O, MgO and CaO promoted the polymerisation whereas acidic SiO_2 depressed the catalytic acticity. Hockey[36] used infrared spectroscopy and microgravimetry to study the reactions of $TiCl_4$ and $Al(CH_3)_3$ vapours with a hydroxylated silica surface. Using this combination he was able to polymerise ethylene and propylene monomers.

vii) Metal Alkyl-Free polymerisation catalysts. Many workers have reported that certain transition metal halides and related compounds are active catalysts for the stereospecific polymerisation of α-olefins in

the absence of added metal alkyls[15]. Matlock and Breslow[37] polymerised ethylene on vanadium and titanium metals while ball-milling the catalyst. Crystalline $TiCl_2$ has been used under a variety of conditions to produce both linear polyethylene[38] and isotactic polypropylene[37]. More recently, stereoregular polymer has been produced using the soluble complex $Zr(allyl)_4$ [39]. Here the stereoregulating power is obviously more fundamental than with either the crystalline catalysts or the soluble bi-metallic complexes. Although such systems do not fall within the definition of Ziegler-Natta catalysts, their polymerisation characteristics are very similar and many workers suggest that a common mechanism is operative in both systems[15].

1A.3) <u>The chemistry of the Ziegler-Natta catalyst.</u>

On mixing the two components of a Ziegler-Natta catalyst, the first reaction is a partial alkylation of the transition-metal compound.[31] It is convenient to illustrate the extent and diversity of this reaction by reference to the system $TiCl_4/AlR_3$. On mixing, the initial reaction proceeded according to[40,41]:

$$TiCl_4 + AlR_3 \longrightarrow RTiCl_3 + AlR_2Cl \qquad (1.1)$$

(2)

The stability of the tetrahedral complex (2) depended upon the nature of the alkyl group (R). If R was methyl then the complex was stable, but if R possessed a β-carbon atom with an attached hydrogen atom (eg. $C_2H_5^-$), then (2) was unstable. The resulting decomposition of

the complex led to reduction of the Ti(IV) species to Ti(III). The appearance of the Ti(III) d^1 system has been followed by electron spin resonance spectroscopy (E.S.R.)[17]. Two mechanisms have been proposed for this reduction but the bi-molecular decomposition (reaction 1.2) has gained more support than a free radical mechanism (reaction 1.3)[40]:

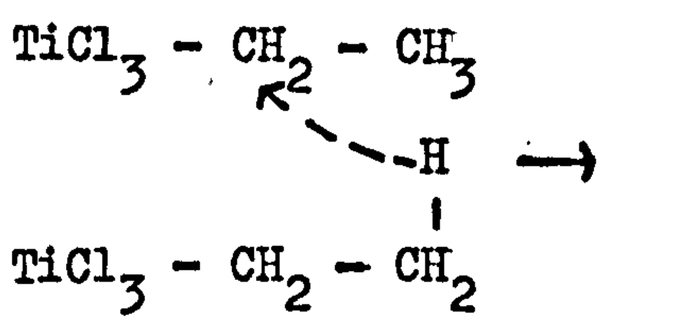

$$TiCl_3 - CH_2 - CH_3 \;\; \longrightarrow \;\; 2\,TiCl_3 + C_2H_4 + C_2H_6 \qquad (1.2)$$

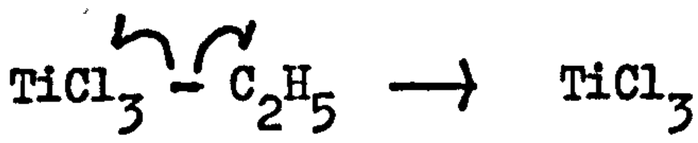

$$TiCl_3 - C_2H_5 \longrightarrow TiCl_3 + C_2H_5\cdot \qquad (1.3)$$

Rodriguez[31] reported that the initial reaction of crystalline α-$TiCl_3$ with AlR_3 vapour (R = CH_3-, C_2H_5-) was a rapid abstraction of chloride ions from the surface of the crystal, forming Ti-alkyl bonds (reaction 1.4):

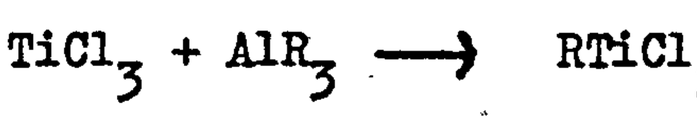

$$TiCl_3 + AlR_3 \longrightarrow RTiCl_2 + AlR_2Cl \qquad (1.4)$$

(3)

Product (3) then reacted in two ways:-

a) Reaction with further AlR_3 led to aluminium fixation in the form of a non-volatile surface compound whose structure was thought to be:

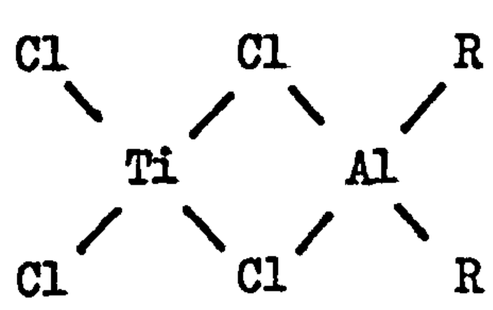

It was assumed that this complex, which was found to cover the majority of the crystal surface, was not the source of the active site.

b) Alternatively (3) may decompose, probably following a similar mechanism to reaction (1.2). In this case, a vacancy was formed in the crystal surface and a titanium atom became accessible from the outside.

Such incompletely coordinated titanium atoms are also present in untreated $TiCl_3$, situated around surface defects in the crystal. It was Rodriguez's contention that these titanium atoms form the basis of the active polymerisation centre. A similar reaction sequence has been reported when $TiCl_3$ and AlR_3 react together in a hydrocarbon medium, although Caunt[42] reported that one of the reaction products ($AlRCl_2$) acted as a catalyst poison.

The reaction of $TiCl_4$ vapour with the hydroxylated surface of SiO_2 has been studied by Hockey[36,43]. He proposed that the titanium moiety may be appended in two ways:-

a) Type A sites

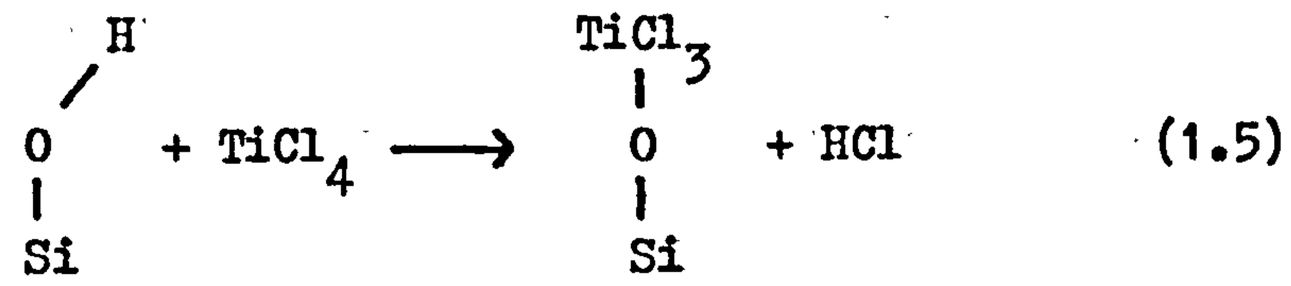

(1.5)

b) Type B sites

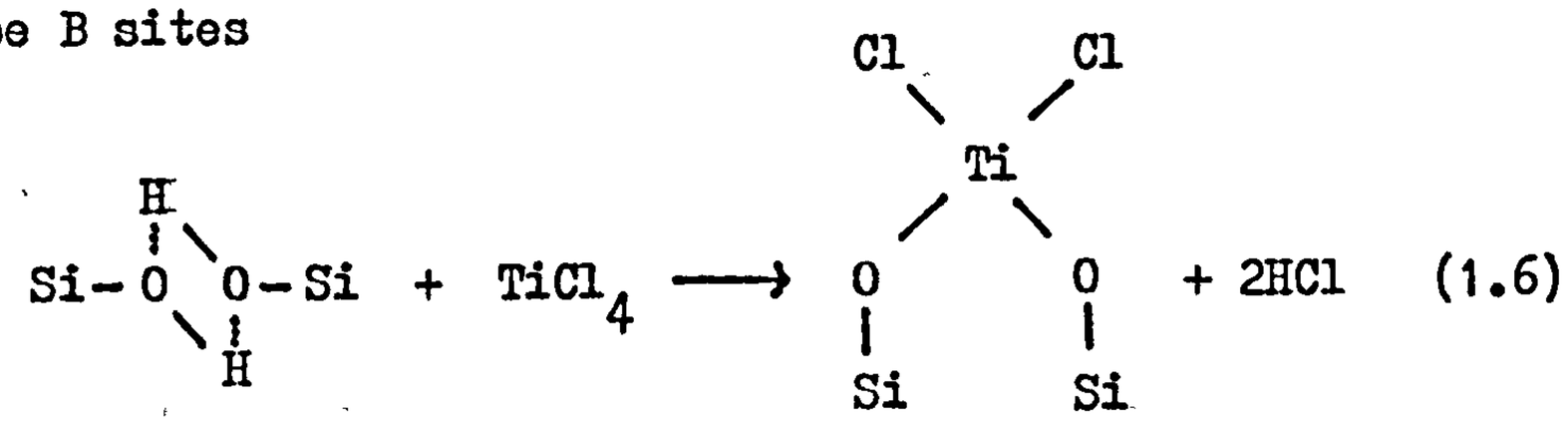

(1.6)

Hockey followed the reaction of the appended Ti species with $Al(CH_3)_3$ vapour using E.S.R. to monitor the appearance of the Ti(III) d^1 system. He concluded that the $Al(CH_3)_3$ vapour reacts to form a surface complex

which then decomposes (or rearranges) to yield a Ti(III)species. Chien[41], using $Al(i\text{-}C_4H_9)_3$ vapour, was unable to achieve reduction of SiO_2 supported Ti(IV) to Ti(III). However, using a hydrocarbon medium, all of the singly coordinated Ti(IV) (type A) was reduced, but only a small proportion of the doubly coordinated Ti(IV) (type B). He argued that the principal reduction mechanism was a bimolecular process (reaction 1.8) and that the steric requirements of such a reaction could not be met by the doubly coordinated Ti(IV) species.

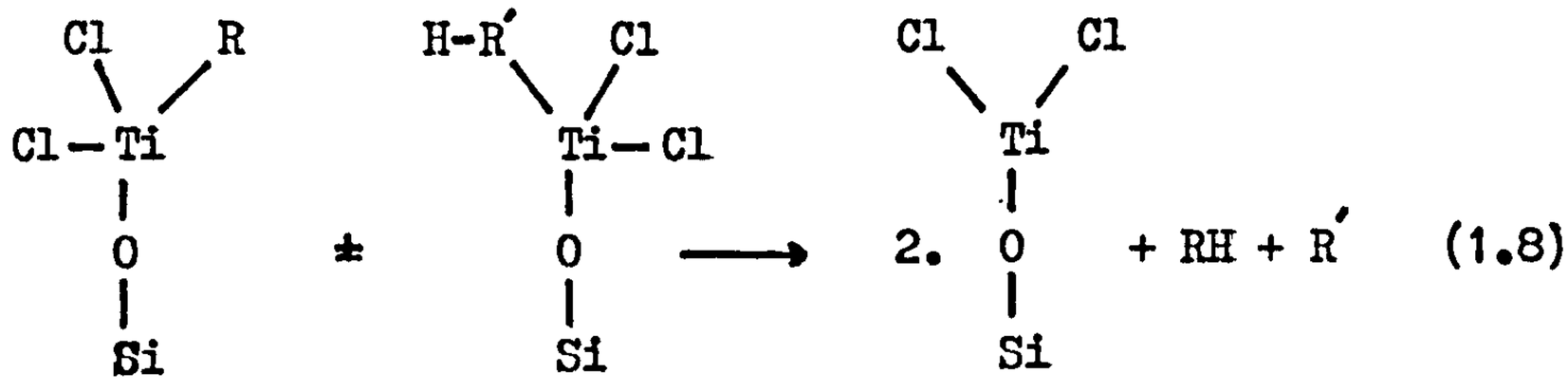

(1.8)

The available evidence appears to suggest that the role of the metal alkyl in producing an active catalyst is two fold - repeated alkylation and reduction of the transition-metal salt until stable centres possessing the correct chemical and geometrical parameters are formed.

1A.4) Mechanism of olefin polymerisation by Ziegler-Natta catalysts

i) Kinetic features of Ziegler-Natta polymerisation. In spite of voluminous kinetic experimentation it is difficult to define precisely the kinetic features which characterise the heterogeneous and homogenous Ziegler catalyst. Assessment of different kinetic investigations brings to light discrepancies in the conclusions reached by different workers, and serves to illustrate the complexity of the Ziegler-Natta system. Berger and Grieveson[30] pointed out that many of the discrep-

ancies can be attributed to the inherent instability of the catalyst chosen. Changes in the composition, crystal structure and valence state of the catalyst can complicate kinetic behaviour and it is therefore important to choose a suitably stable catalyst. The combination of $TiCl_3$ and $Al(C_2H_5)_2Cl$ is reported to possess such stability[14]. Carefully planned experiments to eliminate mass transfer effects and exclude inhibiting impurities are essential. Typical rate curves for propylene polymerisation are shown in figure (1.1)[17]. The initial induction period may be of the build up/decay type (A), obtained with $TiCl_3/Al(C_2H_5)_2Cl$, or of the acceleration type (B), obtained with $TiCl_3/Zn(C_2H_5)_2$. In both cases, a steady rate of polymerisation is attained and in the absence of catalyst decay this persists until very high monomer conversions, when mass transfer becomes important and the rate falls. Ethylene polymerisation curves show similar features but the induction period is generally of much shorter duration.

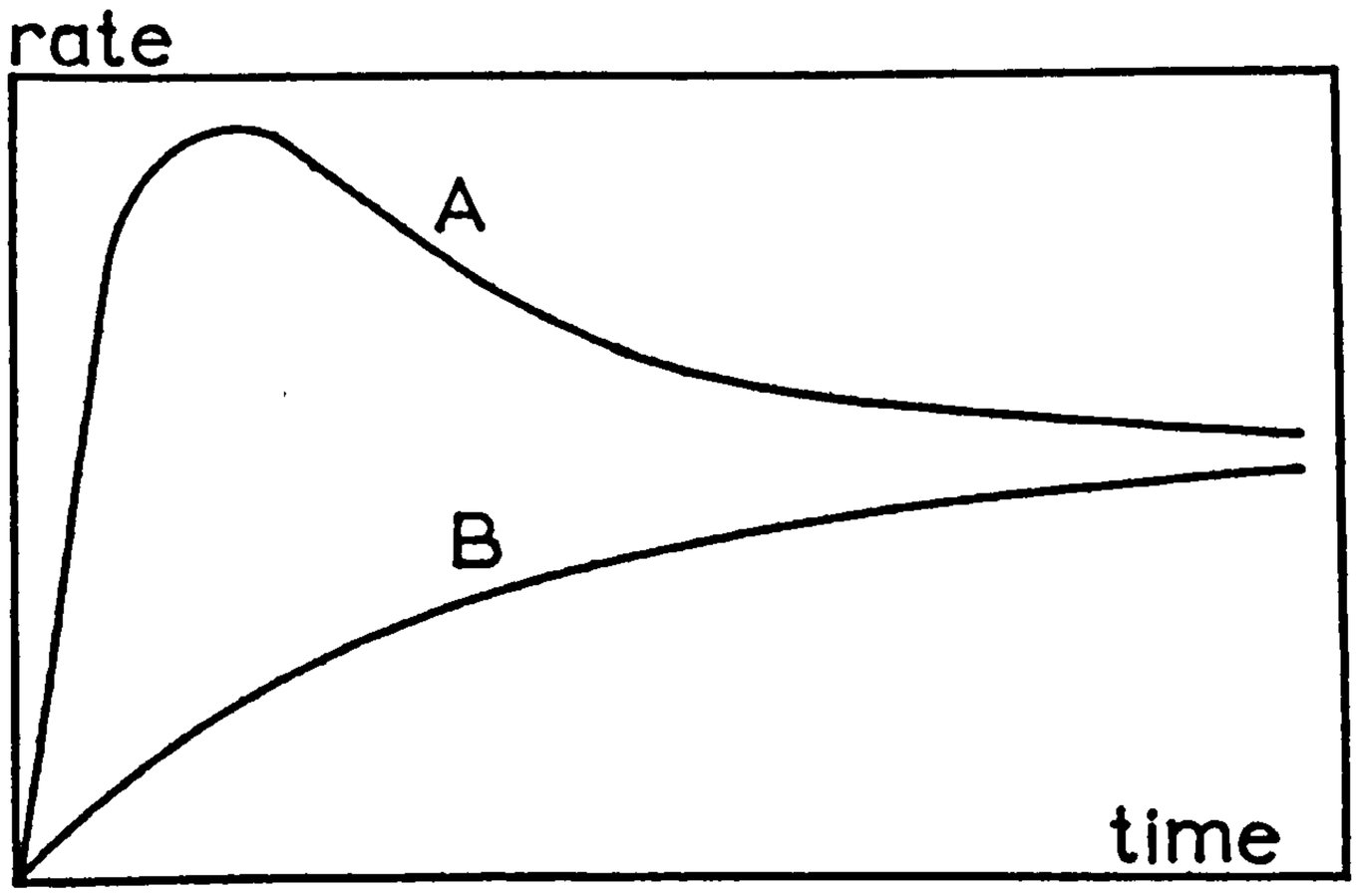

Fig. (1.1). Rate curves for propylene polymerisation.

Several workers have attempted to explain the origin of the induction period. Natta[22] suggested that the 'adjustment' period was necessary for agglomeration or cleavage of catalyst particles under the mechanical action of the growing polymer chains, until a particle size appropriate to the polymerisation conditions was obtained. In support of this, he showed that while finely ground and unground catalyst particles gave curves of type A and type B respectively, the ensuing steady rates were identical in each case. Keii[44] proposed the formation of two types of polymerisation centre, one of which becomes deactivated during the initial stages of polymerisation, while the remaining sites, once activated, are responsible for the ultimate steady rate. In spite of conflicting evidence it is possible to draw the following general conclusions from the kinetic studies[45,15,17]:

a) The rate of polymerisation is effectively independent of metal alkyl concentration, once that a certain minimum concentration is exceeded.

b) Provided that there is a suitable excess of metal alkyl present, the rate is directly proportional to the concentration of the catalyst (i.e. the transition metal salt).

c) For a given catalyst, in the absence of mass transfer effects, the rate is directly proportional to the monomer concentration.

d) The temperature dependence of the rate obeys the Arrhenius law, although values quoted for the activation energy of polymerisation vary widely.

ii) <u>The nature of the active site</u>. Despite early theories proposing a free radical mechanism, it is now generally accepted that the growing

polymer chain is attached to a metal atom and that propagation occurs by monomer insertion into the metal-carbon bond. However the nature of the metal-polymer bond has not yet been precisely defined. Two possibilities are favoured: that the polymer grows by a bimetallic mechanism involving both the transition metal atom and the metal alkyl, or that growth occurs solely by insertion into a transition metal - carbon bond. End group analysis studies of the polymer chains produced during ethylene polymerisation with the soluble catalyst complex (1) led Natta[47] to conclude that growth occurred by monomer insertion into the aluminium - alkyl bond. However, since the direct opening of the

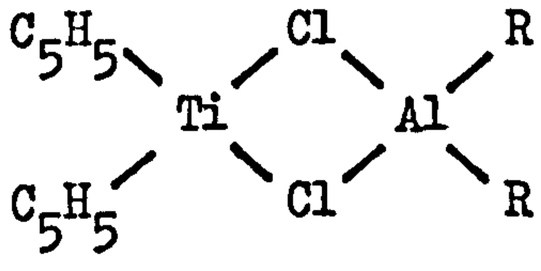

(R = C_2H_5; C_6H_5.)

(1)

aluminium-carbon bond by the incoming monomer appeared unlikely, he proposed a mechanism based on a bimetallic complex centre (figure 1.2)[48]. The incoming monomer is coordinated to the titanium atom, while simultaneously the titanium-polymer partial bond is broken. The coordinated monomer becomes polarised and inserts into the aluminium-carbon bond. Other bimetallic mechanisms have been proposed by Patat and Sinn[49], Huggins[50] and Boor[51]. Although Natta's initial premise, based on end group analysis, has been shown to be ambiguous due to ligand exchange between the aluminium and titanium atoms,[52] a vast amount of experimental evidence has been put forward in support of the

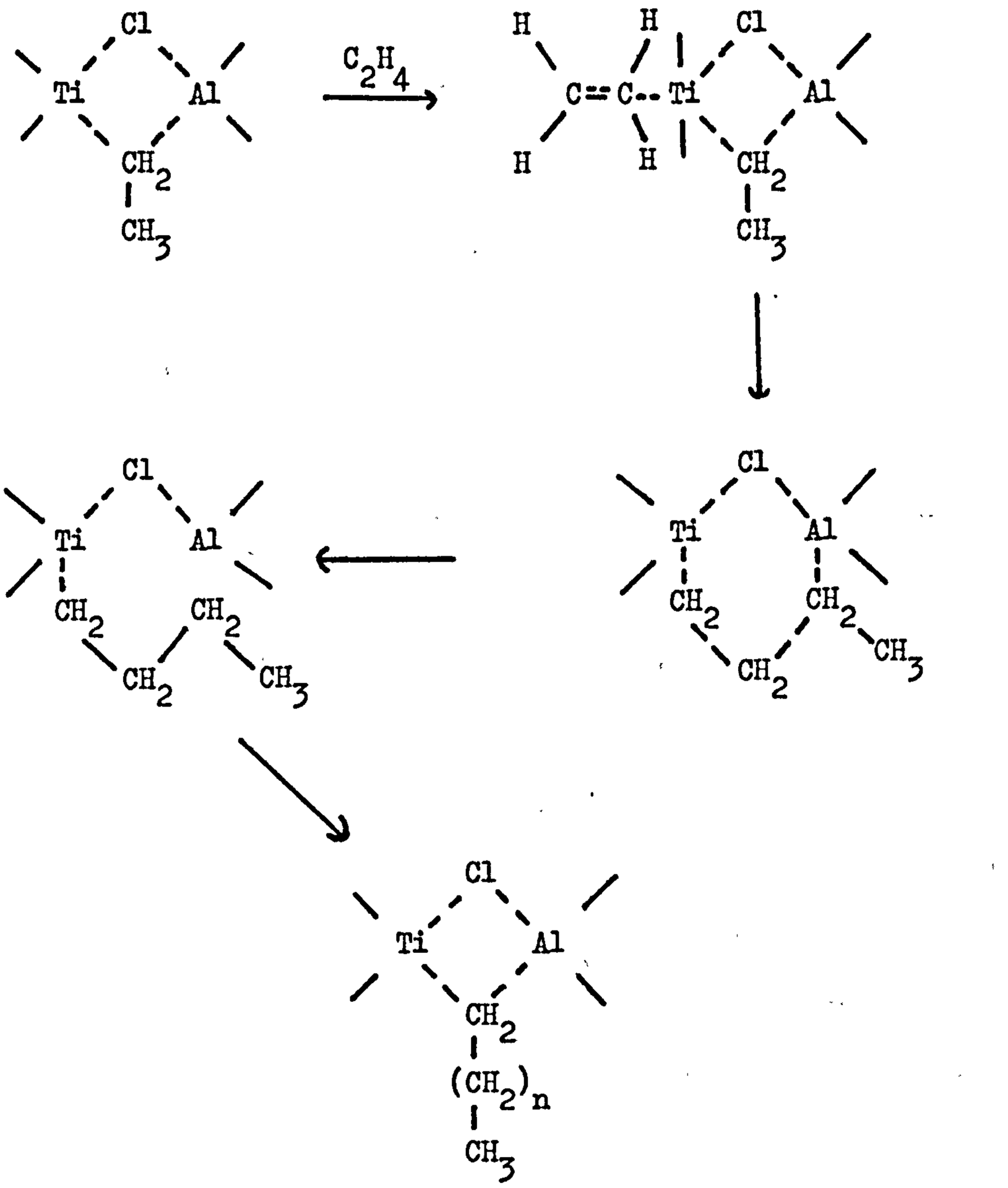

Fig. (1.2). The bimetallic growth mechanism proposed by Natta.

---

bimetallic growth centre. The main points may be summarised:-

a) the sterospecificity of the catalyst depends markedly on the nature of the metal alkyl used,

b) the energy of activation for the propagation step during polymerisation varies with the nature of the metal alkyl,

e.g. $TiCl_3/Al(C_2H_5)_3/C_3H_6$ E_{act} = 42.0 kJ/mole.

$TiCl_3/Zn(C_2H_5)_2/C_3H_6$ E_{act} = 11.3 kJ/mole.

c) the basic shapes of the polymerisation kinetic curves vary with different co-catalysts (section A.4.i).

Exponents of the monometallic polymerisation centre propose that the active site is a transition metal-carbon bond and that the role of the metal alkyl is simply to alkylate the transition metal. Many workers have confirmed that transition metal salts can be alkylated by the organo-metals[19,53]. In fact it has been suggested that in the homogeneous catalyst, $(C_5H_5)_2.TiCl_2/Al(C_2H_5)_3$, the active site is not associated with the soluble complex (1), but with a complex containing a titanium-alkyl bond[54]. In 1964 Cossee[55] proposed as the active site an octahedrally coordinated transition metal atom possessing a metal-alkyl bond and a vacant coordination position (figure 1.3). Polymerisation occurs by coordination of the monomer into the vacancy, followed by concerted insertion into the transition metal-alkyl bond. This proposal has received much support:-

a) Cossee was able to put his hypothesis on a sound theoretical basis using quantum mechanical theory[53] (section A4.iii.).

b) Rodriguez[31] concluded, on the basis of electron microscopy and stoichiometric studies on the $TiCl_3/AlR_3$ system, that polymerisation occurred only in those surface regions where chlorine vacancies (i.e. accessible titanium atoms) might be expected to occur.

c) Studies of the copolymerisation of ethylene and propylene[20,21] with a variety of catalysts showed that while the relative reactivities depended markedly on the transition metal halide nature ($ZrCl_4$, $TiCl_4$,

($COCl_3$, VCl_4), they were completely independent of the metal alkyl structure.

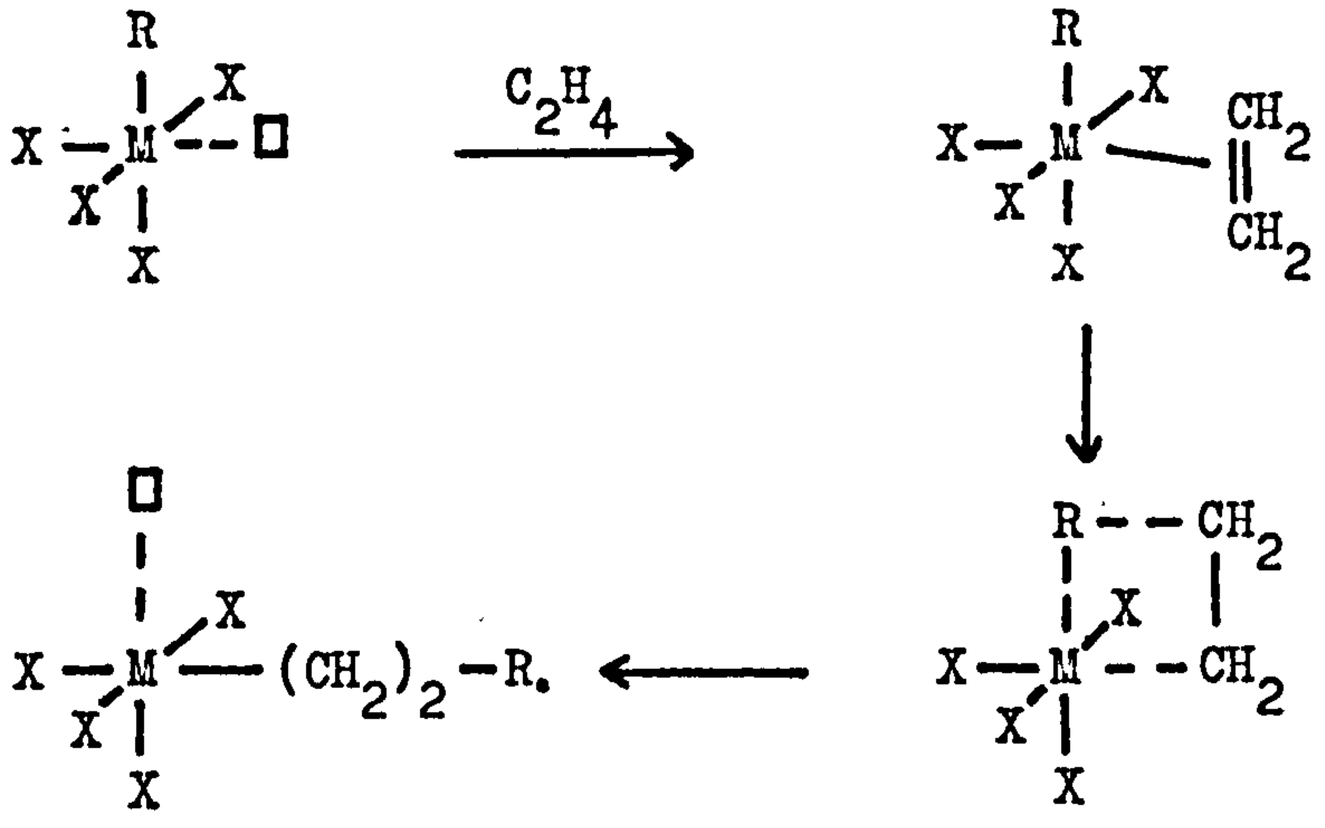

Fig. (1.3). The monometallic mechanism proposed by Cossee.

M = transition metal; X = halide atom;

□ = coordination vacancy.

---

d) studies on metal alkyl free polymerisation catalysts[15] indicate that polymer identical to that produced by conventional Ziegler-Natta catalysts can be obtained. In such cases the propagation occurs by monomer insertion into a transition metal-alkyl bond.

To date, no worker has been able to unequivocally show that growth occurs by either one of the above mechanisms, although taken collectively, the experimental evidence appears to favour polymer chain growth by insertion into a transition metal-carbon bond. Recently, several workers[17,31,56] have proposed that two or more different types

of active centres may be present in the Ziegler-Natta catalyst. This heterogeneous site theory has been invoked to explain the mixtures of atactic and tactic polymer produced during polymerisation. Rodriquez[31] extended Cossee's theory and proposed that in addition to the basic monometallic active structure (figure 1.3), an active bimetallic centre was also present (figure 1.4).

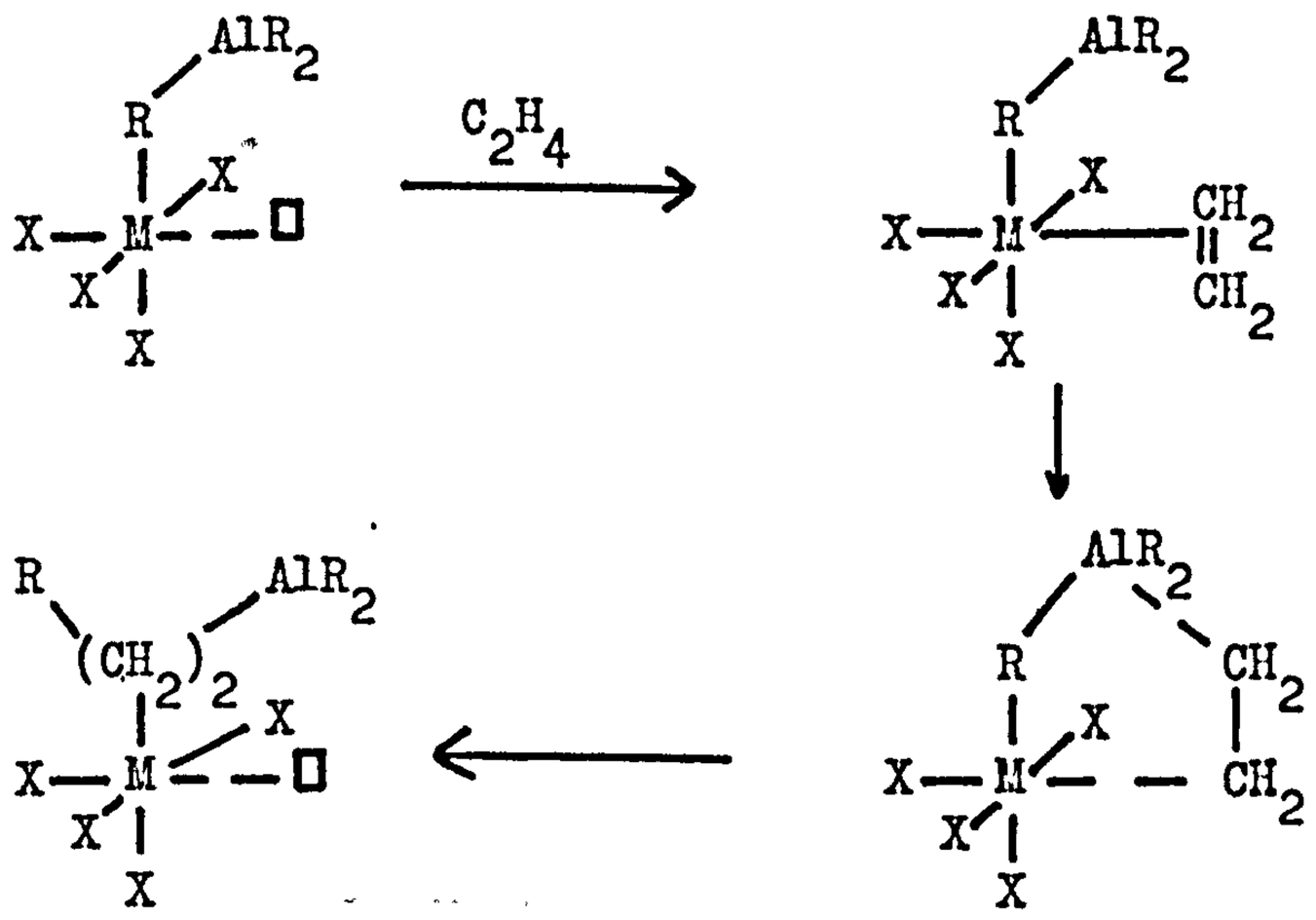

Fig. (1.4). The bimetallic growth mechanism proposed by Rodriquez. M = transition metal; X = halide atom; □ = coordination vacancy.

In view of the importance currently attached to the Cossee type mechanism, the associated theory is discussed in the next section.

iii) <u>The ligand-field theory approach to the Cossee mechanism</u>. The general formulation of the active site proposed by Cossee[55] was of an essentially octahedrally coordinated ion of a transition element, carrying in its coordination sphere one alkyl ligand and having one

vacant octahedral position. In the case of the $TiCl_3/AlR_3$ system, such a complex would occur at the crystal surface, with four lattice chloride ions completing the octahedral formation. Cossee proposed that the first step was coordination of the olefin monomer into the vacant position (figure 1.3). Complex formation between an olefin and a transition metal was discovered over one hundred years ago by Zeise[57]. Chatt[58] proposed that in such complexes the π-bond of the olefin combined with the metal $d_{(x^2 - y^2)}$ orbital. Further overlap between the olefin π^* - anti-bonding orbital and the metal d_{yz} orbital, led to a kind of double bond between metal and olefin, one component having σ, and the other π symmetry. Working from this established complex structure, Cossee expressed the bonding of the octahedral complex $R.TiCl_4(C_2H_4)$ in the form of a molecular orbital energy diagram (figure 1.5).

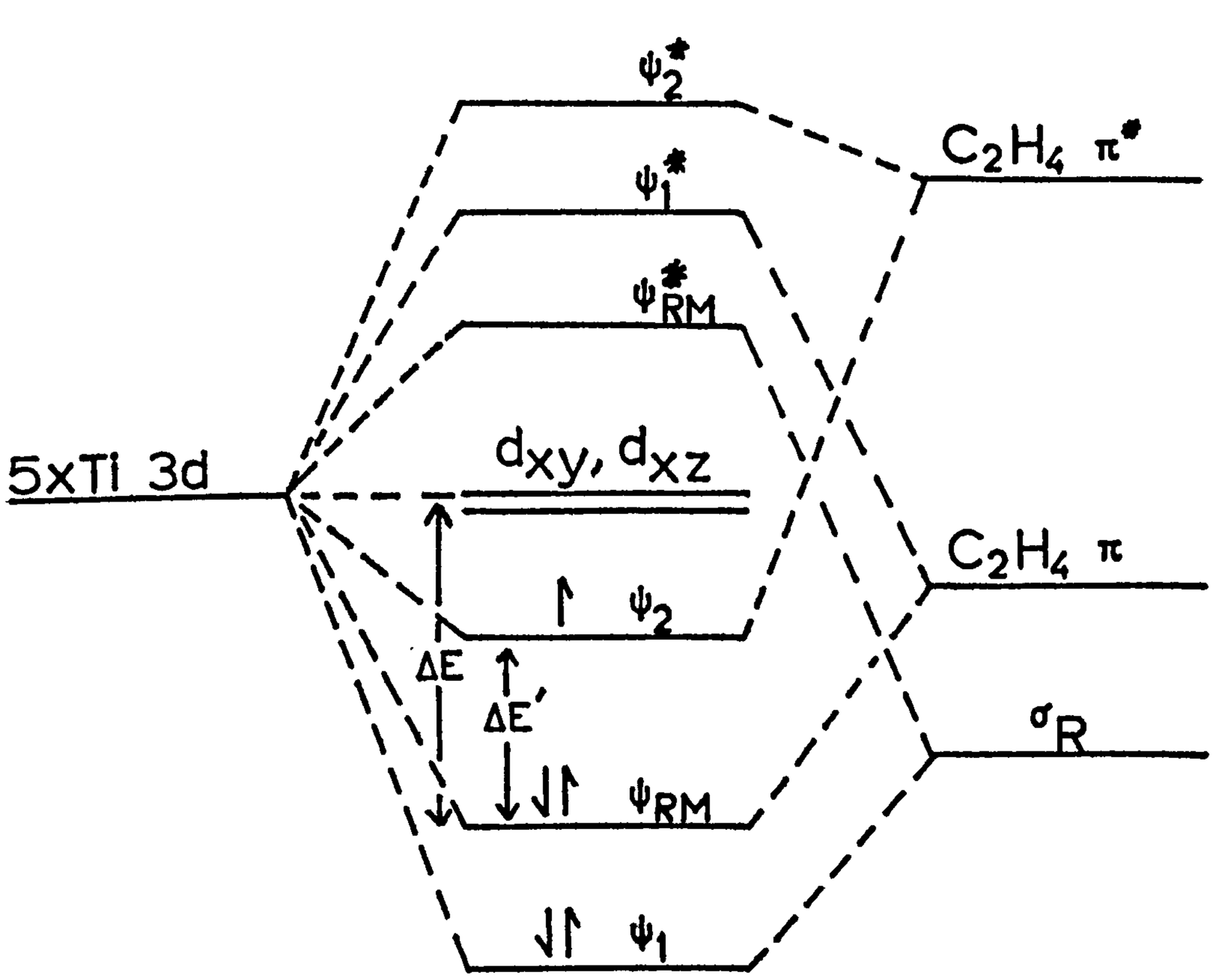

Fig. (1.5). Tentative molecular orbital energy diagram for the octahedral complex $R.TiCl_4$-(C_2H_4)[55].

His considerations were simplified by neglecting the 4s and 4p orbitals and assuming that the titanium-chloride bonds were completely ionic. The prime factor in the insertion step is the strength of the titanium-alkyl bond. For this to break in the required fashion, excitation of one of the bonding electrons from the titanium-alkyl bond to the next highest unfilled orbital must occur. In the absenco of a coordinated monomer, the energy needed, ΔE, is obviously too high for thermal excitation since the complex is stable at ambient temperatures. However, a bonded olefin ligand disturbs the degeneracy of the metal d-t_{2g} orbitals, forming the ψ_2 orbital and lowering the required energy to $\Delta E'$. When $\Delta E'$ is sufficiently small, the alkyl group R is expelled as a radical which attaches itself to the nearest carbon atom of the olefin, while at the same time the other end of the olefin attaches itself to the metal. The concerted nature of this rearrangement lowers the activation energy for the migration of the alkyl group towards the olefinic carbon atom. It follows that for a transition metal to be operative as a catalyst, the metal-carbon bonds must be suffiently stable in the absence of coordinated monomer, while at the same time, olefin coordination must sufficiently destabilise the bond to allow rearrangement to occur. Furthermore only one electron is allowed to be present in the ψ_2 orbital and the transition metal is only suitable when the energy of its 3d level is between the bonding (π) and antibonding (π^*) levels of the olefin. From spectroscopic data, Cossee estimated the approximate values of the energy levels concerned for several transition metals. On the basis of this, he concluded that while the chlorides of Sc, Ti, Yt, Zr, La, Hf and Ta

should exhibit activity, those of Ca, Cr, Sr and Ba should be inactive. His conclusions are in accord with experimental evidence. A more rigorous assessment of the electronic energy levels for the molecular orbitals of the octahedral complex ($R.TiCl_4$-olefin) (4) and the tetrahedral complexes $CH_3.TiCl_3$ (5) and $C_2H_5.Ti.Cl_3$ (6) has recently been made. Begley and Pennella[59] calculated that the energy of the lowest electron transition in the complex (4), corresponding to the initial step in the olefin insertion mechanism proposed by Cossee, was close to the experimental activation energies for polymerisation (42-59 kJ/mole). In addition they showed that on the basis of their electronic energy levels, the complexes (4) and (5) should be stable at ambient temperatures, as observed. The soluble complex (6) was active when used alone for the polymerisation of ethylene, while complex (5) was inactive in the absence of a metal alkyl. This variation in activity was attributed to the difference in the values of the lowest electronic transition energy, only 1.07 electron volt in the former case but 3.20 electron volt in the latter.

The popularity of the Cossee mechanism owes much to this theoretical confirmation. However, any mechanism proposed for a Ziegler-Natta system, must stand or fall on its ability to explain the stereospecificity of the catalyst. The most cogent mechanisms are outlined in the next section.

iv) Origins of Stereospecificity. Since Natta's discovery in 1955[7], the phenomenon of stereospecificity in Ziegler catalysts has occasioned much research, both experimental and theoretical. It is generally

accepted that stereospecificity has its origin in the steric surroundings of the active site. Beyond this premise it has not been found possible to present a unifying theory of stereoregulating catalysts. Of the models proposed to explain the orientating influence in α-olefin polymerisation, the most appealing are those based on monomer-ligand and monomer-polymer interactions, leading to isotactic and syndiotactic placements respectively. With only one reported exception[60], all isotactic polymerisations of α-olefins have required a solid transition metal salt to be present[61]. It is clear however that the inherent stereoregulating properties cannot be assigned to either the individual transition metal, or to the metal alkyl component, but rather to some combination of the two. Since highly isotactic polymer may be produced using metal alkyl free catalysts, it is clear that the isotactic orientation does not require the presence of a metal alkyl molecule as an integral part of the active centre. However, this does not eliminate the possibility that bimetallic growth mechanisms, as proposed by Rodriguez[31], do exist. There is much experimental support for a heterogeneous site theory, invoking active centres of varying stereoregulating power. Progressive complexing of the active centres using electron donors such as amines, led to a higher degree of isotacticity, supporting the view that the more vulnerable exposed sites produce atactic polymer, while the stereo-active centres are based on the accessible metal atoms sheltered in chlorine vacancies[51]. Such results indicate that it is the ligand environment of the active centre which determines the complexing mode of the α-olefin. In the mechanism proposed by Cossee, the incorporation of each monomer unit results in the

positions of the vacancy and the growing chain being interchanged. In a subsequent paper, Arlman and Cossee[62] argued that after each momomer addition, the polymer chain moves back to its more favoured original position before the next monomer unit is coordinated. In this fashion, the α-olefin molecules must assume identical orientations before inserting, leading to isotactic placement.

With the discovery of stereospecific homogeneous catalysts came the necessity to define stereoregulating parameters in the absence of a solid crystal surface. The very existence of syndiotactic polymer led workers to conclude that the steric placement of the incoming α-olefin was determined solely by the interaction with the last inserted monomer unit. In the case of propylene, this monomer-polymer interaction was assumed due to the steric interplay of the methyl groups, so that each newly coordinated propylene molecule had the opposite configuration to the previous one[28]. The more recent discovery, that stereoregular polypropylene can be produced using the soluble catalyst Zr $(allyl)_4$ in the absence of metal alkyls[60] has lent weight to the monomer-polymer interaction theory.

v) Chain termination and chain transfer. Growth of a particular polymer chain at the metal-carbon bond centre can be terminated by suitable choice of additions and experimental conditions. In this way it is possible to control the molecular weight of the polymer. At polymerisation temperatures above 373K, chain termination by thermal cleavage becomes important, as evidenced by the presence of terminal vinyl groups in the polymer[63]. Chain termination by hydrogen is

believed to involve the hydrogenolysis of the metal-polymer bond[64]:

$$H_2 + M\text{- polymer} \longrightarrow M\text{-}H + H\text{- polymer}$$

The use of tritium gas[65] led to the formation of polymer chains with a tritium label at each end, indicating that after termination, the M-H bond is capable of realkylation, reforming the metal-carbon bond centre. In the presence of a partial pressure of hydrogen, the polymerisation rates are generally lower, probably due to the higher activation energy required for monomer insertion into the metal-hydride bond. Recently however, it has been reported[66] that some catalysts show a rate increase on hydrogen addition and this was attributed to modification of the crystalline catalyst by the hydrogen. The use of metal alkyls as chain transfer agents has been reported. Natta[67] showed that transfer by $Zn(C_2H_5)_2$ involves a simple alkyl exchange between the ethyl groups of the alkyl and the growing polymer chains:

$$M\text{-polymer} + Zn(C_2H_5)_2 \longrightarrow M\text{-}C_2H_5 + Zn.C_2H_5\text{-polymer}.$$

PART B Infrared spectroscopic studies of species adsorbed at oxide surfaces.

1.B.1) Introduction

Eischens and Pliskin laid the foundations of this work in the mid 1950's. Their techniques for sample preparation and recording spectra, the principles of which have been adopted in most subsequent studies, have been reviewed[68]. Books by Little[69] and Hair[70] in 1967

gave a comprehensive review of the infrared spectroscopic studies of species adsorbed at oxide surfaces. The recent literature has been covered in a review by Rochester and Scurrell[71].

Transmission spectroscopy, in which the absorption of radiation passing through the oxide is measured, has been used in the majority of studies, although recently the use of reflectance infrared spectroscopy has occasioned some interest[72]. Comparable results are obtained with both techniques. The oxide sample is generally in the form of a compressed disc, although studies on loosely powdered oxide samples have been made[73]. The presence of small amounts of impurity on the oxide surface can markedly affect the infrared spectrum and the sample is generally maintained in an evacuated infrared cell. An electrically heated furnace, either internal or external, has been used both to degas the oxide disc and to study the effect of temper ature on the surface species. Although spectra can be recordéd at elevated temperatures, the usual practice is to allow the sample to cool after a prescribed heat treatment and then record the spectrum at the temperature of the infrared beam (318K). The metal oxides commonly employed in heterogeneous catalysis (silica, alumina, magnesia, zeolites and the transition metal oxides) are transparent to infrared radiation over the range 1,000–10,000 cm^{-1}. Thus infrared spectroscopy has proved a useful tool in studying species adsorbed on catalyst surfaces.

1.B.2) Hydroxylated oxide surfaces.

i) General features. All oxides, providing they have not been subject

to high temperature treatment in vacuo, have a layer of water on their surfaces under ambient atmospheres at room temperature. In infrared spectroscopic studies, this appears as a combination of absorptions due to surface hydroxyl groups (3400-3800 cm^{-1}) and molecular water (1600-1650 cm^{-1}; 3000-3600 cm^{-1}).

The effect of temperature on these absorption bands has been studied on many metal oxides[71]. Following heat treatment of the oxide in vacuo, the bands due to molecular water gradually disappear (up to 473 K), leaving behind the absorptions due to the surface hydroxyl groups. The existence of several peaks in the hydroxyl stretching region has been commonly observed, indicating the presence of several distinct hydroxyl environments. The assignment of such peaks has proved the subject of much controversy in the literature. As a general rule, sharp absorptions at high frequencies (3600-3800 cm^{-1}) have been assigned to isolated hydroxyl groups. Broader bands at low frequencies (3400-3650 cm^{-1}) have been attributed to interacting hydroxyl groups (e.g. hydrogen bonded interactions). The thermal stability of surface hydroxyl groups is such that they have even been detected on oxide surfaces evacuated at temperatures exceeding 2273 K[74].

The sensitivity of both the shape and frequency of the hydroxyl absorption bands to the immediate surface environment of the hydroxyl groups has proved a powerful probe in studying the interactions of chemical species with the oxide surface. In particular, the hydroxyl frequency shifts observed ($\Delta\nu_{OH}$ cm^{-1}) when the oxide surface was exposed to the weakly basic pyridine and ammonia, and the weakly acidic phenols, have proved useful in assessing the pK_a values of the surface hydroxyl groups[70].

ii) <u>The magnesium oxide surface.</u> The formation of high surface area 'active' magnesia by the thermal decomposition of carbonate[75] or hydroxide[74] of magnesium has been described. For the purpose of infrared spectroscopic studies, the second route is to be preferred since carbonate impurities left by the former method absorb strongly in the region 1200-1700 cm^{-1} [77]. Thermal decomposition of magnesium hydroxide leads to a loss of water vapour at about 550 K, corresponding to almost 32% of the sample weight. This weight loss, combined with a change in structure from a hexagonal lattice to the cubic lattice of magnesium oxide, leads to pore formation and a large increase in surface area. Anderson[76], on the basis of gravimetric and infrared studies, proposed a model for the magnesium oxide surface based on the predominance of the (100) crystallographic plane. The (100) plane presents a cubic array of Mg^{2+} and O^{2-} ions. Each chemisorbed water molecule was supposed to form a hydroxyl group adsorbed on a surface Mg^{2+} ion (type A), with the remaining hydrogen forming another hydroxyl group with an adjacent surface O^{2-} ion (type B) (figure 1.6).

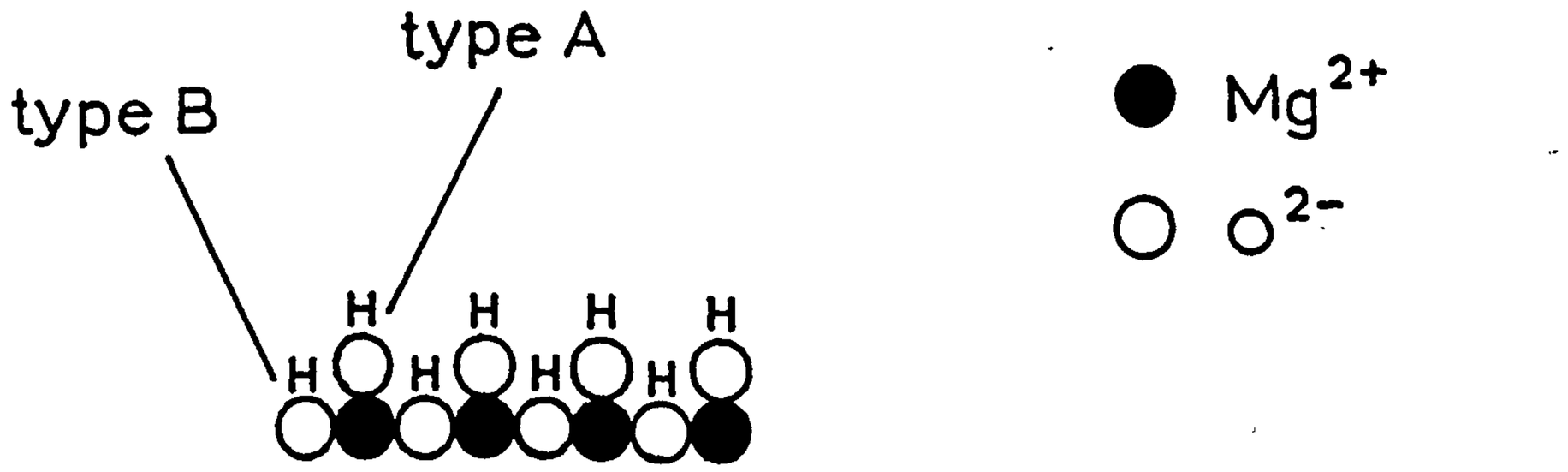

Fig. (1.6). Section through an ideal hydrated (100) face.

After heat treatment at 573 K, two bands were observed in the hydroxyl stretching region (3752 and 3610 cm^{-1}). The strong sharp band at 3752 cm^{-1} was considered to be the stretching vibration of the free hydroxyl groups (type A) and the broad band at 3610 cm^{-1} was assigned to the hydroxyl in the lower lying layer of the magnesium oxide surface. Other workers have assigned the band around 3610 cm^{-1} to a hydrogen bonded surface hydroxyl group[78]. Heating at high temperatures resulted in the gradual removal of both of these bands until at 1020 K only a small peak due to isolated hydroxyl groups remained. Recent studies by a reflectance technique gave comparable results, although the precise positions of the absorption maxima appear to depend upon the nature and thermal history of the sample[72].

It is generally accepted that the surface hydroxyl groups of magnesia are largely ionic (OH^- character). Isotopic exchange using D_2O is thus slow and difficult to accomplish at room temperature. However almost complete exchange may be effected by exposure of the dehydrated surface to D_2O vapour and pumping at 573K [76]. Hair obtained a pK_a value of 15.5 for the isolated hydroxyls (3752 cm^{-1}), illustrating their exceptionally weak acidity[79]. Carbon dioxide undergoes rapid physical adsorption on the surface of magnesium oxide. Progressive chemisorption eventually results in the formation of a broad infrared absorption (1200–1700 cm^{-1}) characteristic of carbonate ions similar to those in magnesium carbonate[80]. It has been reported that the interaction between carbon dioxide and the surface hydroxyl groups of magnesia leads to the formation of bicarbonate species on the oxide surface[81].

iii) The rutile surface. The preparation of rutile samples suitable for spectroscopic studies has been described. Jackson and Parfitt[82] studied the adsorption and desorption of water on rutile and assigned the bands which appeared at 3700 (bridged OH group), 3690 (H-bonded bridged OH group), 3670 (terminal OH group), 3420 (H-bonded terminal OH group) and 3350 and 3400 cm^{-1}. (strongly and weakly physisorbed water) to hydroxyl species on the (110) plane. Two bands at 3615 and 3530 cm^{-1} were thought to be due to either OH groups perturbed by physisorbed water, or to physisorbed water interacting with surface hydroxyl groups. Physisorbed water, amenable to deuterium exchange, was observed to be retained on the rutile surface at temperatures as high as 570K. Jones and Hockey[83] concluded that in addition to the (110) plane, both the (100) and (101) planes influenced the hydroxyl stretching region.

iv) Reactions of $TiCl_4$ and $AlEt_3$ vapours with surface hydroxyls. Because of their high reactivity towards hydroxy species, these reagents have proved useful in the characterisation of surface hydroxyls. The reaction of $TiCl_4$ vapour with the surface hydroxyl groups of silica has been studied by Hockey et al[84]. He proposed that on a fully hydroxylated silica surface there were two types of hydroxyl environment, the single type A (3750 cm^{-1}) and the hydrogen bonded type B (3550 cm^{-1}). Both bands were completely removed by reaction with $TiCl_4$ vapour at room temperature, leading to singly and doubly coordinated titanium species respectively (figure 1.7).

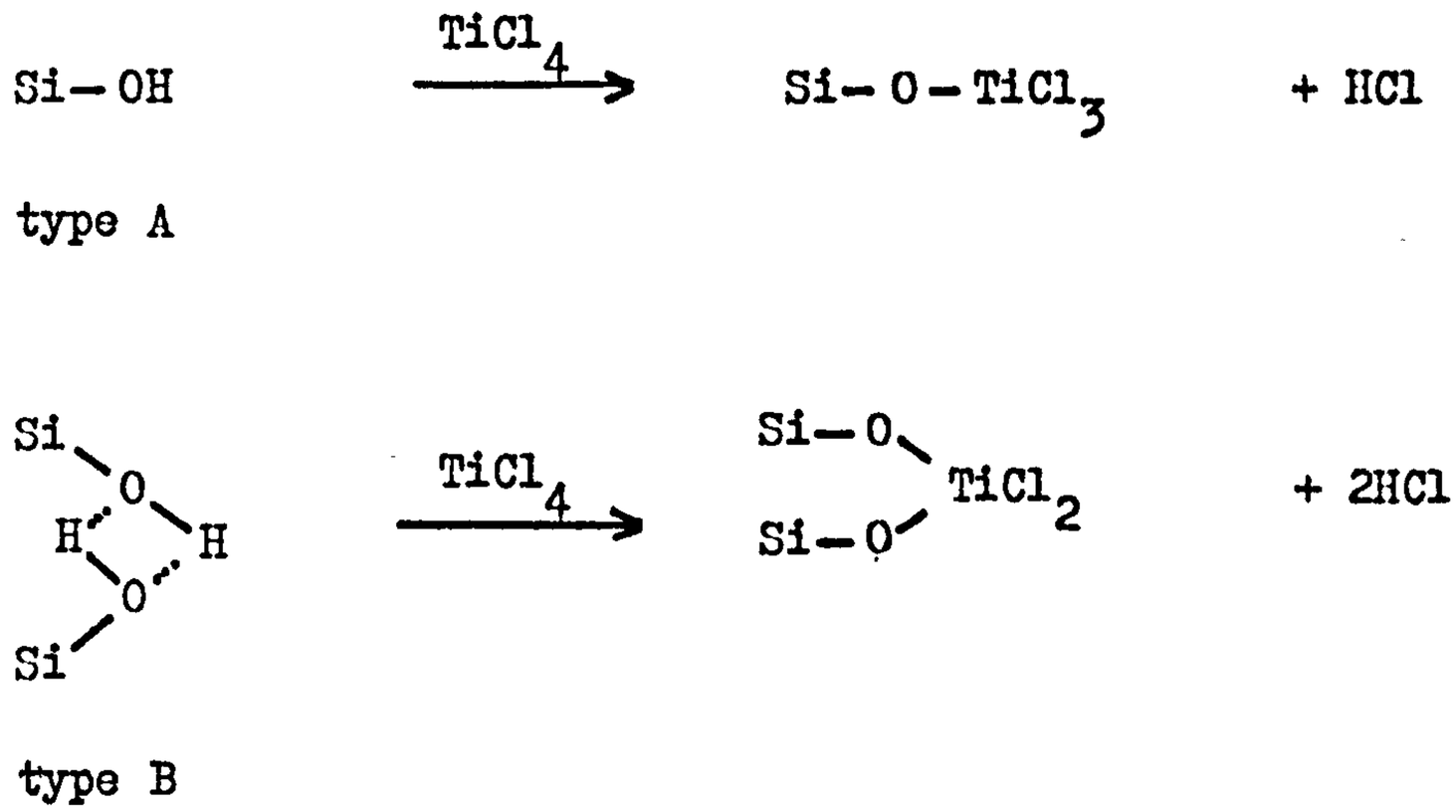

Fig. (1.7). Reaction of $TiCl_4$ vapour with type A and type B surface hydroxyls of silica.

Infrared studies also show that $Al(CH_3)_3$ reacts with all the available surface hydroxyls on the silica surface[85]. In addition, reaction with siloxane bridges has been observed (figure 1.8).

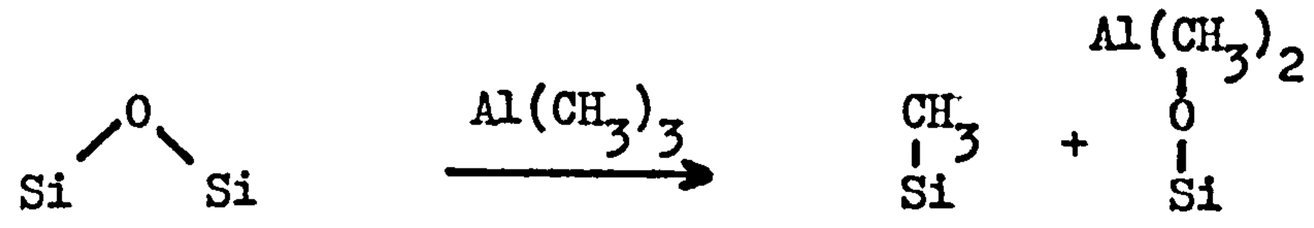

Fig. (1.8). The reaction of $Al(CH_3)_3$ vapour with siloxane bridges in the silica surface.

The consecutive reaction of $TiCl_4$ and $Al(CH_3)_3$ vapours with the silica surface produced a surface species containing a Ti(III) ion.

Exposure of this surface to propylene gas led to the appearance of infrared adsorption bands characteristic of polypropylene[36]. Stoichiometric and E.S.R. studies by Chien have supported these observations[41].

$TiCl_4$ reacted with the surface of rutile to form hydrogen chloride and Ti-O-$TiCl_3$ linkages, with the removal of all accessible hydroxyl groups[86].

1.B.3). Infrared spectroscopy of polyolefins.

With the increasing use of olefin polymers in the late 1950's came the need for reliable techniques for assessing their molecular structure. Extensive studies of the vibrational spectra (both infrared and Raman) of polyethylene and polypropylene have resulted in the assignment of the majority of observed bands, which approach sixty in the case of polyethylene[13,87]. Several absorption bands have been identified as characteristic of particular crystalline modifications of the polymer. These crystalline adsorptions, a consequence of the greater symmetry of crystalline polymer molecules, permit quantitative assessments of the amorphous and tactic contents of polymer samples. The most prominent absorption bands are those of the (C-H) stretching vibration, occuring in the region 2800-3000 cm^{-1}. These bands, four in number, arise from the symmetric and asymmetric stretches of the CH_3 and CH_2 groups. In the spectrum of polyethylene, the asymmetric (2960 cm^{-1}) and symmetric (2870 cm^{-1}) CH_3 stretches, due to terminal methyl groups, are very weak and, if

visible at all, are usually observed as shoulders on the strong asymmetric (2920 cm^{-1}) and symmetric (2850 cm^{-1}) CH_2 absorptions. The growth of polyethylene on the Phillips catalyst[88] and on a supported Ziegler catalyst[36] has been observed using infrared spectroscopy.

All four bands are prominent in the spectrum of polypropylene[87] (CH_3 at 2960 (ν_a) and 2866 (ν_s) cm^{-1}; CH_2 at 2918 (ν_a) and 2840 (ν_s) cm^{-1}). The precise position of these absorptions may vary with the atactic content of the polymer sample.

PART C Diffusion of gases in polymers.

1.C.1). Introduction.

The diffusion of gas molecules through polymer films has been extensively investigated, particularly those aspects pertinent to the packaging and paint industries[89]. In 1937, Barrer[90] reported theoretical and practical techniques for studying the transport properties of penetrants in solids. Subsequent studies, based on Barrer's concepts, have been adequately reviewed[91,92]. A comprehensive mathematical treatment of the underlying theory of the diffusion processes was given by Crank[93].

1.C.2). Definitions and Basic Equations.

The permeation of gas through a plastic membrane is usually

considered to involve three independent physical phenomena:

1) solution or sorption of the gas or vapour at one surface of the membrane,

2) diffusion of the dissolved gas through the membrane

3) re-evaporation or desorption of the gas from the opposite surface.

Since the flow process is generally slow, this permits the use of an equilibrium relationship between the concentrations of absorbed gas at the interfaces and the respective partial pressures[94]. A Henry's law type relationship can be expected to apply:

$$C = Sp \qquad (1.1)$$

where C is the concentration of the solute, p is the external pressure and S is the solubility coefficient for the gas in the polymer (the volume of gas at S.T.P. dissolved in unit volume of polymer at unit pressure). Polymer films in general can be regarded as interspersed crystalline and amorphous regions[91]. The gas molecules are normally assumed to be soluble only in the amorphous regions. They pass through the membrane by an activated diffusion process. Fick[95] first employed the analogy between heat transfer by conduction and the transfer of matter by diffusion, both due to random molecular motion, to state the first law of diffusion:-

$$J = -D \frac{dC}{dX} \qquad (1.2)$$

where J is the diffusion flux and $\frac{dC}{dX}$ is the concentration gradient perpendicular to the surface. The diffusion constant (D) is independent of concentration and has the dimensions ($length^2/time$). Integrating

equation (1.2) under the boundary conditions[93]:-

$$X = 0, \quad C = C_o$$

$$X = 1, \quad C = C_1$$

gives:-

$$J = \frac{D}{l} (C_o - C_1) \qquad (1.3)$$

where l is the film thickness. From equations (1.1) and (1.3):-

$$J = \frac{D}{l} (S_1 p_1 - S_2 p_2) \qquad (1.4)$$

if both surfaces are at the same temperature then

$$S_1 = S_2 = S$$

and

$$J = \frac{DS}{l} (p_1 - p_2). \qquad (1.5)$$

The permeability constant (P) is defined as the volume of gas at S.T.P. passing in unit time through a unit volume cube under unit pressure difference.

$$P = DS = \frac{Jl}{(p_1 - p_2)} \qquad (1.6)$$

The fundamental postulation by Graham[94] that Henry's law applies to the sorption and desorption and that Fick's law applies to the diffusion process has been well established[96] and is generally used as the basis for studying permeation processes.

The above analysis holds only for systems for which the diffusion constant (D) is independent of the sorbed concentration. Permanent gases interact very little with organic solids, the amount sorbed is sufficiently small that the solid structure does not undergo any appreciable strain or swelling. Consequently D is concentration

independent. However with more condensable vapours, for which the penetrant-polymer interaction is appreciable, the polymer structure tends to swell and plasticise. Such structural changes are evidenced by a concentration dependent diffusion coefficient[91].

1.C.3). The effect of temperature.

Over small temperature ranges, the temperature dependencies of P, D and S obey an Arrhenius type law[91]:-

$$P = P_o \exp. (-E_p/RT) \qquad (1.7)$$

$$D = D_o \exp. (-E_D/RT) \qquad (1.8)$$

$$S = S_o \exp. (-\Delta H_S/RT) \qquad (1.9)$$

E_p and E_D are the apparent activation energies for the permeation and diffusion processes; and ΔH_S is the corresponding heat of solution. From equation (1.6) it follows that:-

$$E_p = E_D + \Delta H_S \qquad (1.10)$$

and

$$P_o = D_o S_o \qquad (1.11)$$

Several investigators [91,97] have reported discontinuities in the Arrhenius plots for the coefficients P, D and S. It has been shown that the temperatures at which these discontinuities occur are very close to the glass transition temperatures (Tg) of the polymers.- The values of E_D, E_p and ΔH_S are significantly changed as the temperature is increased through Tg. This is a direct consequence of the drastic change in the freedom of the polymer chains. Accordingly, to obtain meaningful data, it is important to work at temperatures sufficiently removed from Tg that the effects of the molecular rearrangements are negligible.

1.C.4) <u>The nature of the transport process</u>.

The transfer of gas molecules in an amorphous polymer has been qualitatively interpreted in terms of the movement of penetrant molecules through a tangled mass of polymer chains and holes[91]. Segmental motions of the polymer chains, arising from thermal fluctuations, result in the holes being constantly destroyed and reformed. Diffusion takes place by the movement of a gas molecule from hole to hole under the influence of a concentration gradient, in conjunction with a cooperative action of the surrounding structure. The activation energy for diffusion (E_D) is comprised of the energy required for hole formation against the cohesive forces of the medium, and the energy required for the penetrant molecule to move from hole to hole.

The transport properties of a polymer are strongly dependent upon the thermal history[92,98] of the specimen and also on the presence of extraneous substances in the polymer[91,92]. Cold-drawing of the polymer material reduced the value of the diffusion coefficient (D) by several orders of magnitude. E_D remained unaffected, indicating that cold-working did not affect the mechanism of propagation. Annealing of the cold-drawn sample restored the value of D to its unworked value.

Most commercial polymers contain additions to improve or modify the physico-chemical properties of the material. Such additions lead to disruption of the polymer structures, affecting the values of both D and E_D. When the penetrant is present in high concentration, it causes swelling of the polymer. This 'plasticising' effect is evidenced by the dependence of D and E_D upon the sorbed concentration of penetrant.

1.C.5) Determination of P, D and S by permeation studies.

The fundamentals of permeation measurements were developed by Barrer[90]. In a typical permeation experiment, a given polymer film is inserted between two chambers which are then degassed. The required pressure of penetrant gas is introduced into one of the chambers. The penetrant dissolves in one surface of the film, diffusés through the film and evaporates from the other surface at the low pressure side. The amount of penetrant which permeates through unit area (Q(t)) of film is measured as a function of time. When a penetrant diffuses through a membrane in which it is soluble, there is an interval from the time the penetrant first enters the membrane until the steady state of flow is established. The permeability constant (P) may be calculated from this steady flow rate. Typical c.g.s. units are cubic centimetres of gas at S.T.P. passing per second through a 1 cm^2. area of a polymer membrane 1 cm. thick under a pressure differential of 1 cm. Hg. Such values are readily converted into the S.I. Units:- cubic metres of gas(S.T.P.)passing per second through a 1 m^2. area of a polymer membrane 1 m thick under a pressure difference of 1 $kN.m^{-2}$. The intercept on the time axis of the extrapolated linear, steady-state portion of the (Q(t))/t curve is called the time lag (θ) (Figure 1.8).

Barrer[2] has shown that θ is directly related to the diffusion coefficient (D). In the case where D is independent of penetrant concentration, the relationship is:-

$$\theta = \frac{l^2}{6D} \qquad (1.12)$$

where the dimensions of D are length^2/time. Thus P and D may be calculated from the same experiment, and hence the solubility coefficient (S) can be evaluated using equation (1.6).

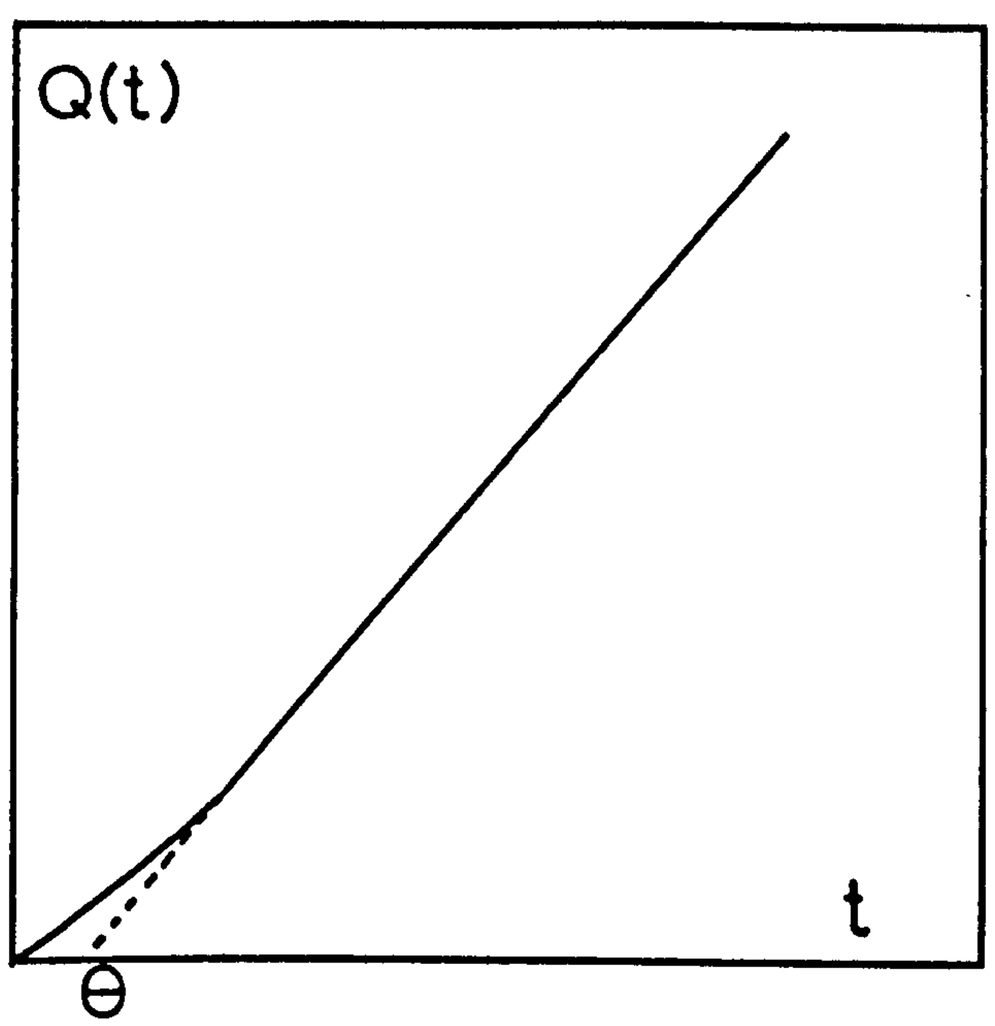

Fig. (1.8). Typical Q(t)/t plot for permeation of gaseous penetrant through a polymer membrane.

1.C.6) Diffusion studies involving polyethylene and polypropylene.

The use of polyethylene and polypropylene for commercial packaging films has resulted in extensive investigation into their permeation properties. The diffusion behaviour of permanent gases (O_2, H_2, N_2, CO_2, CH_4), vapours (H_2O, CH_3Cl) and liquids (C_6H_6, CCl_4) have been reported[89]. The use of polyethylene and polypropylene

membranes for separating gas mixtures by differential permeation has been discussed in detail[99,100]. It has been emphasised that the gases dissolve and diffuse only in the amorphous polymer regions[101].

Studies of the transfer of ethylene gas through polyethylene have been made. Li and Henley[102], working at pressures between 1×10^2 and 8×10^2 $kN.m^{-2}$, reported that the permeability constant (P) was pressure dependent. Russian[103] workers investigated diffusion in the pressure region 2×10^3 to 2×10^4 $kN.m^{-2}$. and found that the diffusion coefficient (D) was pressure independent in this range. From their data it is possible to calculate a value for E_D of around 30 kJ/mole over the temperature range 298K to 333K. Leitao[104] studied the permeation and solubility of propylene in polyethylene films as functions of the relative vapour pressure of the penetrant $\frac{p_1}{p_o}$ between 253K and 298K. He showed that at low values of $\frac{p_1}{p_o}$, D, S, P, E_D, E_P and ΔH_S were independent of the penetrant pressure. At higher values of $\frac{p_1}{p_o}$, E_D, E_P and ΔH_S fell. ΔH_S was negative for all values of $\frac{p_1}{p_o}$ and as $\frac{p_1}{p_o}$ approached unity, E_P became negative and E_D approached zero. At small values of $\frac{p_1}{p_o}$ equation (1.10) was obeyed.

$$E_P = E_D + \Delta H_S \qquad (1.10)$$

There are no reports in the literature of low pressure studies ($< 1 \times 10^2$ $kN.m^{-2}$) where the plasticising effect of the penetrant ethylene is negligible.

Peterlin[98] has studied the effects of cold-working and annealing processes on the transport properties of tetrachloro-ethylene in polyethylene. Cold-drawing of the polymer drastically reduced the value of D, but subsequent annealing at temperatures above 373K almost

restored it to its undrawn value. His results are in agreement with those of other workers[105,106] who were able to correlate the change in D on drawing and annealing with the change in the amorphous content of the polymer. The activation energies for gas diffusion in polyethylene and polypropylene were independent of the crystallinity and thermal history of the polymer.

PART D The Present Work.

During the plastics industry's search for increasingly efficient polymerisation catalysts, the recent patent literature has shown much interest in the use of supported Ziegler catalysts - particularly those having a magnesium compound as support[34]. The present work was carried out in view of the need for a physico-chemical study of such a system. Magnesia was chosen as the support material, partly because its surface characteristics had been extensively researched and also because it had been claimed to form an active supported catalyst[34].

Four basic investigations were undertaken:

a) The catalyst activation procedure was studied using micro-gravimetric, infrared spectroscopic and analytical techniques.

b) The polymerisation of ethylene and propylene on the catalyst surface was followed by the same techniques. The analysis of these results permitted the investigation of the kinetics of polymerisation.

c) The analysis of the kinetic experiments indicated the possibility of the diffusion control of the polymerisation rate.

In the absence of suitable data in the literature, the mass transfer properties of ethylene and propylene in their respective polymers were studied.

d) An initial infrared spectroscopic survey of the suitability of rutile (TiO_2) for use as a Ziegler catalyst support was made.

The basic aims of the work were to examine the types of surface species present at various stages of the activation and polymerisation reactions and to elucidate the role of these species in the overall reaction mechanism.

CHAPTER 2. EXPERIMENTAL.

PART A. Apparatus.

2.A.1) General description.

A high-vacuum system constructed in Pyrex glass was used. The apparatus was evacuated via an electrically heated mercury diffusion pump backed by a Speedivac oil rotary pump. Dynamic vacua of 2×10^{-6} kN.m^{-2} were consistently obtained, and measured by means of a Penning gauge. A schematic diagram of the system is shown in figure (2.1). Mercury vapour was excluded from the system by the use of liquid nitrogen traps T_1 and T_2. The apparatus was maintained free of grease by using grease-free valves (Youngs', Acton.) in place of the conventional greased taps. This precaution was necessary to prevent reaction of the catalyst components ($TiCl_4$ and $Al(C_2H_5)_3$) with the stopcock grease and also to prevent contamination of oxide samples, arising from grease vapour[107].

Gas phase pressures were measured using a mercury manometer and a glass spiral gauge. The spiral gauge proved cumbersome in use and was later replaced by a transducer gauge calibrated between 0.2 and 60.0 kN.m^{-2}. A bulb of known volume was used for volume calibration of the system.

2.A.2) Studies using infrared spectroscopy.

i) The infrared spectroscopy cell. The cell was of Pyrex

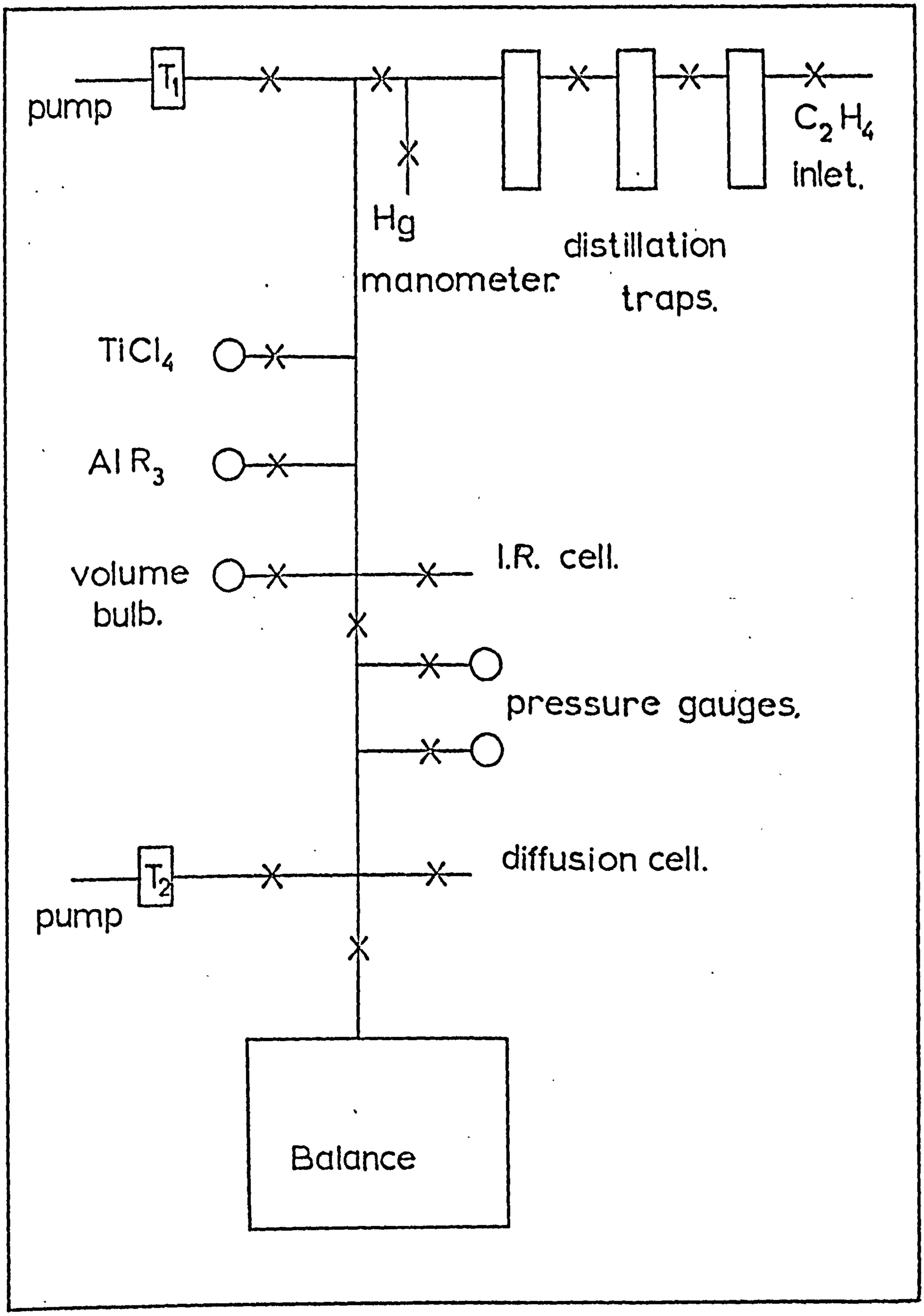

Figure 2.1 Schematic representation of the vacuum system.

construction with fluorite (5 cm. diameter) windows. The windows were cemented to ground glass flanges using M-V No. 38 brick-red enamel (A.E.I. Ltd.). The adhesive was allowed to dry overnight at room temperature and then cured for twenty-four hours at 383 K. The oxide disc sample was supported in a pyrex holder and secured with a stainless steel cover slip. Pyrex rails, running the length of the cell, enabled the sample holder to be moved along the cell by means of an external magnet. In this fashion the sample could be moved from the heating region to the recording position between the fluorite windows. Heating was by means of an external electric furnace, the temperature being controlled at temperatures up to 723 ($\pm$2) K by an ETHER 'DIGI' controller and measured using a chromel-alumel thermocouple. The cell could be isolated from the frame by means of two grease free taps, in series to ensure a good seal. To record a spectrum, the cell was isolated by means of these taps and then cut off the frame and removed to the spectrometer. After each spectrum had been recorded, the cell was glassblown back onto the vacuum system.

ii) <u>The infrared spectrometer</u>. Two instruments, a Perkin-Elmer 521 and a Perkin-Elmer 457, were used, subject to suitability, to record the infrared spectra. Both instruments were double beam, grating spectrometers and comparable results were obtained from both instruments although the resolution of the PE 521 was slightly higher than that of the PE 457. The higher source intensity of the PE 457 was useful in recording the spectra of samples having low transmittance.

The oxide discs were responsible for a high level of radiation scattering and attenuation of the spectrometer reference beam with an adjustable comb attenuator was necessary. To ensure that sufficient energy was received by the detector, wide slits had to be employed throughout the frequency range. The gain and balance control settings of the instrument were frequently checked and adjusted when necessary in order to ensure that spectra were recorded under optimum conditions. Scanning speeds employed were never greater than 100 cm^{-1}/min. and usually much slower in the region of the peak to be investigated. Facilities were available for flushing the sample-well of the spectrometer with dry nitrogen when spectra were being recorded. This technique did not lead to any marked improvement in the spectra and was not extensively used.

2.A.3) <u>The Diffusion Cell</u>.

The cell, shown in figure (2.2), was constructed of mild steel. The two hollow chambers were clamped together using six brass nuts and bolts. The polymer membrane was held between the chambers, supported on the low pressure side by a porous, stainless steel disc. Gas leaks around the edge of the membrane were eliminated by use of a polyethylene gasket on each side of the film. After assembly, the exterior of the cell was coated with a vinyl spray (Seal-Cote, Jencons Ltd.). This eliminated rusting of the mild steel when immersed in a water thermostat, and reduced the possibility of an atmospheric leak into the system. Glass-metal seals were brazed

1). End-view.

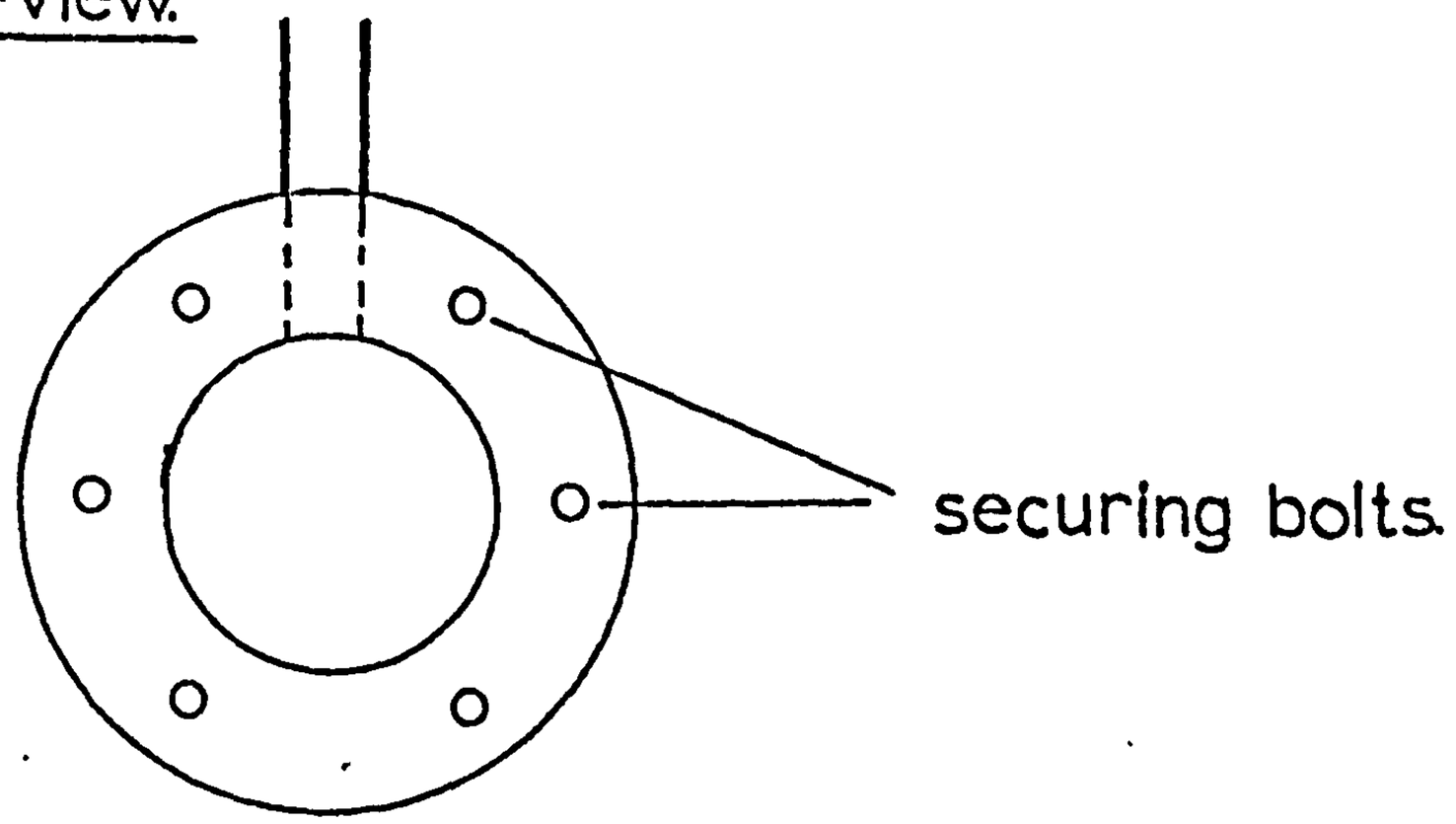

2). X-Section.

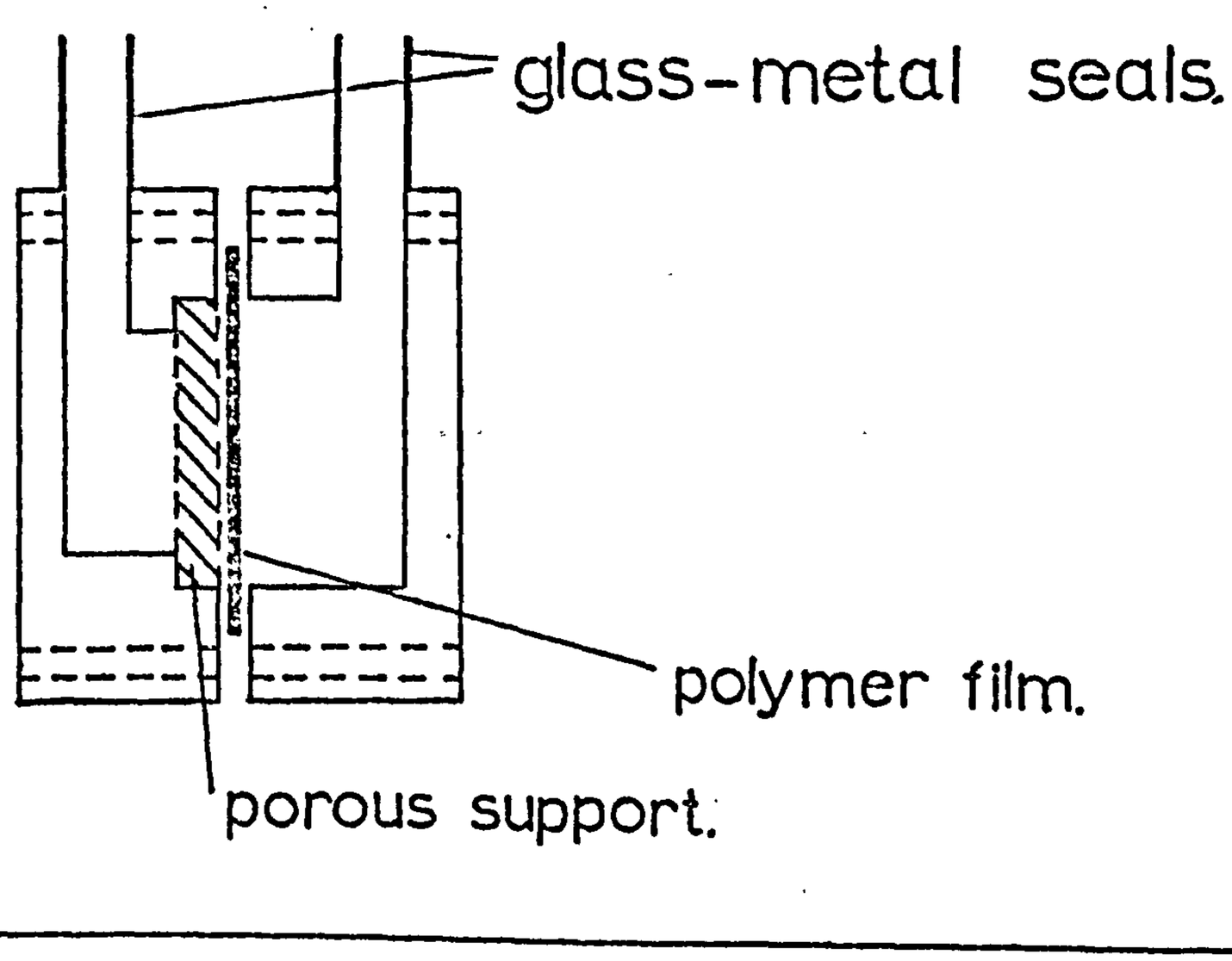

Figure 2.2. The diffusion cell.

directly onto the mild steel and the cell was glass blown onto the vacuum system. The low pressure side of the cell (including a Mc.Leod gauge to measure the pressure) was volume calibrated by gas expansion from the known volume of the Mc.Leod gauge (volume = 66.7 cc.; diameter = 3 mm.). The mean of three separate determinations gave 153 cc. for the volume of the low pressure side.

2.A.4) The Vacuum Microbalance.

i) Structural considerations. A beam balance has a high sensitivity if a small weight change on one of the weight pans causes a large deflection of the beam. To investigate the factors which affect the sensitivity of a balance, suppose a weight (W_1) is placed

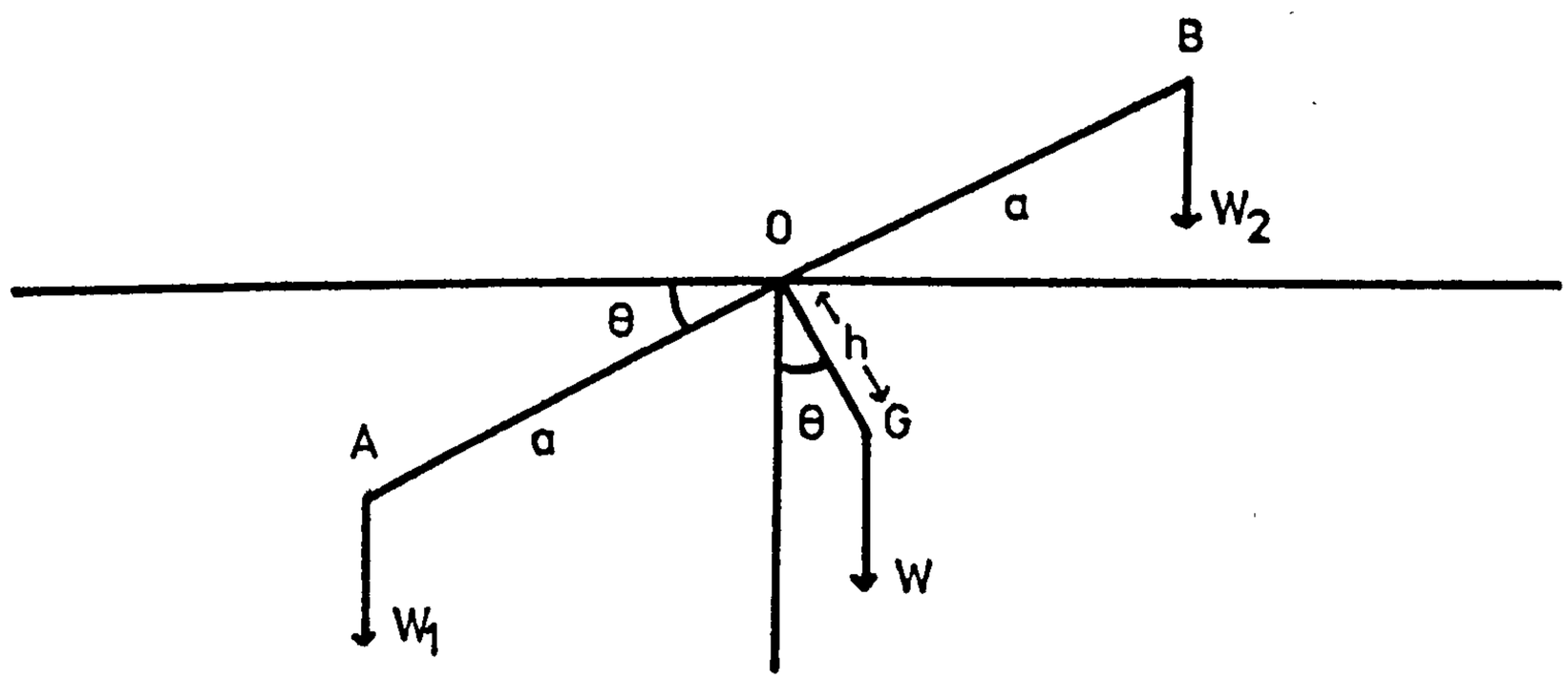

Figure 2.3. Schematic diagram of the beam balance.

on the left scale pan and a slightly smaller weight (W_2) is placed on the right scale pan (figure 2.3). The beam AOB, pivoted about O,

will then be inclined at angle Θ to the horizontal. The weight of the beam (W) acts at G, a distance h below O.

If AO = OB = a, then taking moments about O:-

$$W_1 \, a \cos\theta = W \, h \sin\theta + W_2 \, a \cos\theta$$

$$\therefore \quad \tan\theta = \frac{(W_1 - W_2)a}{Wh}$$

Thus for a given weight difference between the scale pans $(W_1 - W_2)$, θ is directly dependent on a, and varies inversely with W and h. In theory then, a sensitive beam balance must be light, have long arms and its centre of gravity must be very close to the fulcrum. In practice a compromise must be made between beam lightness and rigidity, and also between beam length and the associated period of oscillation.

If the suspension points of the scale pans and the pivot of the beam are in the same plane, then the balance sensitivity does not vary with load. However, if the scale pan pivots lie above or below the beam pivot, then sensitivity becomes load dependent. A full discussion of these pivots has been presented by Rhodin[108] and Gulbransen[109].

ii) Construction. The balance, of the beam type, was constructed in the Glass Workshop of Nottingham University Chemistry Department (figure 2.4). A similar instrument has been described in the literature[110]. As far as practicable, the balance was constructed in Pyrex to minimise the corrosive action of the vapours used in the course of this project. The beam, 26 cm. in length, was made from Pyrex tubing (o.d. 5 mm). Agate knife edges were attached at the centre and at each end of the beam using Araldite cement. The beam was shaped so that all three knife edges

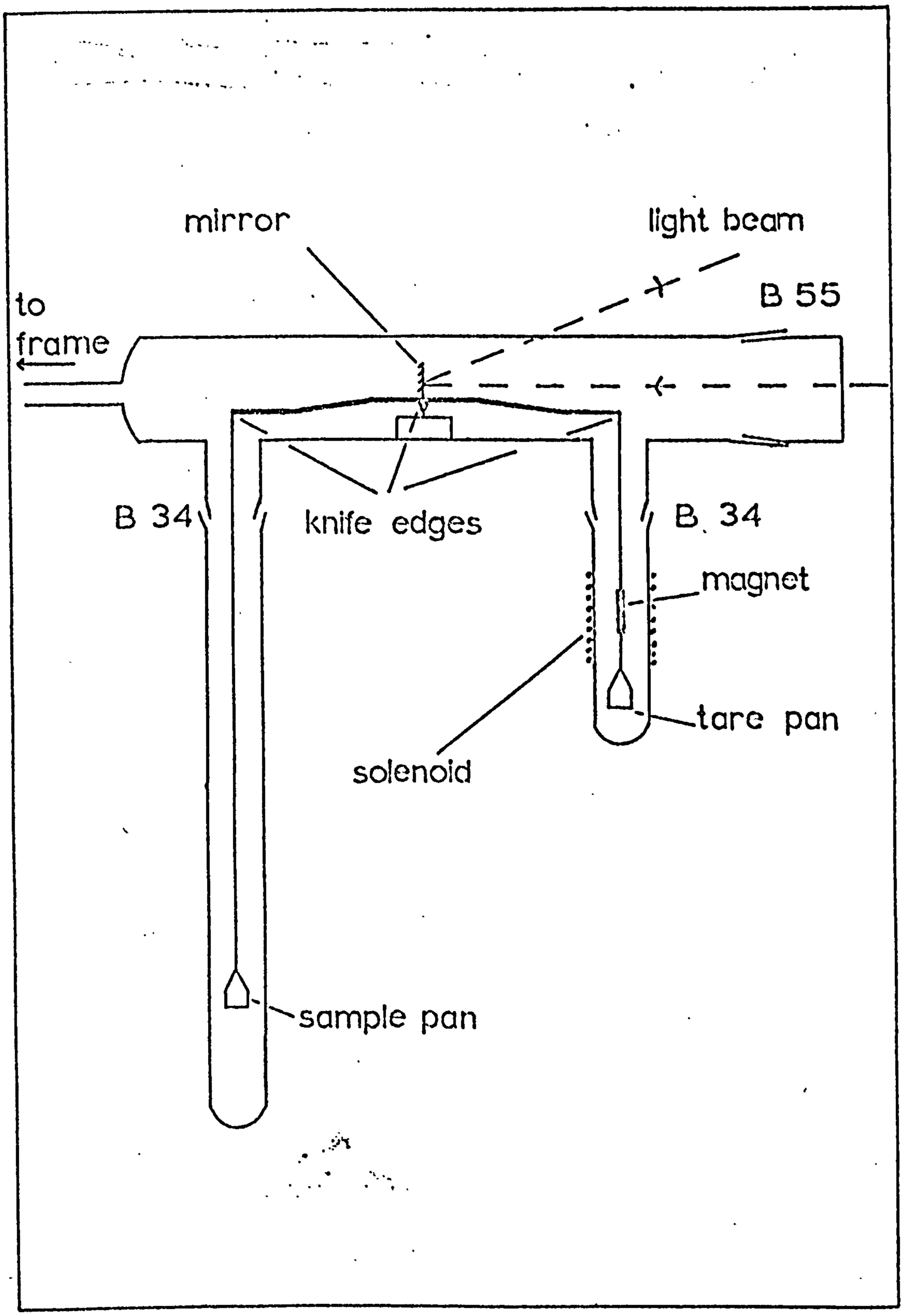

Figure 2.4. The vacuum microbalance.

lay in one plane, ensuring that the balance sensitivity was load independent. The sample pan (Pyrex, 2 cm. diameter) was suspended by means of a Pyrex fibre, 70 cm. long. A glass encased permanent magnet suspended in a solenoid field by a Pyrex fibre (10 cm. long) provided the balancing force. To eliminate hysteresis effects, the magnet was made from Alnico, having a square hysteresis loop. A glass bucket was suspended beneath the magnet, providing a means for taring the balance using Pyrex beads. The solenoid, 9 cm. in length and 4.5 cm. in diameter, consisted of approximately 2500 turns of 30 S.W.G. copper wire, having a resistance of 90 ohms. The electrical circuit used in the balancing operation is shown in figure (2.5). Power was supplied by an eighteen volt stabilised D.C. supply unit and the current could be continuously varied up to a maximum of 200 ma. by means of the variable resistance (R_v). The current

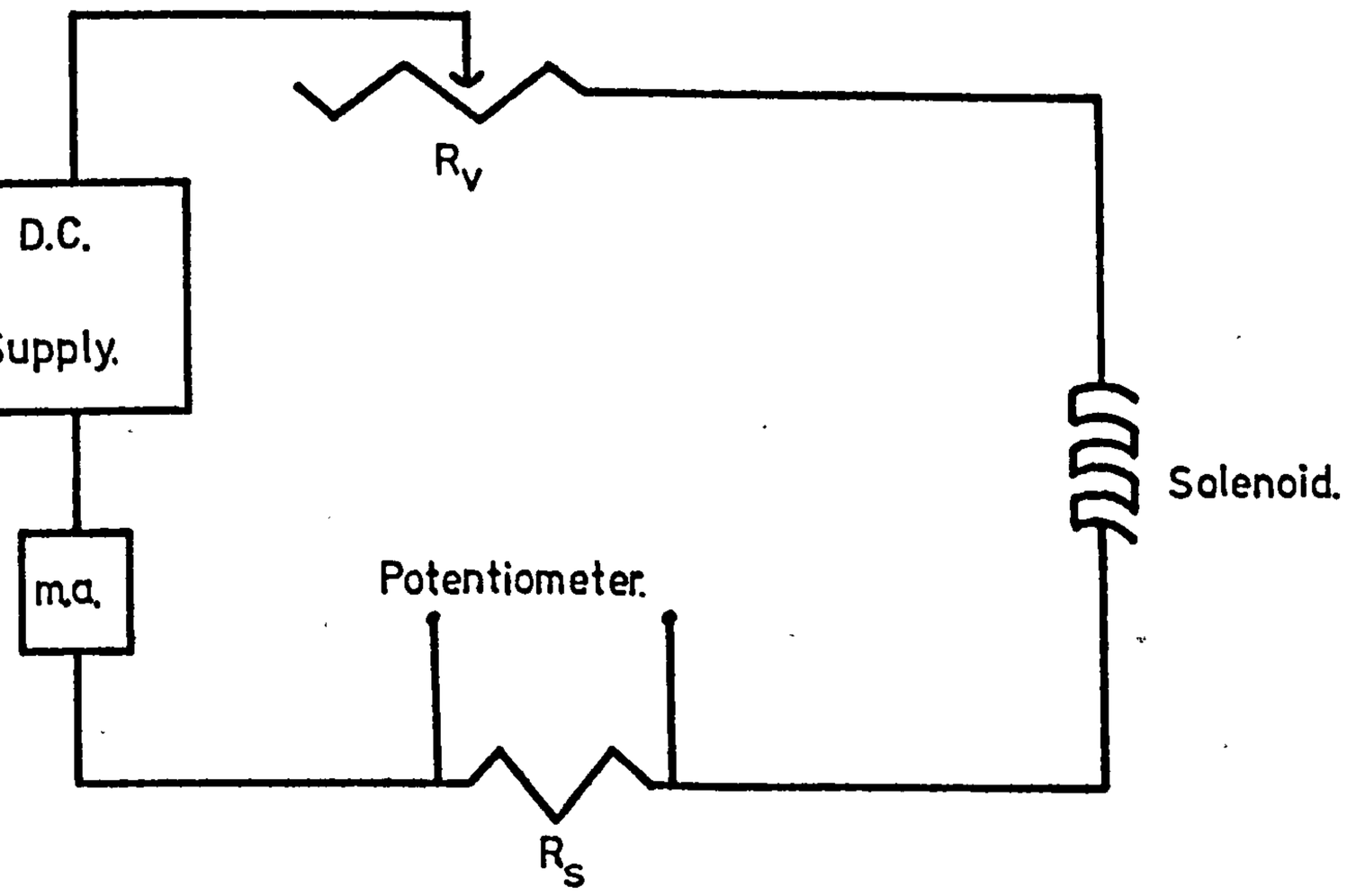

Figure 2.5. The balancing circuit.

flowing was indicated on a milliameter and accurately measured via the potential drop across a standard resistance (R_s = 15 ohm., temp. coeff. = 0.01% per degree). A calibration was made of sample weight against the current required to balance the beam. Imbalance was detected by an optical method. A light beam, entering and leaving the balance case through optically flat windows, was reflected from a small circular mirror attached by Araldite cement to the centre of the balance beam. The reflected light was directed onto a pair of matched photo-electric cells (Evans Electroselenium, Ltd.) connected in opposition. In the balanced position, zero deflection of a galvanometer connected directly to the photo-electric cells was observed. A slight displacement of the balance beam gave rise to a deflection of the galvanometer light. The imbalance could then be corrected by adjustment of the solenoid current to restore the galvanometer light to the null position. The sensitivity of such a detection system depends directly upon the length of the optical lever and the intensity of the light falling on the photo-electric cells. After much experimentation a compromise between these two parameters was adopted, the optical lever having a length of 110 cm. folded between two plane mirrors. Picein wax, chemically inert and possessing a very low vapour pressure was used to seal the balance 'Quick-fit' joints (one B55 and two B34 joints). The balance was enclosed in a wooden box lined with Jabolite. This protected the photo-electric cells from the effects of daylight and also restricted temperature change in the balance case to an acceptably low value. The sample hangdown tube projected through a hole in the base of the box, allowing

the use of an external furnace for degassing oxide samples. Furnace temperature was controlled by an Ether 'Digi' controller and measured by means of a chromel-alumel thermocouple inserted into a glass pocket in the hangdown tube. Interference with the balance from external vibrations was reduced by mounting the micro-balance assembly on a rigid metal frame and standing it on a sheet of slate (4 cm. thick).

iii) Calibration and Sensitivity. The balance was calibrated using standard weights (Cahn calibration weights; 1-200 mg. range). The linear relationship between weight (M) and balancing current (I) is illustrated in figure (2.6). To check the reproducibility, three initial calibrations were carried out, the balance being dismantled and reassembled in between each one. The slope of these plots varied by less than 0.5%. No hysteresis was observed as weights were removed from the balance. This calibration was checked periodically during the course of this project and no significant drift in the value of the gradient was observed. Figure (2.6) indicates that 2.98 mg. of excess weight require 1.0 ma. to restore balance. All calibrations were carried out in air. The effect of buoyancy on the balance reading was investigated by measuring the current required to balance a given excess weight at different pressures of dry nitrogen gas. At a nitrogen pressure of 9.3×10^{1} $kN.m^{-2}$ the buoyancy correction was 1×10^{-4} gm. At pressures below 2.0×10^{1} $kN.m^{-2}$ it was found that no correction was necessary. All the experiments to be described were carried out in the region where buoyancy corrections were not required.

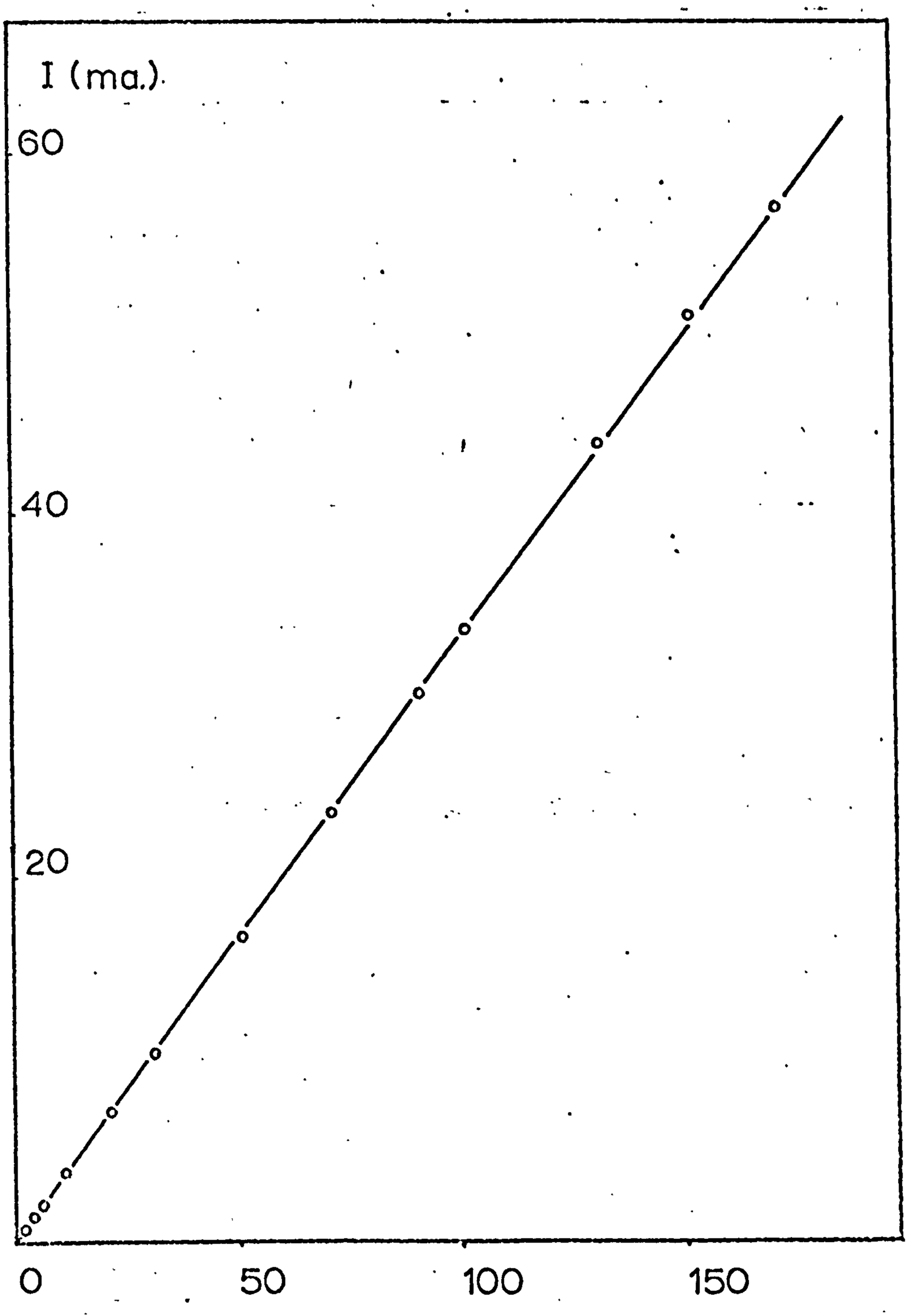

Figure 2.6. Calibration curve for the vacuum microbalance.

$$\frac{1}{\text{slope}} = 2.98 \text{ mg/ma.}$$

The practical range of the balance covered a weight change of 400 mg. with a maximum sample weight of 1 gm. (tared using Pyrex beads). The sensitivity of the instrument was estimated by determining the smallest detectable signal from the photo-electric detector circuit. This corresponded to a 1 cm. deflection on the galvanometer, which when zeroed, was equivalent to a change of approximately 7×10^{-3} ma. in the solenoid current. Using the calibration factor of 2.98 mg./ma., the smallest weight change measurable with the balance was 2×10^{-5} g. The stability of the balance zero was checked by zeroing the instrument and checking for drift of this reading with time. The maximum drift in any one 24 hour period was found to be equivalent to a weight change of 8×10^{-5} g. This was not considered to be significant when compared with the weight changes involved in the reactions investigated during the course of this project.

PART B. Materials.

2.B.1) Support materials.

i) Magnesium oxide. The preparation of high surface area active magnesia by thermal decomposition of the carbonate or hydroxide has been reported[75]. Four samples of magnesium oxide were considered:

a) Following the method of Anderson[76], magnesium hydroxide was prepared by hydrolysis of magnesium methylate. After vacuum calcination of the hydroxide at 673 K, an off-white sample of magnesium oxide was

obtained. The slight brown discolouration was attributed to a decomposition product of an organic contaminant, possibly residual magnesium methylate. B.E.T. measurements, using nitrogen gas at 77K (area/mol = 16.2 $Å^2$) gave the surface area as 250 m^2/g.

b) Thermal decomposition of reagent grade basic magnesium carbonate ($MgCO_3.Mg(OH)_2.3H_2O$) in vacuo at 673 K yielded white magnesium oxide. Infrared spectroscopy revealed the presence of absorption bands (1200–1700 cm^{-1}) characteristic of residual carbonate species. The surface area of this material was found to be 310 m^2/g.

c) A high purity sample of magnesium oxide (Johnson Matthey Ltd., grade 2, batch B2296) revealed very weak absorptions in the carbonate region of its infrared spectrum. After evacuation at 673 K for twelve hours the surface area of this sample was 50 m^2/g.

d) Precipitation of magnesium hydroxide from an aqueous solution of magnesium nitrate by ammonium hydroxide, followed by thermal activation of the precipitate at 673 K in vacuo, yielded a white solid with very weak carbonate infrared bands and a surface area of almost 180 m^2/g.

Each of these four samples formed the basis for an active supported polymerisation catalyst, although the polymerisation conditions did not allow for a quantitative comparison of the catalyst activities. However, sample (d), in view of its low surface contamination combined with a high surface area, was chosen as the most suitable support material. Accordingly, a master batch of magnesium hydroxide wasprepared following the method outlined by Malinowski[111]. Stringent precautions were taken to exclude contaminants. All the

water used in the preparation was doubly-deionised and triply distilled from alkaline potassium permanganate. Glassware was cleaned with a 1% HF solution and thoroughly rinsed with clean water. Ammonia gas was distilled over metallic sodium and passed into an aqueous solution of magnesium nitrate ($Mg(NO_3)_2.6H_2O$; A.R. grade). The resulting fine, white precipitate of magnesium hydroxide was separated by centrifugation, and thoroughly washed with cold water. After drying in an oven at 393 K the material was ground using an agate mortar and pestle. The surface area was determined by the conventional B.E.T. method (77 K, N_2 gas, area/molecule = 16.2 $\mathring{A}^2$) to be 176 ($\pm$7) m^2/g. Since the basic magnesium surface reacts chemically with atmospheric carbon dioxide, the support material was kept in a screw-top jar and unnecessary contact with the atmosphere was avoided. This carrier material is subsequently referred to as 'Carrier E'.

ii) Rutile. A sample of titanium dioxide (rutile) was kindly supplied by Dr. C. H. Rochester, Nottingham University Chemistry Department. This material (sample no. CL/D428) had been subjected to four cycles of alternate sohxlet extraction with boiling water and heating in air at 673 K to lower the chloride fraction. The surface area was 24 m^2/g.

2.B.2) Chemical reagents.

i) Titanium tetrachloride - obtained from B.D.H. Ltd., in 100 g sealed glass ampoules (98.5%). The light brown liquid was distilled

under vacuo in dry glass apparatus. The first and last thirds of the distillate were rejected and the middle-fraction collected as a clear liquid. (B.pt. 409K at 10^2 kN.m^{-2}). The purified material was stored in an inverted pear-shaped flask, sealed by a teflon valve and protected from any adverse effects of daylight by a coating of black paint on the exterior of the flask.

ii) Aluminium tri-ethyl. This material, colourless when pure, was supplied in a steal container by Koch-Light Ltd., (90-95%). It is a very hazardous chemical to work with, igniting spontaneously when exposed to oxygen in the atmosphere and exploding when mixed with water. The following safety precautions were found to be effective in handling aluminium tri-ethyl:

a) The compound was maintained under an inert atmosphere (N_2 or He gas) and all apparatus used for containing or processing was scrupulously dried and flushed with dry nitrogen gas.

b) Protective clothing(laboratory coat, goggles, face-shield and rubber gloves) was worn whenever the material was handled.

c) A dry powder fire extinguisher (Pyrene) was always available.

d) All apparatus which had been used for $Al(C_2H_5)_3$ was rinsed with a 50:50 (V:V) mixture of concentrated hydrochloric acid and methanol to destroy residual traces of the compound.

e) All purification operations were carried out in a fume cupboard, the floor of which was lined with a commercial fire powder (a mixture of vermiculite and Na_2CO_3).

An initial attempt to transfer some of the $Al(C_2H_5)_3$ from its steel container to a distillation apparatus using a positive nitrogen

pressure to force out the liquid was unsuccessful due to leakage around the container head. Subsequent transfers were made by use of a glass syringe with a 15 cm. stainless steel needle. It was not convenient to handle samples greater than 15 ml. volume. The liquid was distilled in glass apparatus under a reduced pressure of nitrogen. Pure material was collected as a colourless liquid (B.pt. 341K at 0.40 $kN.m.^{-2}$)[112] in an inverted pear-shaped glass flask and sealed by a teflon valve. After joining to the main vacuum system, the liquid was carefully degassed by means of four freeze-thaw cycles using liquid nitrogen as coolant. The containing flask was covered with a protecting layer of P.V.C. tape.

iii) Deuterium Oxide D_2O (Koch-Light Ltd.; 99.7%), after degassing was used as supplied.

iv) Hydrogen chloride. Dry HCl gas was prepared by the action of concentrated sulphuric acid on sodium chloride (A.R. grade).

v) Silicon tetrachloride. Supplied in a sealed glass ampoule (B.D.H. Ltd. 98%) and used without further purification.

2.B.3) Olefin monomers.

1) Ethylene. Supplied in a lecture cylinder by B.D.H. Ltd., (99.8%). The cylinder was connected to the vacuum system using nylon tubing. Immediately before use, ethylene gas was purified by freezing

at 77K and pumping for thirty minutes, followed by two trap to trap distillations from an n-pentane slush bath (142K). The middle third was collected in each distillation. Mass spectrometric analysis of the purified monomer did not detect oxygen or water impurities.

ii) Propylene. Supplied by B.D.H. Ltd., (99%). Purification details were as for ethylene except that the slush bath for distillation was methanol (175K).

2.B.4) Polymer Samples for Diffusion Studies.

i) Marlex polyethylene. This material, produced using a chromium oxide catalyst, was kindly supplied by Dr. Cundall, Nottingham University Chemistry Department, (density = 0.954).

ii) Anti-oxidant free polyethylene. Manufactured by a conventional Ziegler process, this sample was supplied by Dr. A.N. Roper, Shell Carrington, Manchester. It was specially prepared without added anti-oxidants. (density = 0.918 g/cc.).

iii) Polypropylene. A sample of isotactic polypropylene, made by the Ziegler process (I.C.I., Welwyn, Ltd.) was kindly supplied by Mr. D. Reynolds, Nottingham University Chemistry Department. The high purity of this material was indicated by an exceptionally low phosphorescence spectrum.

PART C Experimental Technique.

2.C.1) Studies on the microbalance.

i) Preparation of the magnesium oxide support. Each sample of magnesium oxide was prepared in situ by calcination of magnesium hydroxide. Sufficient hydroxide (about 73 mg.) was used to give an oxide sample of 50 mg. The sample was loaded onto the microbalance and the balance case sealed using Picein wax. After recordingthe zero, the balance case was carefully evacuated and the sample pumped to constant weight. Using an external furnace, the magnesium hydroxide was heated to 548K. Decomposition to the oxide occurred at this temperature (reaction 2.1) accompanied by a structure change from the hexagonal hydroxide lattice to the cubic structure of magnesium oxide.

$$Mg(OH)_2 \xrightarrow{548K} MgO + H_2O \qquad (2.1)$$

Too fast a heating rate in the region of 548K led to spluttering of the sample powder, caused by the explosive expulsion of water vapour. When decomposition was complete, the temperature was raised to 673K and the magnesium oxide degassed for between 14 and 18 h. The sample was cooled to 308K and the weight loss associated with the calcination was recorded.

ii) Reaction of $TiCl_4$ with the support surface. A small amount of freshly distilled $TiCl_4$ was thermostatted (308K) and its vapour allowed to react with the magnesium oxide surface for three minutes.

Excess reactant was removed by pumping, and the sample was evacuated to constant weight. Initially it was not found possible to reproduce the weight change associated with this reaction. $TiCl_4$ reacted with the surface hydroxyls of the oxide and the irreproducibility was attributed to variations in the surface hydroxyl concentration. This concentration was most likely a function of the vacuum achieved in the immediate vicinity of the oxide surface during calcination. Accordingly the pumping system was redesigned to place a diffusion pump closer to the microbalance and to reduce the number of obstructions (bends, taps etc.) in the pumping line. Subsequently it was found possible to reproduce the weight gain to within 5% when the oxide was reacted with $TiCl_4$. An analytical technique to determine the amount of Ti on the oxide surface was developed (section 2.C.3).

iii) Reaction with $Al(C_2H_5)_3$. The titanium modified surface of the oxide was allowed to react with $Al(C_2H_5)_3$ vapour at 308K. The vapour pressure of $Al(C_2H_5)_3$ at this temperature is of the order of 1.3×10^{-3} $kN.m^{-2}$. To facilitate evaporation of the dimeric metal alkyl species from the liquid surface, a magnetic stirring device was employed to agitate the organometal. An exposure time of 30 minutes followed by evacuation for 15 minutes was adopted as standard procedure.

iv) Gas-phase polymerisation of C_2H_4 and C_3H_6. Freshly distilled olefin monomer was admitted to the balance and the increase in weight due to polymerisation on the supported catalyst surface was followed as a function of time. The change in monomer pressure during the course of the polymerisation was recorded via the pressure transducer

gauge. During the initial runs the overall fall in pressure was of the order of 10-15%. In later runs the incorporation of a large 'dead' volume (7 litre) in the polymerisation system reduced this pressure decrease to an acceptable level (4%).

Throughout these early runs the polymerisation rate was found to be completely irreproducible. After each run, the sample pan and the glass surround were heated in air to 823K to burn-off the thin layer of polymer formed on the glass under polymerisation conditions. This obviated the deposition of carbonaceous decomposition products on the magnesium oxide surface during the calcination procedure of the next polymerisation experiment. Over the course of ten identical polymerisation experiments the catalyst activity gradually diminished and finally vanished, even though the catalyst activation steps were apparently unaffected. An exhaustive investigation was made of this phenomenon.

The entire vacuum system was systematically tested for atmospheric leaks using the Penning gauge and a high tension tesla coil as indicators. The number of greasefree, teflon valves was reduced as far as possible and all of the residual taps were renewed. The Picein wax joints of the microbalance case, showing signs of deterioration after repeated exposure to the catalyst components, were remade. Such precautions did not result in the restoration of catalyst activity.

The monomer was purified by four trap to trap distillations before exposure to the catalyst surface. Mass spectrometry again failed to reveal the presence of any impurities in the purified gas.

The stock samples of $TiCl_4$ and $Al(C_2H_5)_3$ were replaced by freshly distilled materials. Variation of the exposure times of both catalyst components to the support surface failed to restore the catalyst activity.

During the course of catalyst activation, the component vapours also reacted with the surface of the Pyrex apparatus. Subsequent exposure to olefin monomer resulted in the formation of a thin film of polymer over the apparatus. After a number of polymerisation experiments the collective effect of this side-reaction was the formation of a substantial layer of extraneous material covering the glass surfaces of the reaction system. This material was clearly visible to the naked eye. It was removed by dismantling the balance assembly and 'scouring' the affected surfaces with a mildly abrasive paste ($NaHCO_3/H_2O$). Subsequent annealing (823K) in air, followed by a soaking in hot chromic acid (excepting the balance beam which, having Araldite joints, was vulnerable to heat and strong acid), revealed a 'clean' glass surface. On reassembling the apparatus it was found that catalyst activity had been restored.

The inhibiting influence of this polymer film was attributed to the sorption of catalyst poisons (oxygen, moisture) while the balance was open to the atmosphere between experiments. Gradual release of such poisons throughout the activation procedure would lead to a reduction in the ultimate polymerisation activity of the catalyst. This inherent irreproducibility of the polymerisation rate necessitated the use of split-temperature and split-pressure techniques for kinetic investigations. About ten such runs were possible before the catalyst activity fell to an unacceptably low level. Then the balance assembly was again treated in the manner described above.

In studying the temperature and pressure dependencies of the polymerisation rate, the points were taken in random order to average out the effects of systematic errors. The effect of hydrogen, oxygen and deuterium oxide on the ethylene polymerisation rate was investigated.

In an established polymerisation, the monomer was withdrawn into a cold trap (77K) and allowed to mix with gaseous hydrogen to form a 5% v/v mixture. This mixture was then readmitted to the active catalyst. Treatment with O_2 and D_2O involved withdrawing the monomer and treating the active catalyst with the additive for 3 minutes. Excess additive was removed by pumping before the monomer was restored to the system.

2.C.2) Infrared studies.

i) Magnesium oxide. The powder (~100 mg.) was compressed at (3.8×10^5 kN.m^{-2}) in an evacuated (0.40 kN.m^{-2}) stainless steel die to form a self-supporting disc (diameter 2.54 cm.). Two such discs, clamped into the sample holder (section 2.A.2) were sealed inside the infrared spectroscopy cell. The cell was evacuated and the discs heated to 673K using an external furnace. After degassing (14-18 h.) at this temperature, the cell was cooled and an infrared spectrum of the oxide surface was recorded (at the temperature of the infrared beam, ~ 320K). The oxide was not transparent to infrared radiation below 1000 cm^{-1}. Interpretation of spectra in the region 1200-1600 cm^{-1} was complicated by the presence of a small surface concentration of a carbonate species[80]. Following the procedure outlined in section (2.C.1), the magnesium oxide disc was allowed to react with $TiCl_4$ and $Al(C_2H_5)_3$ vapours. After each activation step an infrared spectrum was recorded. Ethylene and propylene polymerisation on the activated catalyst surface was followed spectroscopically. To assist with the characterisation of the surface reactions of MgO, the behaviour of $SiCl_4$, HCl and D_2O vapours at the

oxide surface was studied. Complete oxchange of tho surface hydroxyl groups of magnesia was achieved by heating the discs with D_2O vapour at 523K and evacuating at 673K. A reversed activation procedure, in which $Al(C_2H_5)_3$ was dosed onto the oxide surface before tho $TiCl_4$, was also carried out.

ii) Rutile. Sample discs (2.54 cm. diameter; 150 mg.) were pressed at 1.3×10^5 $kN.m^{-2}$. Tissue paper circles were used to prevent the oxide powder adhering to the stainless steel die. On heating (673K) the discs turned greyish in colour, characteristic of a reduced rutile surface. An oxygen-wash treatment (13 $kN.m^{-2}$; 30 mins; 673K) removed this discolouration. The dehydrated discs were then rehydrated with water vapour (298K; 20 mins.) and evacuated for 15 h. at 493K. Infrared spectra of the rehydrated oxide surface, the catalyst formation steps and the polymerisations of ethylene and propylene were recorded.

2.C.3) Analytical techniques.

i) Titanium analysis. With an acidic titanium (IV) solution, hydrogen peroxide produces a yellow colour, the intensity of which (up to 400 ppm. Ti) is proportional to the titanium concentration. The coloured species has been identified as $Ti(H_2O_2)_4^{4+}$ and the analysis of titanium is based on the colourimetric determination of this species. Following the method outlined by Vogel[113], standard titanium solutions were made up. Using a Unicam SP.800 ultra-violet spectrophotometer,

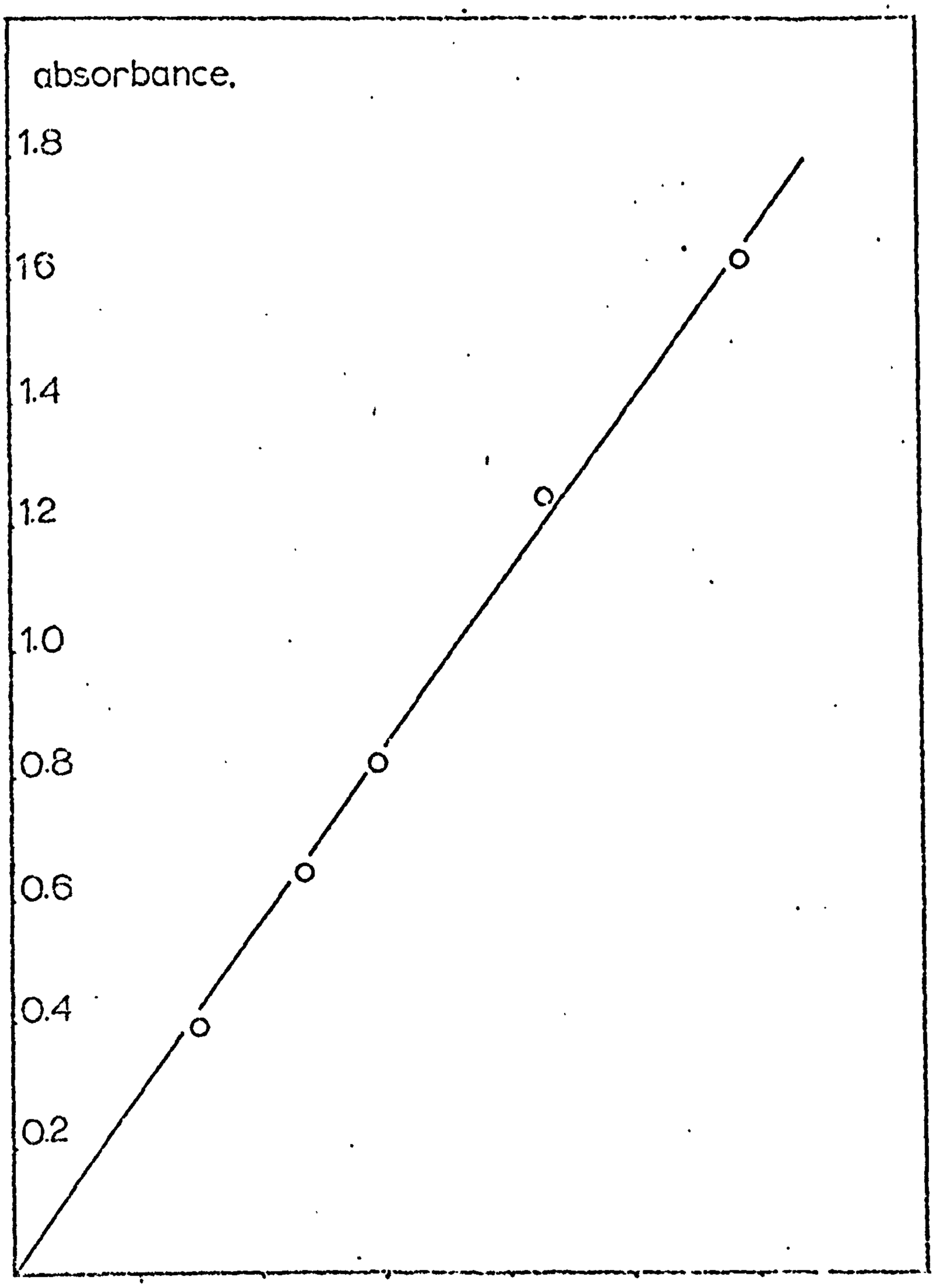

Figure 2.7. Colourimetric analysis of Titanium. Calibration of Ti^{4+} concentration against absorbance at 24000 cm^{-1}.

a calibration curve of titanium concentration (ppm) against absorbance (24000 cm^{-1}) was constructed (figure 2.7). No interference was detected from any of the other species in solution and distilled water was used in the reference cell. Titanium modified samples of magnesium oxide were prepared using the microbalance as described in section (2.C.1). Each sample was dissolved in concentrated sulphuric acid (3 ml.), 3% hydrogen peroxide (5 ml.)was added and made up to 50 ml. with deionised water (final acidity ∿ 2N). The absorptionsof the sample solutions were determined at 298K and their titanium concentrations read off the calibration plot. Sensitivity was one ppm. Ti, equivalent to .05 mg. Ti on a 50 mg. oxide sample.

ii) Aluminium analysis. A Southern-Analytical A3000 model flame absorption spectrophotometer was used to determine aluminium contents of catalyst samples. Aluminium analysis is complicated by the refractory nature of its oxide, which requires a high temperature flame to produce the necessary decomposition[114]. A nitrous oxide/ acetylene flame (∿3220K) was used and optimum response was obtained under the following conditions:-

Absorption line	3093 Å
Fuel	C_2H_2; 8.4 l/min.
Oxidant	N_2O; 8.0 l/min.
Burner height	4.5
Lamp current	18 ma.
Slit width	2

When usingthis flame, operating under explosive conditions, great care was taken to avoid the risk of an explosion when igniting and extinguishing

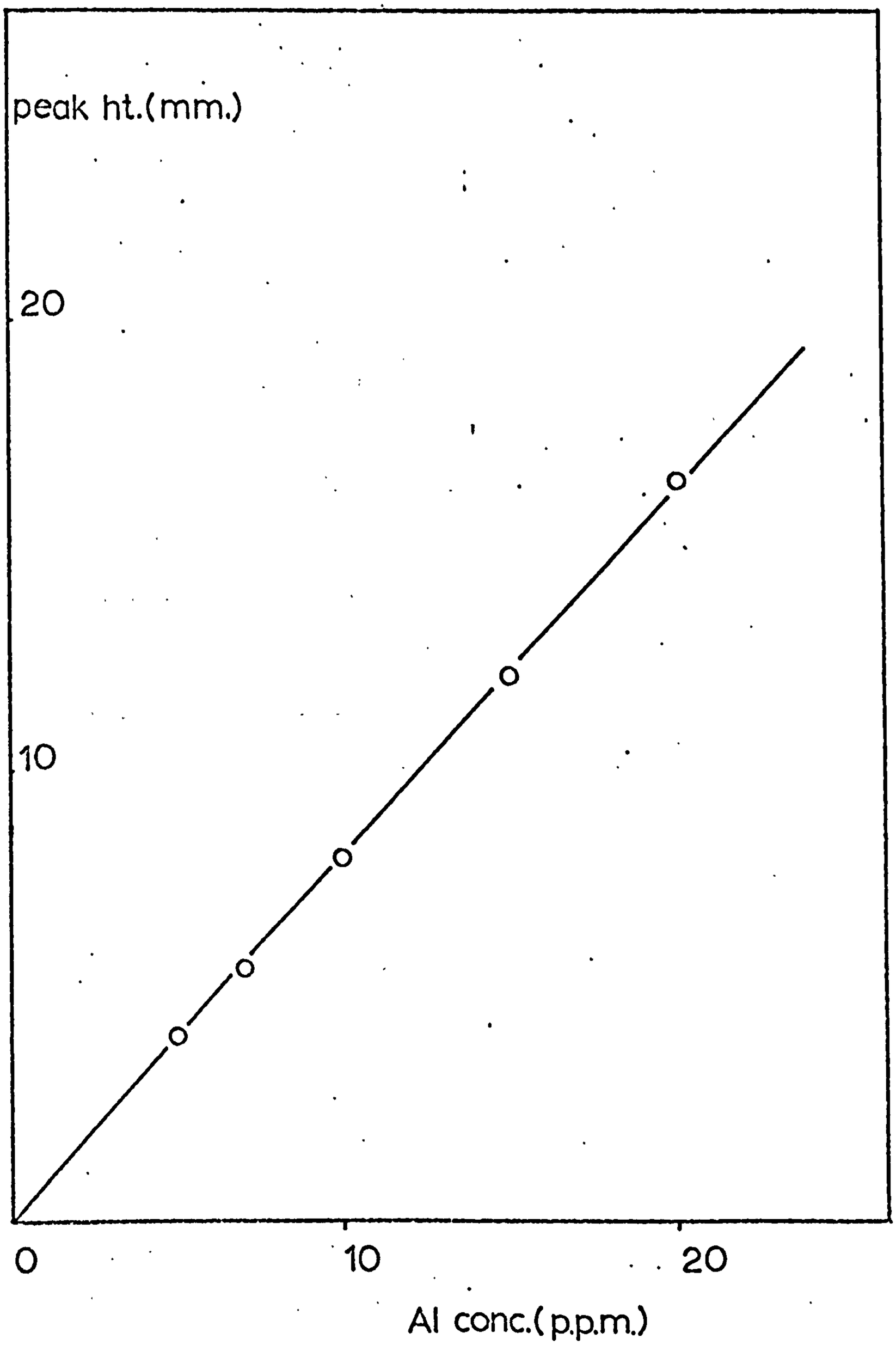

Figure 2.8. Analysis of Aluminium. Calibration curve for Al determination by Flame Absorption Spectroscopy.

the flame. The exciting light was supplied by a hollow aluminium cathode lamp (Activon Glass Products, Ltd.,). Initial tests revealed that, of the foreign species present in the standard and sample solutions, only potassium ions interfered, giving slight enhancement of the aluminium absorption peak. Accordingly both sets of solutions were matched for K^+ content (50 ppm.) using a standard KCl solution. Standard aluminium solutions (between 5–20 ppm.) were made up from $AlK(SO_4)_2 \cdot 12H_2O$ (A.R. grade). A linear calibration was obtained of aluminium concentration (ppm.) against absorption peak height. (figure 2.8). The sensitivity for 1% absorption was 3 ppm. Samples for analysis were prepared on the microbalance as follows:-

a) a control sample of MgO was treated with $Al(C_2H_5)_3$ vapour (section 2C.1), dissolved in concentrated sulphuric acid (3 ml.) and made up to 50 ml. with water,

b) two catalyst samples were prepared in the normal way (section 2C.1) and made up as above,

c) a catalyst sample was exposed to ethylene gas to confirm its polymerisation activity. It was then dissolved in hot concentrated sulphuric acid (3 ml.), diluted and filtered (to remove insoluble polymer) and made up to 50 ml. with water.

The aluminium content of these samples was determined from the calibration plot (detection sensitivity was equivalent to 0.10 mg Al on a MgO sample of 50 mg).

2.C.4) Catalyst solubility studies.

The solubility of catalyst samples in hot and cold, dilute and concentrated mineral acids were tested. Similar tests were applied to samples after ethylene polymerisation. Difficulties experienced in 'wetting' the surface of these samples were overcome by the use of a surface active agent (Sunlight Lemon Liquid). The preweighed samples, after suspension in acid solution (12h), were filtered, dried and reweighed to determine the weight loss. Removal of the polymer from the catalyst surface using boiling tetralin allowed the solubility of the catalyst residue in acid solution to be tested.

2.C.5) Scanning Electron Microscopy.

This investigation was hindered by the low surface conductivity of the polymer coated samples, even after the deposition of a gold surface film. However, micrographs of the fresh magnesium oxide surface and of polymerised samples, did allow for comparison of surface features.

2.C.6) Diffusion studies.

Polymer samples were supplied in pellet form (polyethylene) or as a powder (polypropylene). The films necessary for permeation measurements were made by compressing the virgin polymer between smooth aluminium plates at 433K. Pressure was applied via a torque wrench through a screw-press. After compression the plates were allowed to cool slowly

to room temperature before separating. It was found that uniform polymer films (between .05 and .15 mm. in thickness) were formed without the use of spacers between the plates. Film thickness was measured using a screw-gauge micrometer (accuracy ± .005 mm.). A circular disc (3.2 cm. diameter) was punched from the polymer film and inserted in the diffusion cell between two polyethylene gaskets. The cell was reassembled and glass-blown onto the vacuum system. After outgassing the polymer film overnight (1.3×10^{-4} kN.m^{-2}, 308K), a known pressure of olefin monomer was admitted to the high pressure side of the cell. The rate of permeation of the gas through the film was monitored by following the pressure increase on the low pressure side, using a Mc.Leod gauge. A volume calibration of the low pressure side was made by gas expansion from the known volume of the McLeod gauge.

CHAPTER 3. RESULTS.

PART A Results of infrared spectroscopic studies.

3.A.1) Magnesium Oxide as catalyst support (support E).

a) Activation of the magnesium oxide. The changes in the infrared spectrum of a self-supporting disc of calcined magnesia during catalyst activation in vacuo are shown in figure 3.1. The magnesia surface (trace a), freshly calcined for 14h. at 673K under vacuo, showed hydroxyl absorption bands at 3770 and 3640 cm^{-1}. Treatment with $TiCl_4$ vapour resulted in the replacement of these bands by a broad absorption at 3650 cm^{-1} and a shoulder at 3450 cm^{-1} (trace b). The action of $Al(C_2H_5)_3$ upon this titanium modified surface produced four bands in the (C-H) stretching region (2955, 2920, 2880 and 2860 cm^{-1}) but did not disturb the hydroxyl absorptions (trace c).

b) Polymerisation of ethylene gas on the activated catalyst disc. Magnesium discs activated at room temperature were active for ethylene polymerisation (figure 3.2). Traces b) and c) were recorded after 10 mins. and 2h. polymerisation respectively. The absorption peaks at 2920 and 2860 cm^{-1} increased in intensity as a function of the polymerisation time, while those at 2955 and 2880 cm^{-1} were gradually absorbed into the growing peaks as polymerisation progressed. Long polymerisation times (> 20h.) led to the coalescence of the growing peaks, giving an intense, broad band at 2900 cm^{-1}.

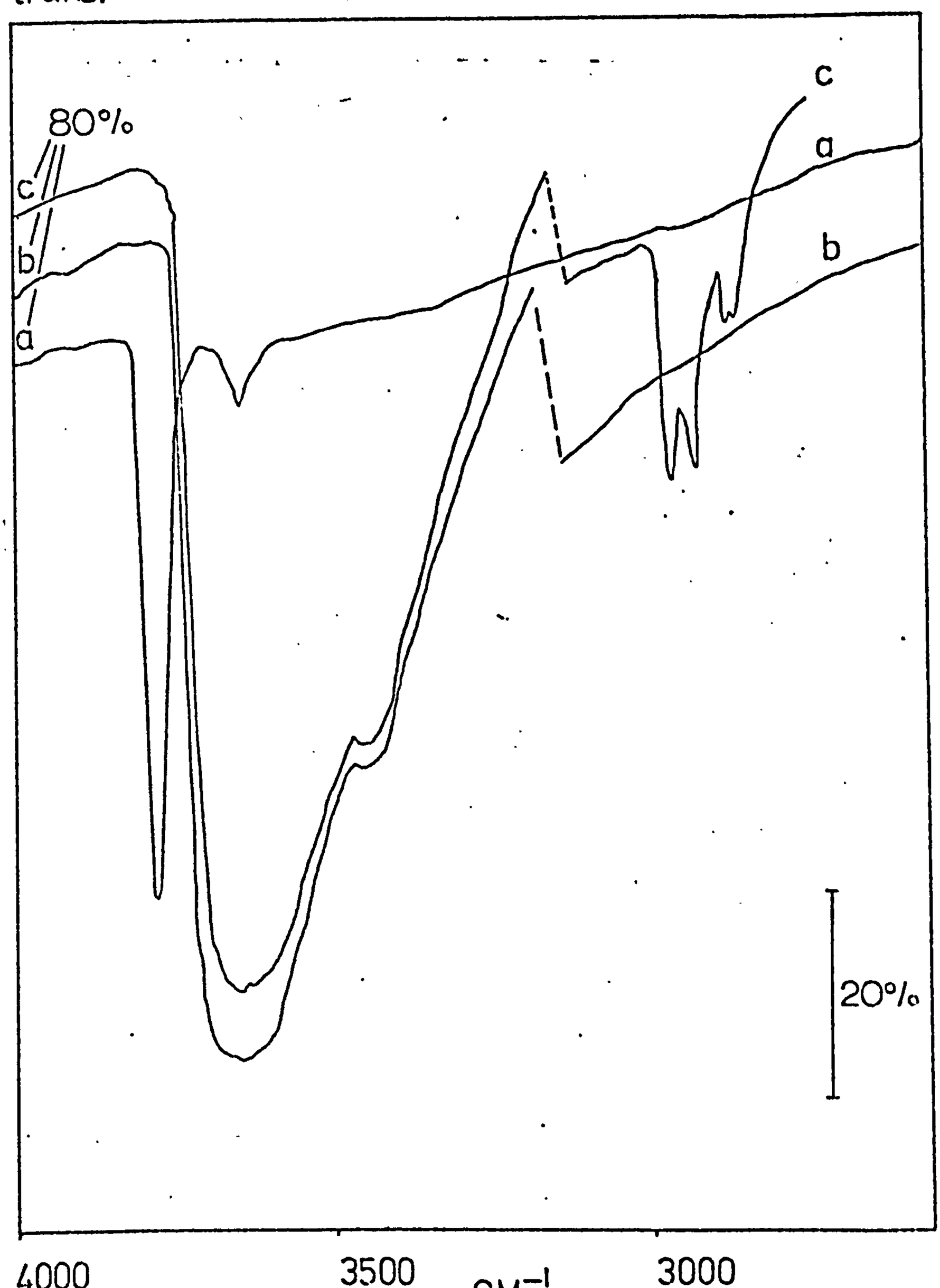

Figure 3.1. Infrared study of the preparation of the magnesia-supported Ziegler Catalyst. a) hydroxylated MgO; b) after $TiCl_4$ treatment; c) after $Al(C_2H_5)_3$ treatment.

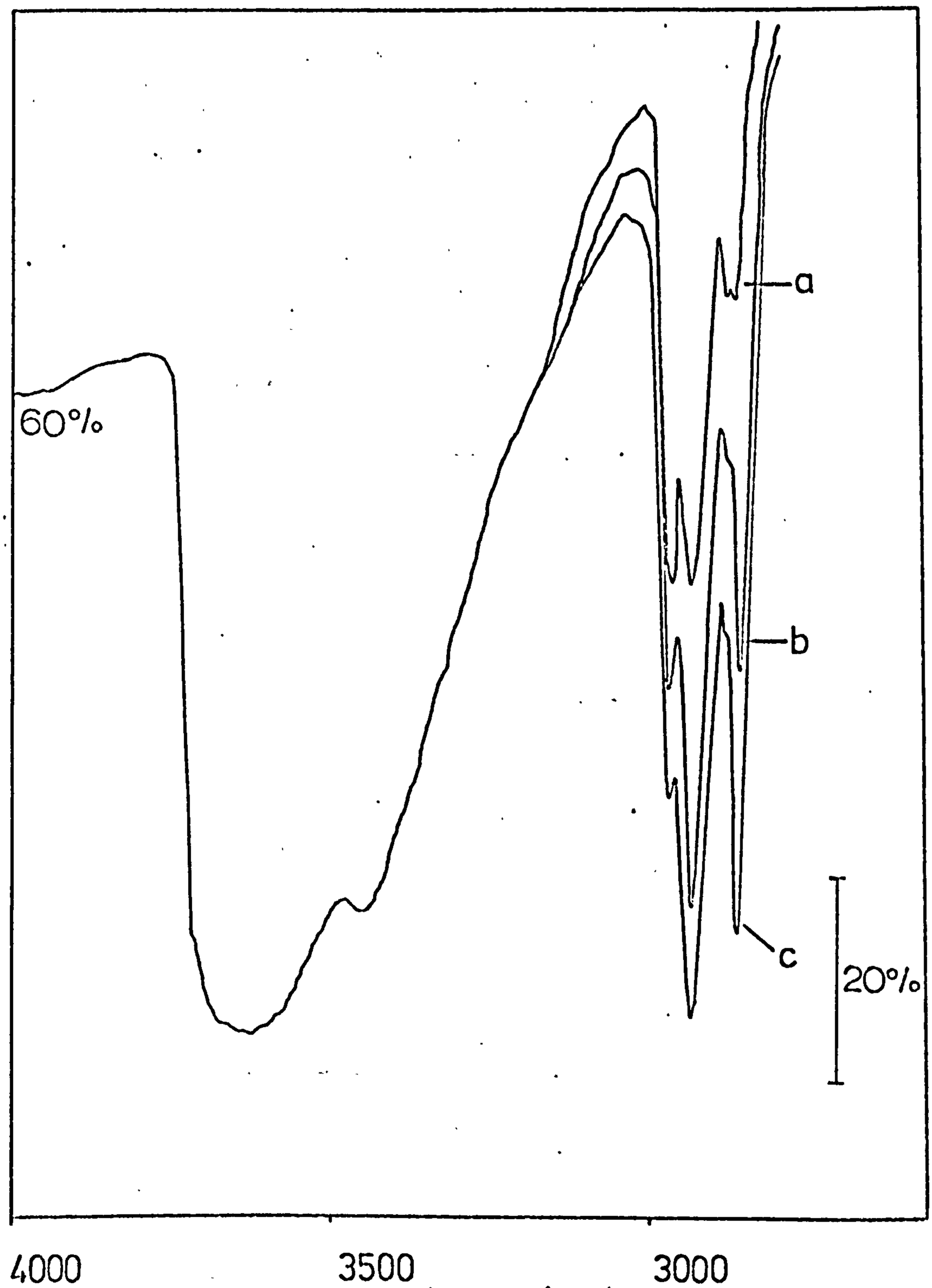

Figure 3.2. Ethylene polymerisation on a magnesia supported Ziegler catalyst. a) the catalyst surface; b) 10 mins. reaction; c) 2h. reaction. ($P_{C_2H_4}$ = 7.7 kN.m^{-2})

Figure 3.3. Propylene polymerisation on a magnesia supported Ziegler catalyst: a) the catalyst surface; b) 10 mins. reaction; c) 12 h. reaction. ($P_{C_3H_6}$ = 7.6 kN.m^{-2})

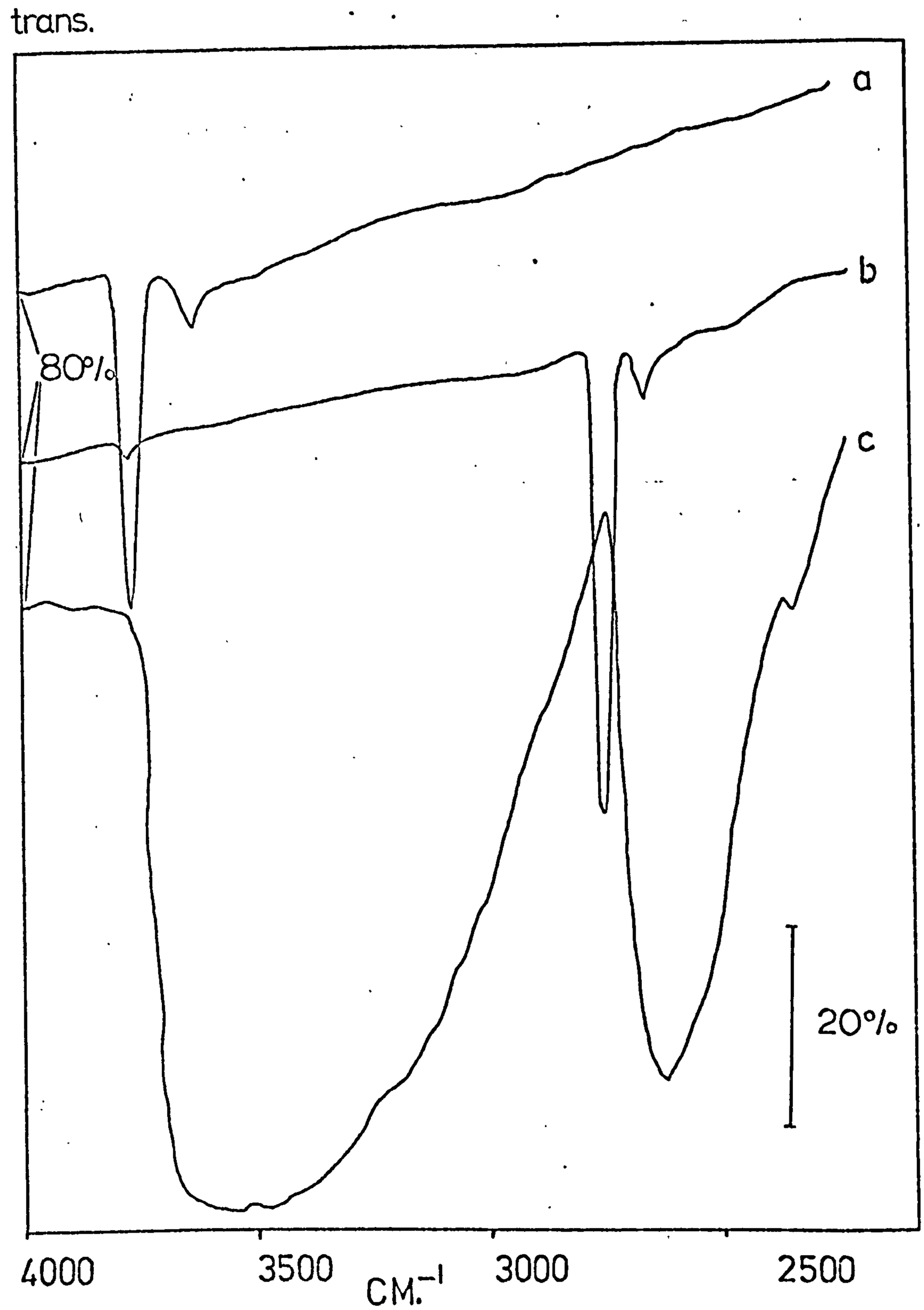

Figure 3.4. Exchange of the magnesia hydroxyl groups with D_2O. a) MgO surface after evacuation at 673K; b) after exchange with D_2O at 573K and evacuation at 673K; c) after treatment with HCl at room temperature.

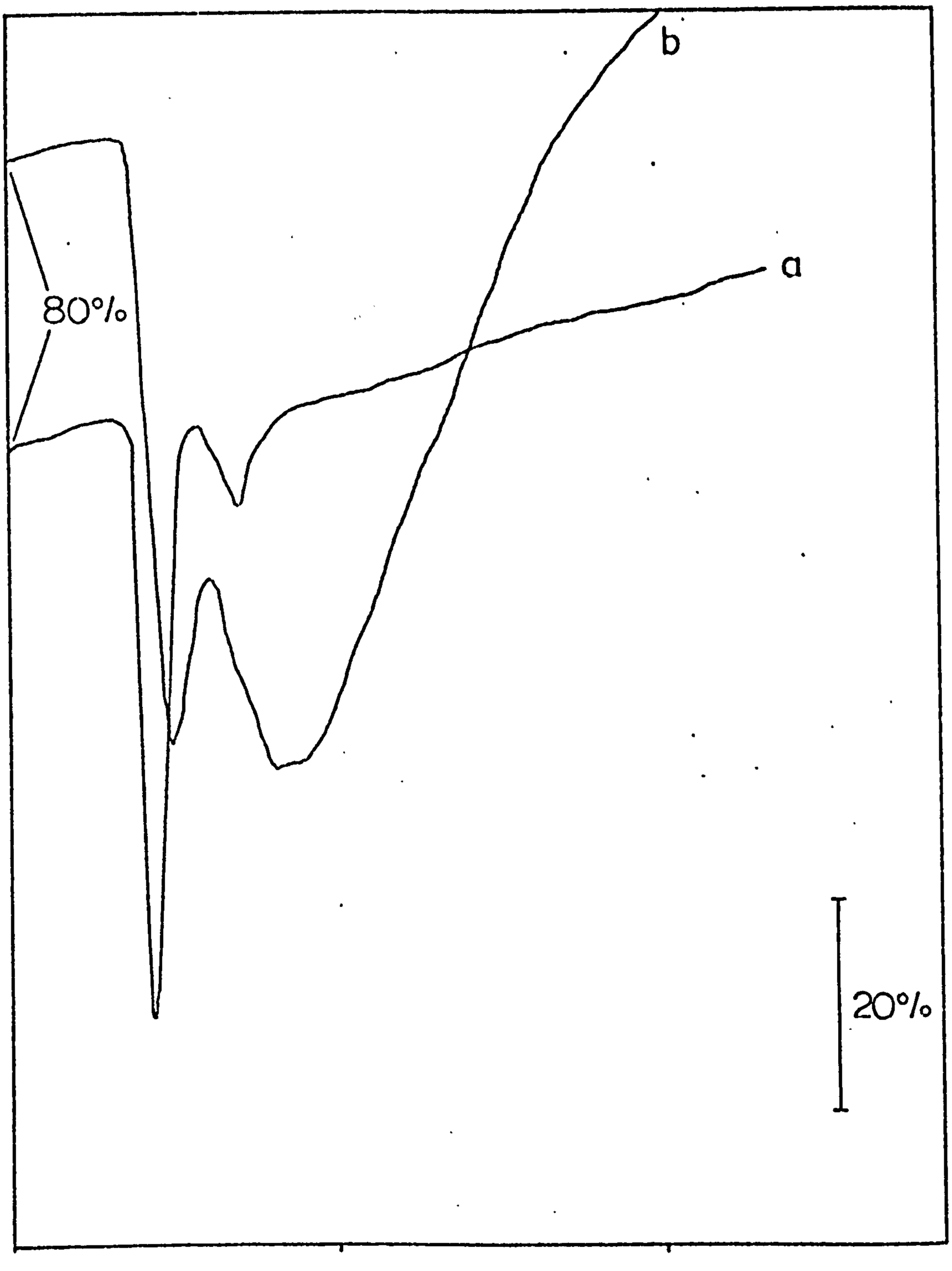

Figure 3.5. Reaction of $SiCl_4$ with the magnesia surface.
a) the MgO surface after evacuation at 673K;
b) after treatment with $SiCl_4$ vapour at room temperature.

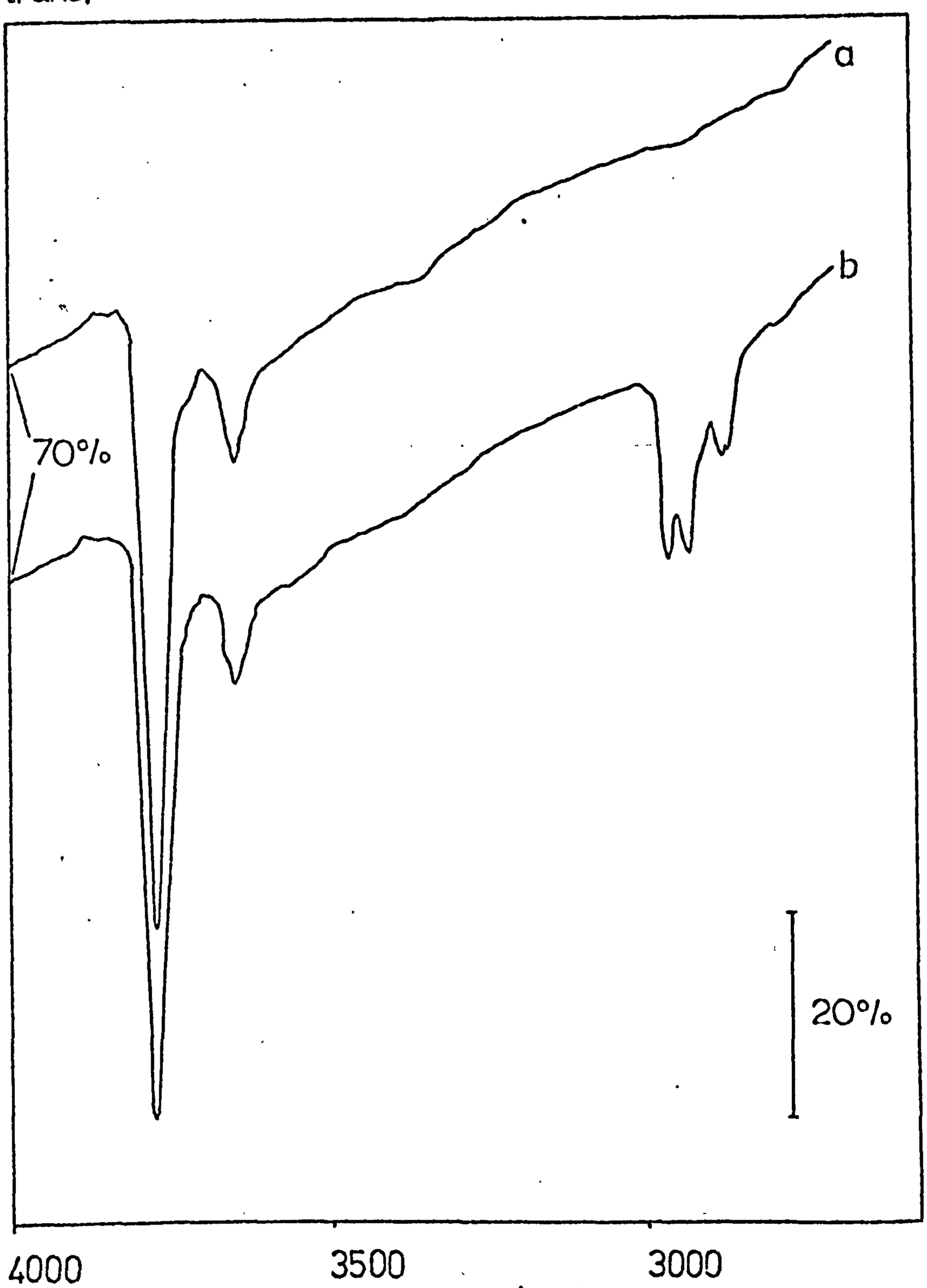

Figure 3.6. 'Reversed' catalyst activation a) the MgO surface after evacuation at 673K; b) after treatment with $Al(C_2H_5)_3$ vapour at room temperature.

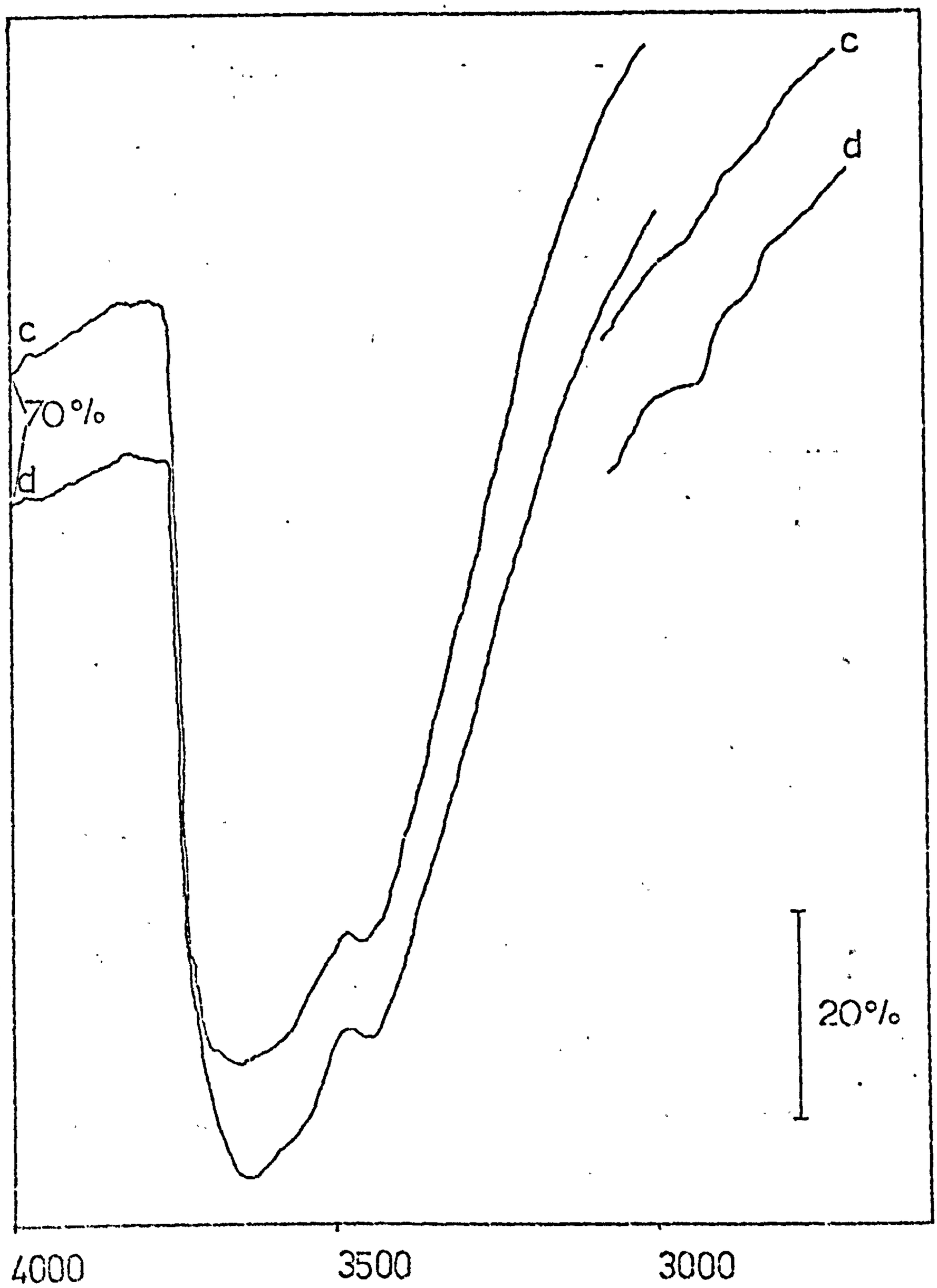

Figure 3.7. 'Reversed' catalyst activation (contd.). c) after treatment with $TiCl_4$ vapour; d) after exposure to C_2H_4 (8.6 $kN.m^{-2}$) for 24 h.

c) Polymerisation of propylene gas on the activated catalyst disc. The progressive polymerisation of propylene on the surface of the active catalyst (trace b) is shown in figure 3.3. Spectra recorded after 10 mins. and 12h. (traces c) and d) respectively) showed that absorption peaks at 2955, 2920 and 2880 cm^{-1} increased in intensity as polymerisation proceeded. Long polymerisation times led to the loss of this fine structure, resulting in a broad, intense band centred at 2900 cm^{-1}.

d) Deuteroxyl exchange with the magnesia surface and subsequent reaction with HCl gas. (figure 3.4). The hydroxyl stretching bands of the magnesia surface (3770 and 3640 cm^{-1}, trace a) were completely exchanged by equilibrating with D_2O vapour at 573K and evacuating at 673K. The deuteroxyl bands appeared at 2780 and 2680 cm^{-1} (trace b), shifted to lower frequencies by a factor of approximately $1/\sqrt{2}$ from the original hydroxyl absorptions. Admission of HCl gas to this deuteroxylated surface produced broad bands at 3500 and 2620 cm^{-1} and a shoulder at 2360 cm^{-1} (trace c). Further absorption peaks were observed at 1620 (strong), 1430 (medium) and 1190 cm^{-1} (weak).

e) Reaction of $SiCl_4$ vapour with the magnesia surface (figure 3.5). At room temperature, $SiCl_4$ vapour reacted readily with the hydroxylated magnesia surface (trace a) to produce two new absorptions at 3740 and 3560 cm^{-1} (trace b).

f) 'Reversed' catalyst activation (figures 3.6 and 3.7). Treatment of the magnesia surface (trace a) with $Al(C_2H_5)_3$ vapour produced four

bands in the (C-H) stretching region (2955, 2920, 2880 and 2860 cm^{-1}) but did not perturb the hydroxyl absorptions of the magnesia (trace b). Subsequent exposure to $TiCl_4$ vapour (trace c) yielded a very broad peak at 3650 cm^{-1} with a shoulder at 3450 cm^{-1} (identical to the spectrum produced by direct interaction of $TiCl_4$ with the magnesia surface) accompanied by complete removal of the (C-H) absorptions introduced in the previous reaction. Following exposure to ethylene gas this surface did not display any polymerisation activity (trace d).

3.A.2) Titanium dioxide (rutile) as support.

a) Activation of the rutile surface (figure 3.8). Thermal activation of a rutile disc sample at 493K (section 2.C.2) produced the spectrum of the hydroxylated surface (trace a) with peaks at 3730, 3700, 3670 and a broad absorption at 3420 cm^{-1}. There was no absorption band in the region of the water bending - mode at 1600 cm^{-1}. Exposure of this surface to $TiCl_4$ vapour (trace b) caused the complete removal of the bands at 3730, 3700 and 3670 cm^{-1} and a shift in the position of the broad absorption peak to 3370 cm^{-1}. The reaction of $Al(C_2H_5)_3$ vapour with this surface led to the appearance of four peaks in the (C-H) stretching region, 2955, 2920, 2880 and 2860 cm^{-1}.

b) Polymerisation of ethylene gas on the activated rutile surface. The rutile surface, activated at room temperature, was active for ethylene polymerisation (figure 3.9). The progressive polymerisation at the rutile surface is shown in traces b) and c), recorded after 3 mins. and

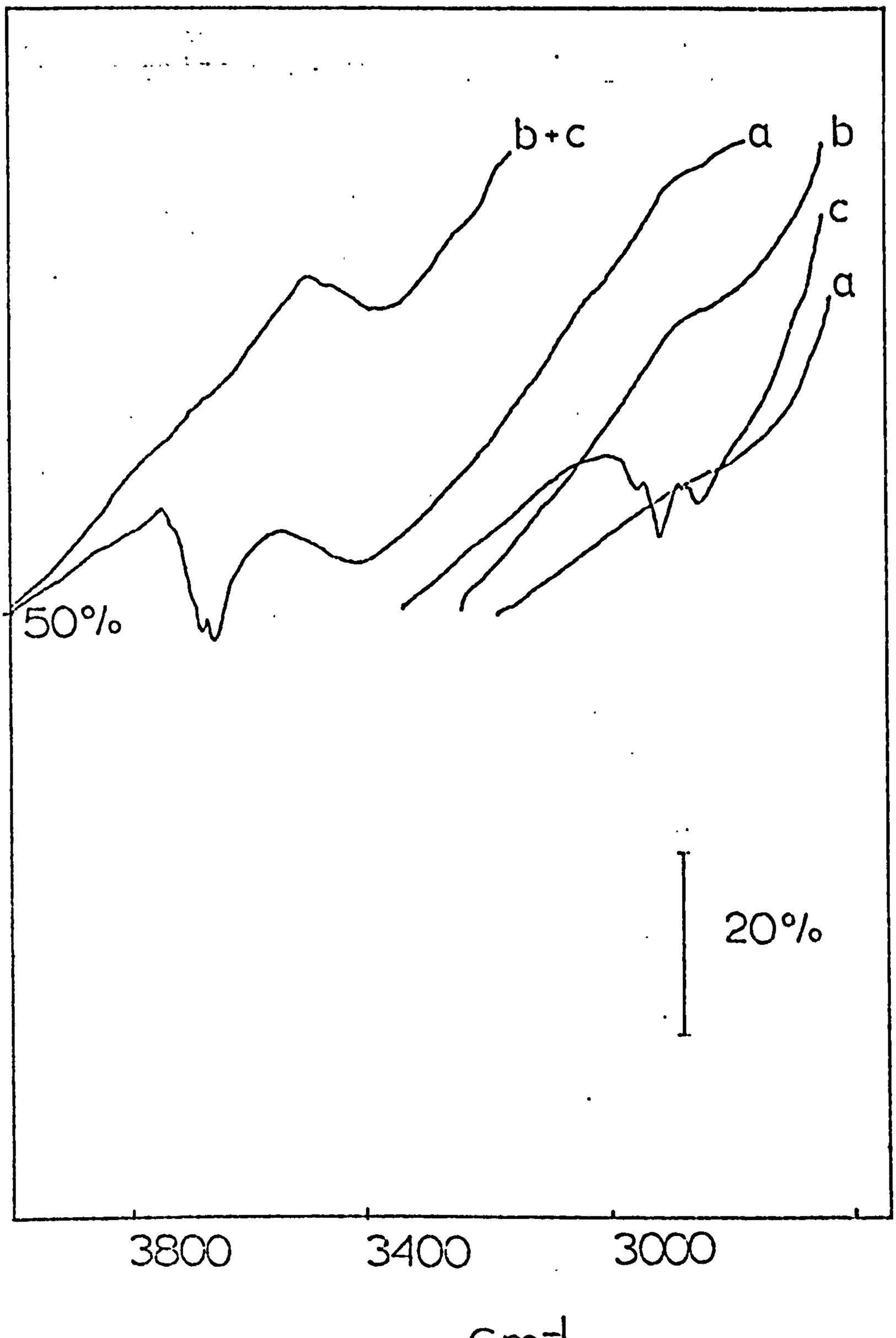

Figure 3.8. Infrared study of the preparation of the TiO_2 (rutile) supported Ziegler catalyst. a) TiO_2 surface after oxygen wash at 673K, rehydration at 293K and evacuation at 493K.; b) after $TiCl_4$ vapour; c) after $Al(C_2H_5)_3$ treatment.

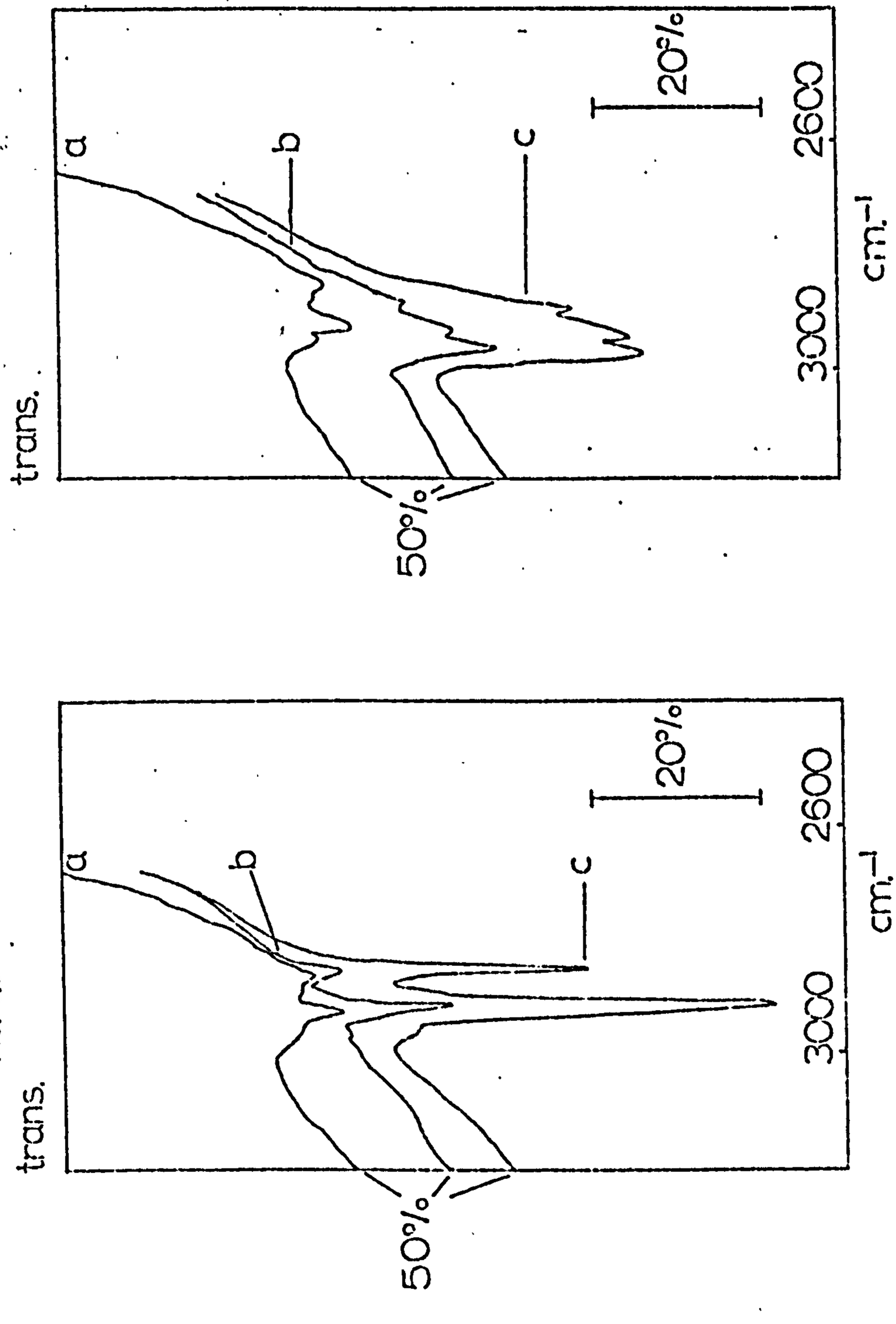

FIG. 3.10

FIG. 3.9

Olefin polymerisation on a rutile supported Ziegler catalyst.

Figure 3.9. C_2H_4 polymerisation. a) catalyst surface; b) 3 mins. reaction; c) 30 mins. reaction ($P_{C_2H_4}$ = 7.6 kN.m^{-2}).

Figure 3.10. C_3H_6 polymerisation. a) catalyst surface; b) 5 mins. reaction; c) 1 h. reaction ($P_{C_2H_6}$ = 7.8 kN.m^{-2}).

30 mins. respectively. Absorption peaks at 2920 and 2860 cm^{-1} increased in intensity as a function of the polymerisation time.

c) Polymerisation of propylene gas on the activated rutile surface.

Figure 3.10 shows the changes which occur in the infrared spectrum of the activated rutile surface (trace a) during the polymerisation of propylene. Traces b) and c) were recorded after 5 mins. and 1 h. respectivoly. Absorption bands at 2955, 2920 and 2880 cm^{-1} increased in intensity as a function of exposure time.

PART B. Changes in sample appearance during catalyst activation and polymerisation.

3.B.1) Magnesium Oxide.

Exposure of this white solid (in either powder or compressed disc form) to $TiCl_4$ vapour produced a faint yellow-brown colouration. Subsequent treatment with $Al(C_2H_5)_3$ vapour caused the sample to turn grey in colour. The intensity of the grey colour appeared to reach a maximum after an exposure time of about ten minutes. Exposure of such samples to oxygen at room temperature led to rapid removal of the discolourations. Polymerisation of either ethylene or propylene gas on activated powder samples caused the agglomeration of the fine catalyst particles, eventually forming a 'spongy' mass. A shiny, transparent film was clearly visible on infrared disc samples after prolonged polymerisation.

3.B.2) Titanium dioxide.

During activation, the colour of white rutile discs changed through pale yellow-brown (after $TiCl_4$ vapour) to grey-black (after $Al(C_2H_5)_3$ vapour). The original white colour was regenerated by oxygen treatment at room temperature. Polymerisation of ethylene or propylene on the disc surface produced a shiny, transparent surface film.

PART C. Gravimetric and analytical results of the activation process.

3.C.1) Thermal activation of $Mg(OH)_2$.

The average weight loss recorded during the calcination of magnesium hydroxide at 673K was 29.6% (theoretical weight loss for complete decomposition = 30.8%). A sample of hydroxide (70 mg) produced an oxide sample of about 50 mg.

3.C.2) Reaction of $TiCl_4$ with MgO.

The results of gravimetric and analytical studies of the reaction between $TiCl_4$ vapour and the magnesia surface are given in Table 3.1. The average amount of titanium in the recorded weight gain was found by analysis to be 25.5 ($\pm$ 0.5)%. This figure was subsequently used to estimate the amount of titanium in polymerisation catalysts prepared in identical fashion to the samples in table 3.1. The

Sample	$\frac{MgO\ wt.}{mg.}$	$\frac{TiCl_4\ wt.}{mg.}$	$\frac{wt.\ of\ Ti}{mg.}$	$\frac{Ti}{TiCl_4} \times 100$	$\frac{Heating\ time}{h}$
1T	49.7	8.85	2.23	25.1	15.0
2T	48.4	8.45	2.13	25.2	18.5
3T	50.2	8.10	2.13	26.3	15.8
4T	49.1	8.70	2.20	25.3	19.0

Table 3.1. Reaction of $TiCl_4$ vapour with the MgO surface at 308K.

weight gain during the $TiCl_4$ reaction was not dependent upon the outgassing time of the oxide sample for heating times between 15 and 19 h.

3.C.3) Reaction of $Al(C_2H_5)_3$ with the $TiCl_4$/MgO surface.

The reaction of $Al(C_2H_5)_3$ vapour with the titanium modified magnesia surface was found to be irreproducible. Following initial exposure of the surface to the vapour, a small weight gain was invariably observed ($\sim$3 mg.). Evacuation of the activated sample prior to polymerisation experiments led to complete or partial loss of this weight increase. In several instances the recorded overall weight change was negative. Catalyst polymerisation activity was not related to the nature of the weight change during this activation reaction. Analysis of four samples (three controls and one active catalyst, section 2.C.3) failed to detect the presence of aluminium. The lower detection limit of the analytical technique corresponded to 0.1 mg. of aluminium on a

magnesia sample of 50 mg. The direct interaction of $Al(C_2H_5)_3$ vapour with a fresh magnesia surface gave a small weight gain but again, no aluminium was detected on analysis of the sample.

PART D. Kinetic investigation of the polymerisation of C_2H_4 and C_3H_6 on the activated magnesia surface.

3.D.1) Introduction.

Polymerisation was followed gravimetrically. A standard weight of catalyst was used in all polymerisations to minimise variations in the geometry of the catalyst bed. The weight of polymer formed after time t mins. (m_t) was expressed as milli-moles of monomer polymerised per mg. of titanium present in the catalyst. The observed rate of polymerisation fell off rapidly from its initial value. It was found that for a particular polymerisation, the weight of polymer formed (m_t) had a $t^{\frac{1}{2}}$ dependence. As previously noted (section 2.C.1) it was not possible to reproduce the polymerisation curves. The adherence of the data to the $t^{\frac{1}{2}}$ relationship is shown for three samples in figure 3.11 in which m_t^2 is plotted against the polymerisation time (t). Since all three samples had the same weight and were treated in identical fashion, figure 3.11 also serves to illustrate the inherent irreproducibility of the polymerisation system. Experiment showed that at constant temperature and pressure, the gradients of such plots remained effectively constant for reaction times of up to five hours. Thus for the purpose

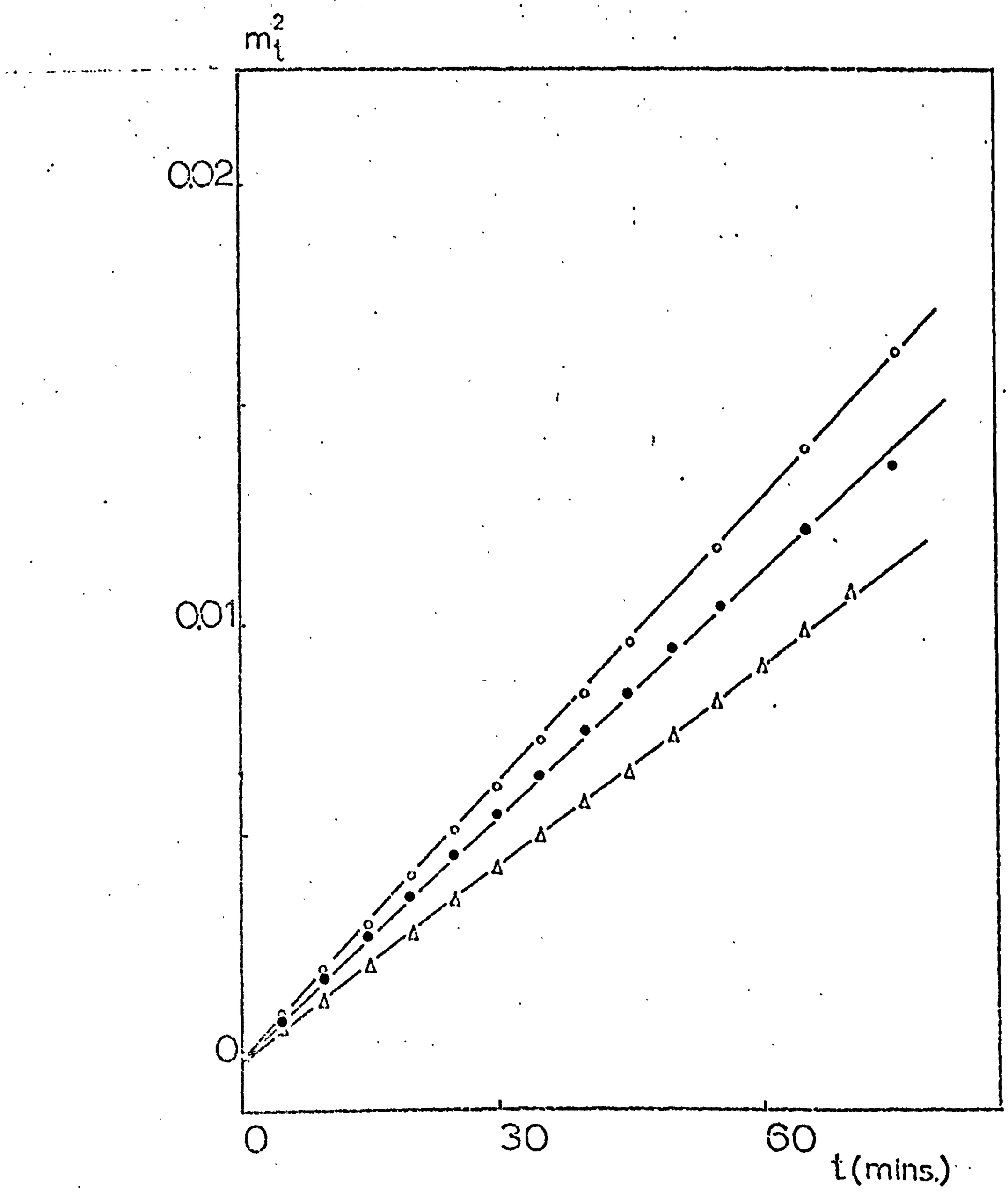

Figure 3.11. Polymerisation of C_2H_4 on a magnesia supported Ziegler Catalyst. T = 308 K; p = 7.6 kN.m^{-2}. (o run 1E; • run 2E; Δ run 3E).

of investigating the pressure and temperature dependencies of the polymerisation reactions, split temperature and split pressure techniques were developed. In this fashion it was possible to obtain pressure or temperature parameters from a single catalyst sample.

3.D.2) Treatment of polymerisation data.

The rate of weight increase during polymerisation was found to obey a law analagous to the parabolic law followed by tarnishing reactions at metal surfaces. In such reactions, the rate determining step is the diffusion of reactants to the reaction surface through a growing surface film. The parabolic law may be expressed as:

$$\frac{dX}{dt} = k\left(\frac{C_o - C_s}{X}\right) \qquad (3.1)$$

where X is the thickness of the surface film at time t; C_o and C_s are the concentrations of the diffusing species at the exterior and interior surfaces respectively; and k is the rate constant.

The weight (M) of a polymer film of density (ρ) and thickness (X) extending over an effective catalyst surface area (a), is given by:

$$M = Xa\rho \qquad (3.2)$$

Differentiating with respect to time (t),

$$\frac{dM}{dt} = a\rho\,\frac{dX}{dt} \qquad (3.3)$$

and from equation (3.1):

$$\frac{dM}{dt} = (a\rho)^2 k\left(\frac{C_o - C_s}{M}\right) \qquad (3.4)$$

Integrating between limits,

$$\int_{m_o}^{m_t} M.dM = (a\rho)^2 \; k \; (C_o - C_s) \int_{t_o}^{t} t \; dt. \qquad (3.5)$$

gives:

$$(m^2_t - m^2_o) = 2k(a\rho)^2(C_o - C_s)(t - t_o) \qquad (3.6)$$

where m_o, m_t represent the mass of polymer formed after times t_o and t respectively. Since C_s, the concentration of monomer at the catalyst surface, is small under conditions where transfer is rate determining, then:

$$(C_o - C_s) \simeq C_o$$

Assuming that sorption of monomer at the exterior of the polymer film obeys a law of the form:

$$C_o = k' \; p^n \qquad (3.7)$$

where k' is a constant and p is the external gas pressure, then:

$$(m_t^2 - m_o^2) = 2kk' \; p^n(a\rho)^2(t - t_o) \qquad (3.8)$$

Thus a plot of $(m_t^2 - m_o^2)$ against $(t - t_o)$ should yield a straight line of gradient $2kk' p^n(a\rho)^2$. This gradient can be expressed in the form:

$$2kk' p^n(a\rho)^2 = K \; p^n \qquad (3.9)$$

where K is a constant at constant temperature. In this form, equation 3.8 can be applied to polymerisation reactions during the course of which either the temperature or the monomer pressure is varied. If t_o is zero, then m_o becomes zero and equation (3.8) reduces to:

$$m_t = (K \; p^n \; t)^{\frac{1}{2}} \qquad (3.10)$$

the relationship obeyed by the plots shown in figure 3.11.

3.D.3) Determination of n-Pressure dependence of olefin polymerisation.

The pressure dependence (n) of the reaction at constant temperature was determined by application of equation (3.8).

a) C_2H_4 polymerisation. The results of one polymerisation (run 4E) are reproduced here in their entirety, illustrating the principles described in section 2.C.a. In subsequent cases only those details pertinent to equation 3.8 and to the later stages of the kinetic analysis are given.

Table 3.2 shows how the (mass of polymer/time) data (figure 3.12) was adapted for equation 3.8. Values of m_o and t_o were chosen to give polymerisation times of around 30 minutes for each monomer pressure.

Table 3.2.

The polymerisation of C_2H_4 at different monomer pressures

(Run 4E; figures 3.12, 3.13.)

time (t) mins	polymer mass (m) (m.moles C_2H_4/mg.Ti)	pressure (p) kN/m^2	$(m_t^2 - m_o^2)$	$(t - t_o)$
0	0	6.00		
3	0.129			
5	0.180			
8	0.240			
10	0.274			
12	0.303			
14	0.331			
16	0.357			
18	0.381			
20	0.405			

Continued/....

t	m	p	$(m_t^2 - m_o^2)$	$(t - t_o)$
22	0.427			
24	0.449			
26	0.469			
28	0.489		0	0
30	0.509		0.019	2
32	0.527		0.038	4
34	0.545		0.057	6
36	0.562		0.076	8
38	0.579		0.096	10
40	0.595		0.115	12
42	0.611		0.135	14
44	0.628		0.154	16
46	0.643		0.174	18
48	0.657		0.193	20
50	0.671		0.212	22
52	0.686		0.471	24
54	0.700		0.490	26
56	0.714		0.510	28
58	0.728		0.530	30
60	0.741		0.549	32
	Pressure change	2.00		
64	0.758		0	0
66	0.762		0.007	2
68	0.767		0.014	4
70	0.771		0.020	6
72	0.775		0.027	8

Continuod/.....

t	m	p	$m_t^2 - m_o^2$	$t - t_o$
74	0.779		0.033	10
76	0.783		0.039	12
78	0.788		0.045	14
80	0.791		0.052	16
82	0.795		0.058	18
84	0.799		0.065	20
86	0.802		0.070	22
88	0.807		0.076	24
90	0.810		0.082	26
92	0.815		0.090	28
94	0.819		0.096	30
96	0.822		0.101	32
	Pressure change	9.35		
98	0.832		0	0
100	0.851		0.033	2
102	0.872		0.068	4
104	0.893		0.105	6
106	0.913		0.142	8
108	0.934		0.180	10
110	0.953		0.217	12
112	0.972		0.254	14
114	0.992		0.292	16
116	1.010		0.329	18
121	1.056		0.424	23
122	1.065		0.443	24
124	1.083		0.481	26

Continued/.....

t	m	p	$m_t^2 - m_o^2$	$t - t_o$
126	1.100		0.517	28
128	1.117		0.556	30
130	1.133		0.592	32
132	1.150		0.632	34
	Pressure change	3.61		
138	1.188		0	0
142	1.200		0.028	4
144	1.206		0.042	6
146	1.211		0.056	8
148	1.217		0.068	10
150	1.222		0.081	12
152	1.228		0.096	14
154	1.233		0.109	16
156$\frac{2}{4}$	1.239		0.122	18
158	1.244		0.135	20
160	1.249		0.147	22
162	1.254		0.161	24
164	1.259		0.172	26
166	1.264		0.186	28
168	1.269		0.199	30
170	1.274		0.211	32
172	1.279		0.223	34
174	1.284		0.236	36

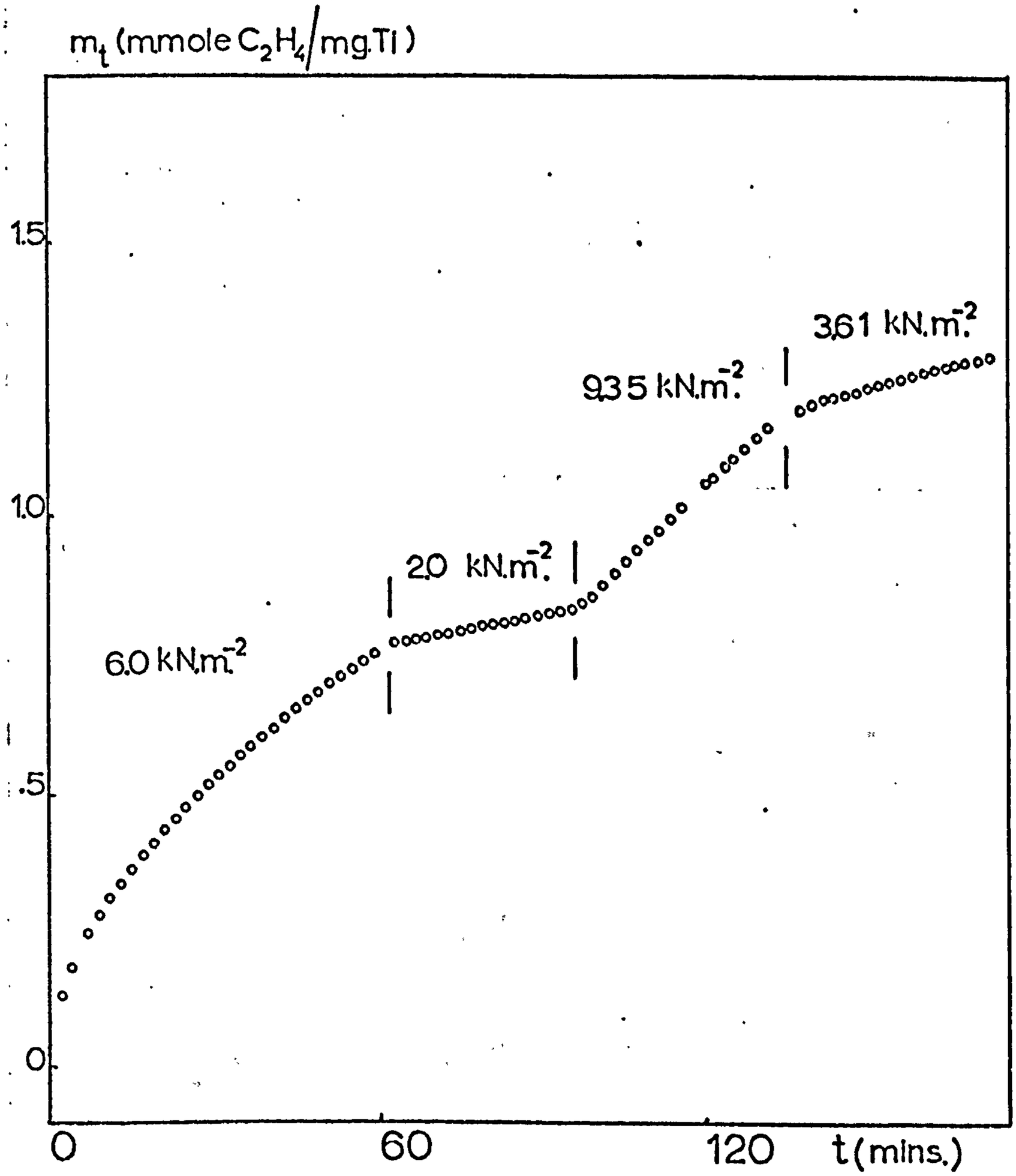

Figure 3.12. C_2H_4 polymerisation. The effect of changing the monomer pressure on the polymerisation rate; T = 308K. (run 4E; table 3.2).

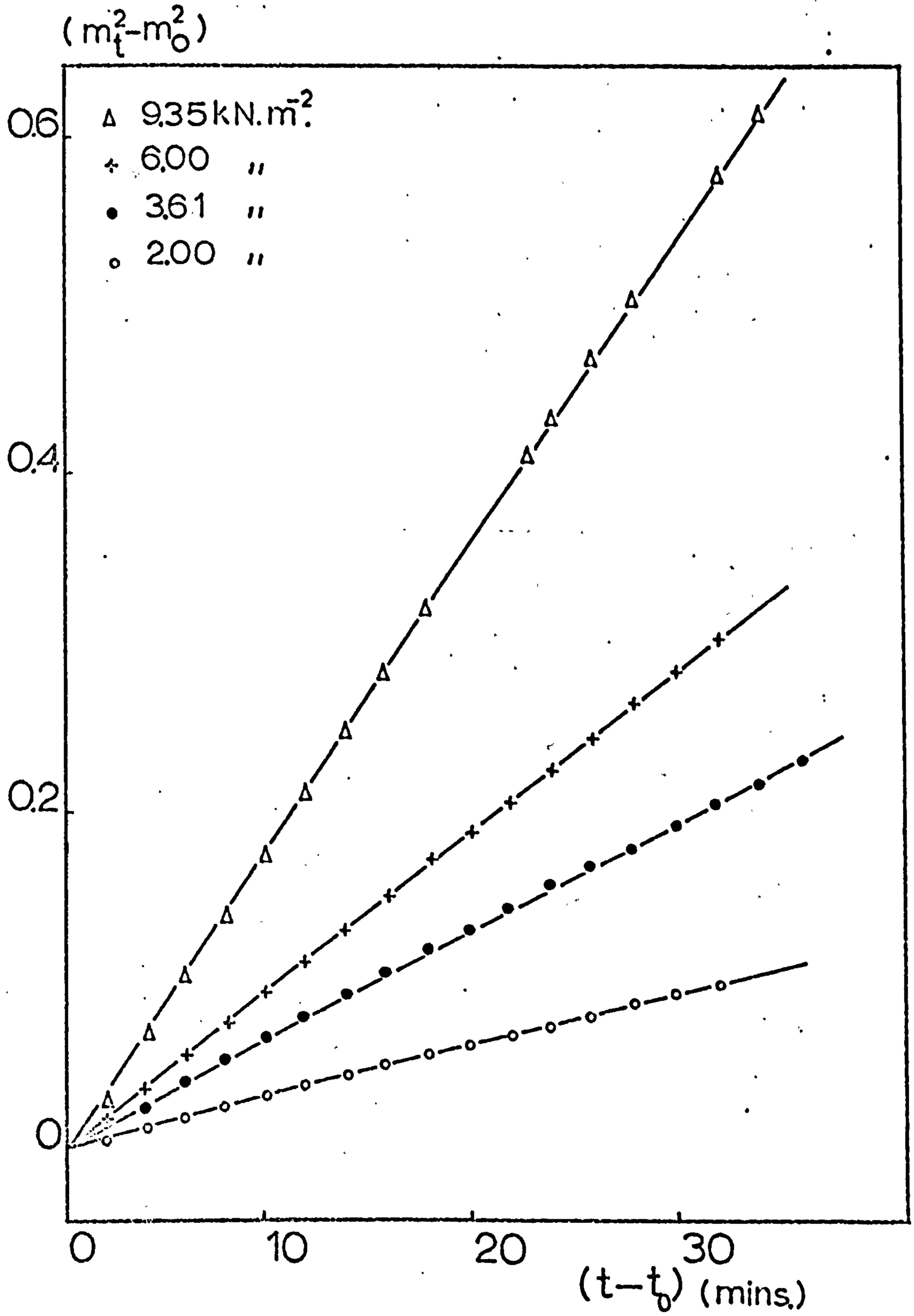

Figure 3.13. C_2H_4 polymerisation. Variation in polymerisation rate with monomer pressure; T = 308 K. (run 4E; table 3.2).

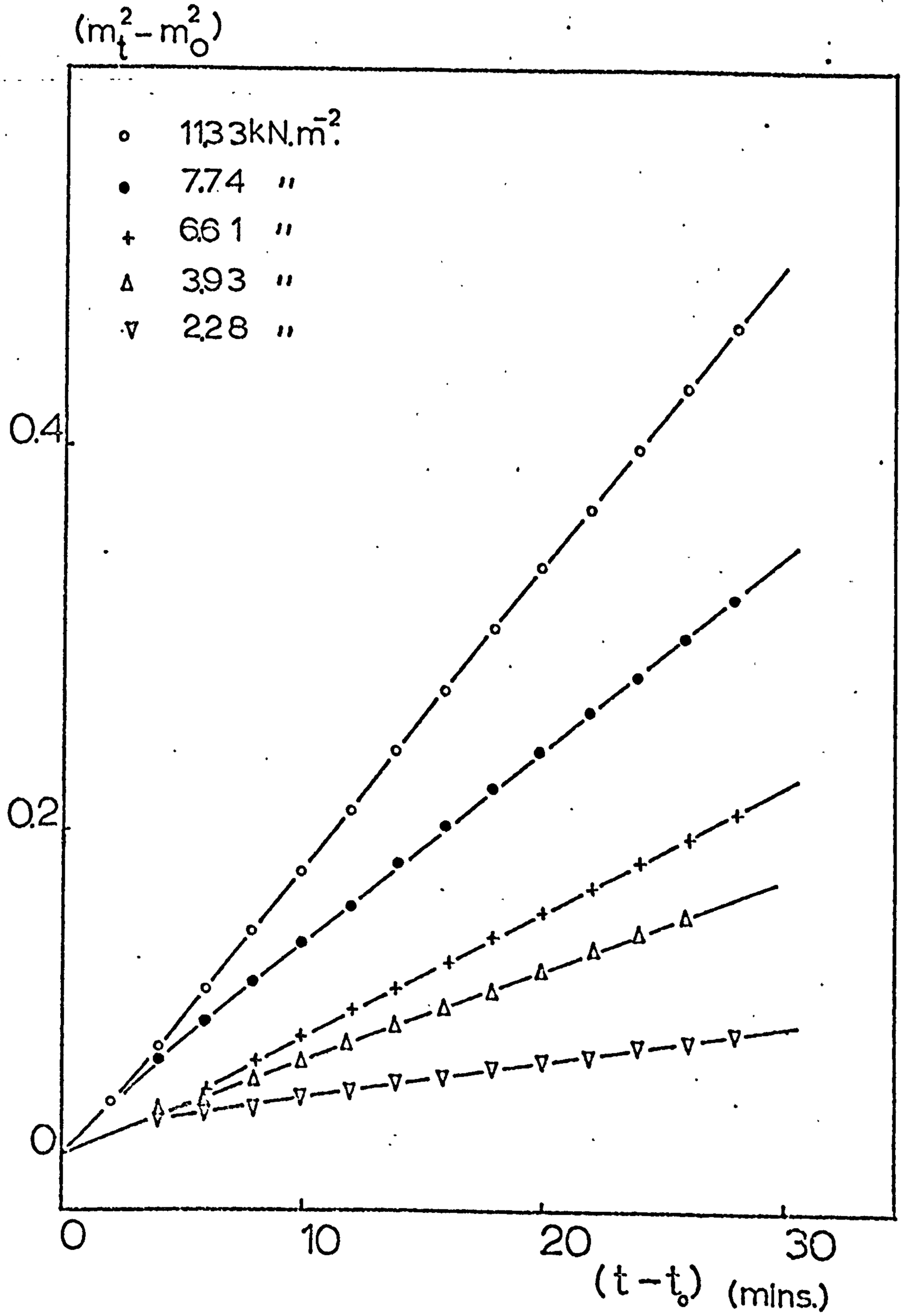

Figure 3.14. C_2H_4 polymerisation. Variation in polymerisation rate with monomer pressure; T = 308 K. (run 5E).

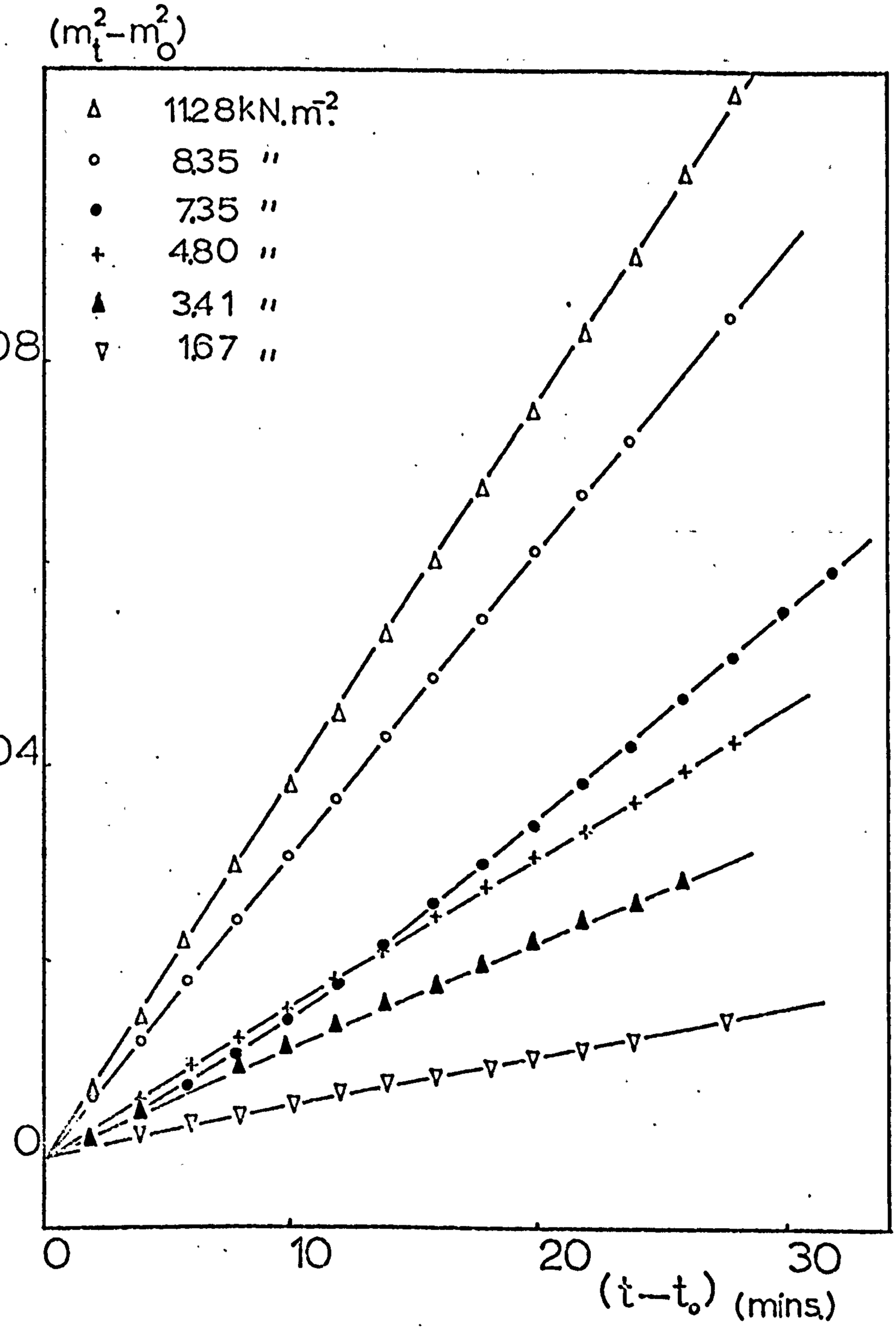

Figure 3.15. C_2H_4 polymerisation. Variation in polymerisation rate with monomer pressure. T = 308 K. (run 6E).

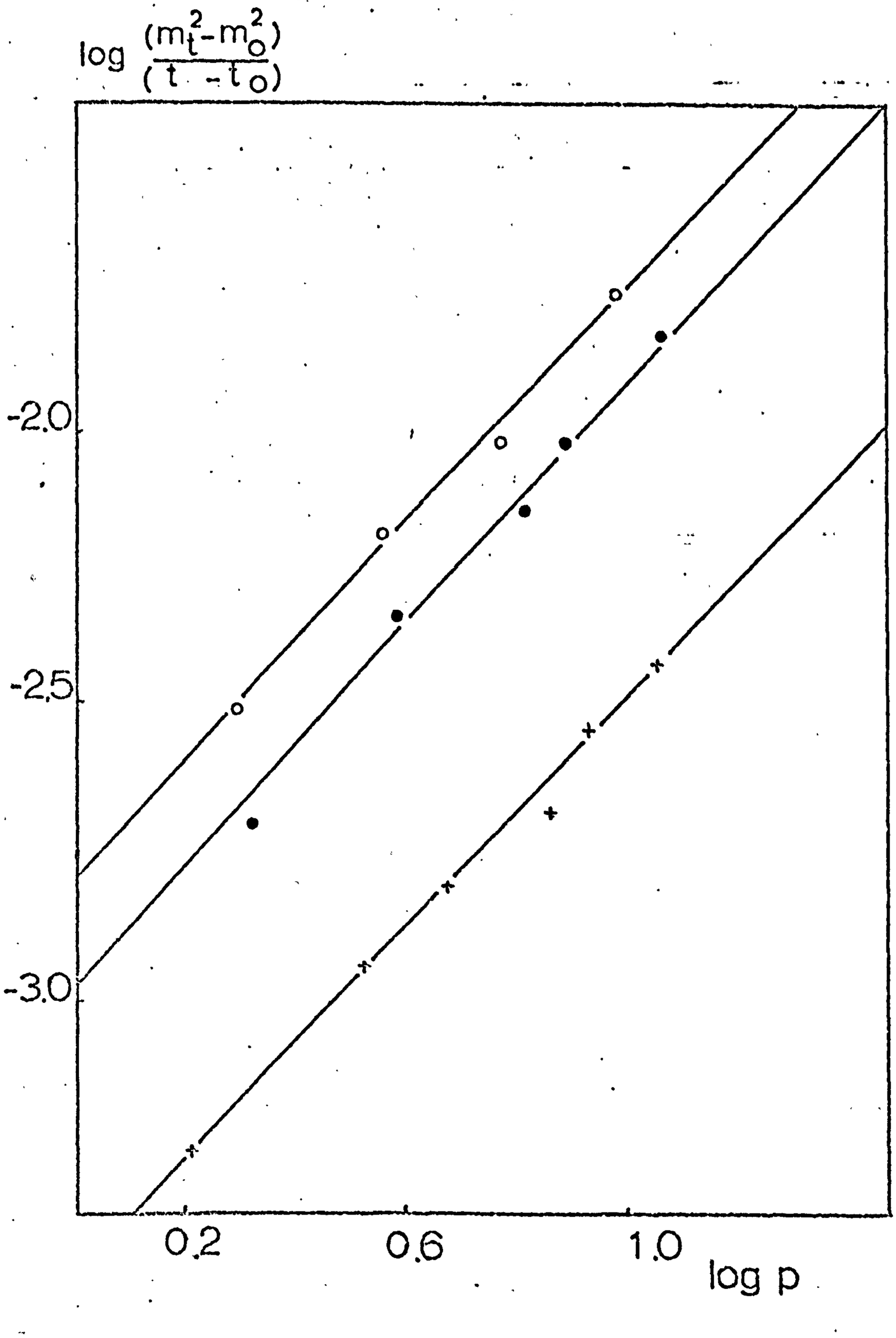

Figure 3.16. C_2H_4 polymerisation. Pressure dependence of the polymerisation rate. (o run 4E; • run 5E; + run 6E; table 3.3).

Figure 3.12 shows the increase in weight of the catalyst sample as a function of time, following exposure to a range of ethylene monomer pressures. Application of equation 3.8 to this data yielded a linear plot for each of the pressure regions (figure 3.13; table 3.2). Data for two similar polymerisations (runs 5E, 6E) is plotted in figures 3.14 and 3.15 respectively. At low values of $(t - t_o)$, curvature of the plots is evidence that after a pressure change, some time is required for the attainment of the ambient polymerisation rate. From equation 3.9, the gradients of the straight line plots for runs 4E, 5E and 6E can be expressed as:

$$\frac{(m_t^2 - m_o^2)}{(t - t_o)} = Kp^n.$$

The values of the gradients are given in table 3.3. (n) was determined

Table 3.3. The pressure dependence of C_2H_4 polymerisation.

(T = 308K) The units of Kp^n are (m.moles C_2H_4/mg.Ti)^2 min.$^{-1}$

(runs 4E, 5E, 6E; figure 3.16).

Run No.	Pressure (p) / (kN.m^{-2})	$\log_{10}$ p / kN.m^{-2}	$Kp^n \times 10^3$	$\log_{10} Kp^n$
4E	9.35	0.971	18.73	-1.727
	6.00	0.778	9.63	-2.016
	3.61	0.558	6.52	-2.186
	2.00	0.301	3.09	-2.510
5E	11.33	1.055	15.78	-1.802
	7.74	0.888	9.40	-2.027
	6.61	0.820	6.52	-2.186
	3.93	0.595	4.84	-2.315
	2.28	0.358	2.09	-2.691
6E	11.28	1.052	3.86	-2.413
	8.35	0.922	3.11	-2.507

Continued/....

Table 3.3 continued.

Run No.	Pressure (p) ($kN.m^{-2}$)	$\log_{10}$ p ($kN.m^{-2}$)	$Kp^n \times 10^3$	$\log_{10} Kp^n$
	7.35	0.866	2.16	-2.665
	4.80	0.682	1.53	-2.819
	3.41	0.533	1.11	-2.955
	1.67	0.223	0.54	-3.274

Table 3.4. Values of n for C_2H_4 and C_3H_6 polymerisation (figures 3.16, 3.19).

Monomer	Run No.	n
C_2H_4	4E	1.09
	5E	1.12
	6E	1.07
C_3H_6	7E	1.09
	8E	1.10

from the slopes of the corresponding log/log plots (figure 3.16) and the values are tabulated (table 3.4). The mean value of n for ethylene polymerisation was found to be 1.1.

b) C_3H_6 polymerisation. Polymerisation of propylene on the supported catalyst was found to obey the rate law proposed in equation 3.8. The application of this law to two propylene polymerisations (runs 7E and 8E)

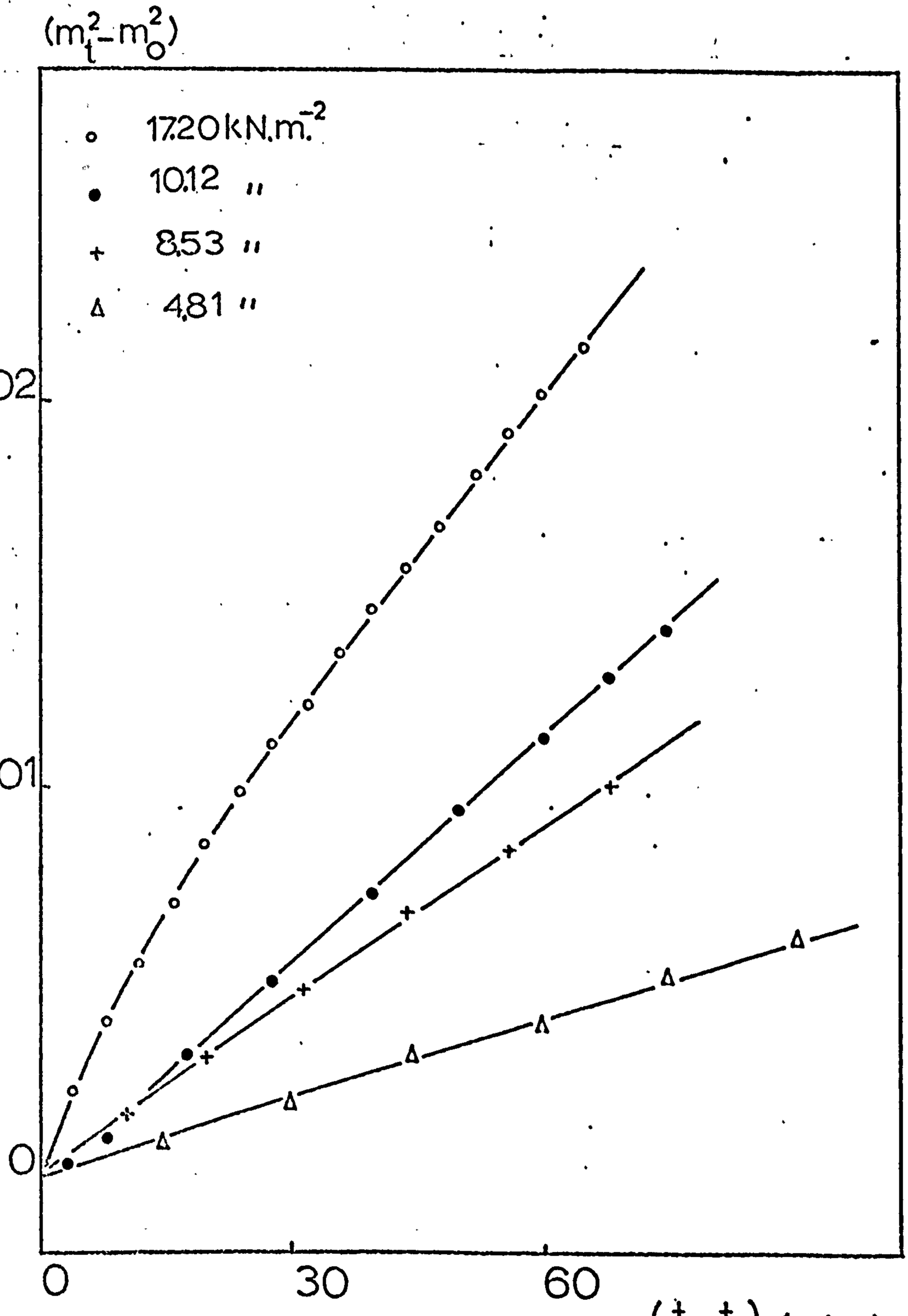

Figure 3.17. C_3H_6 polymerisation. Variation in polymerisation rate with monomer pressure. T = 308 K (run 7E).

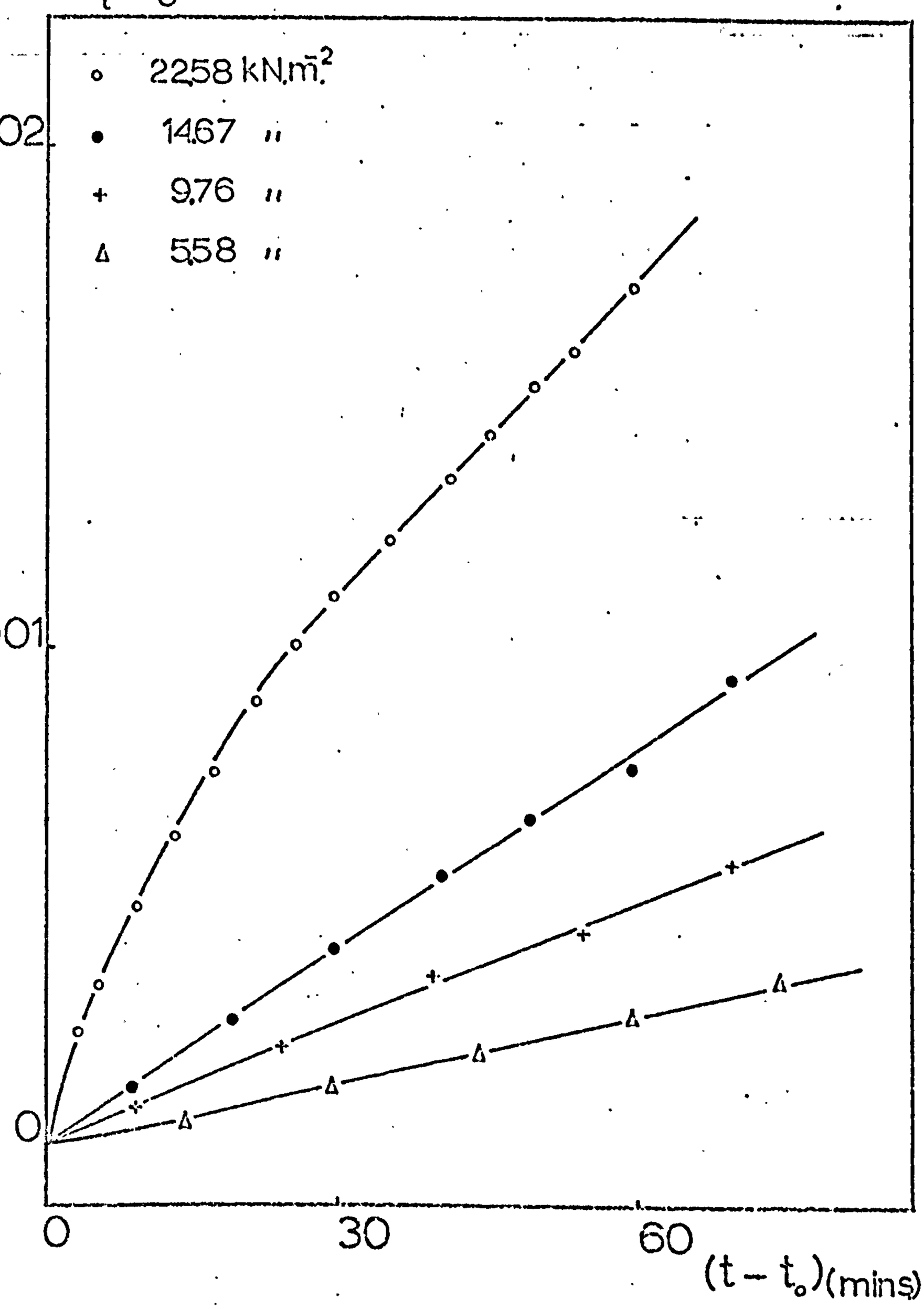

Figure 3.18. C_3H_6 polymerisation. Variation in polymerisation rate with monomer pressure. T = 308K (run 8E).

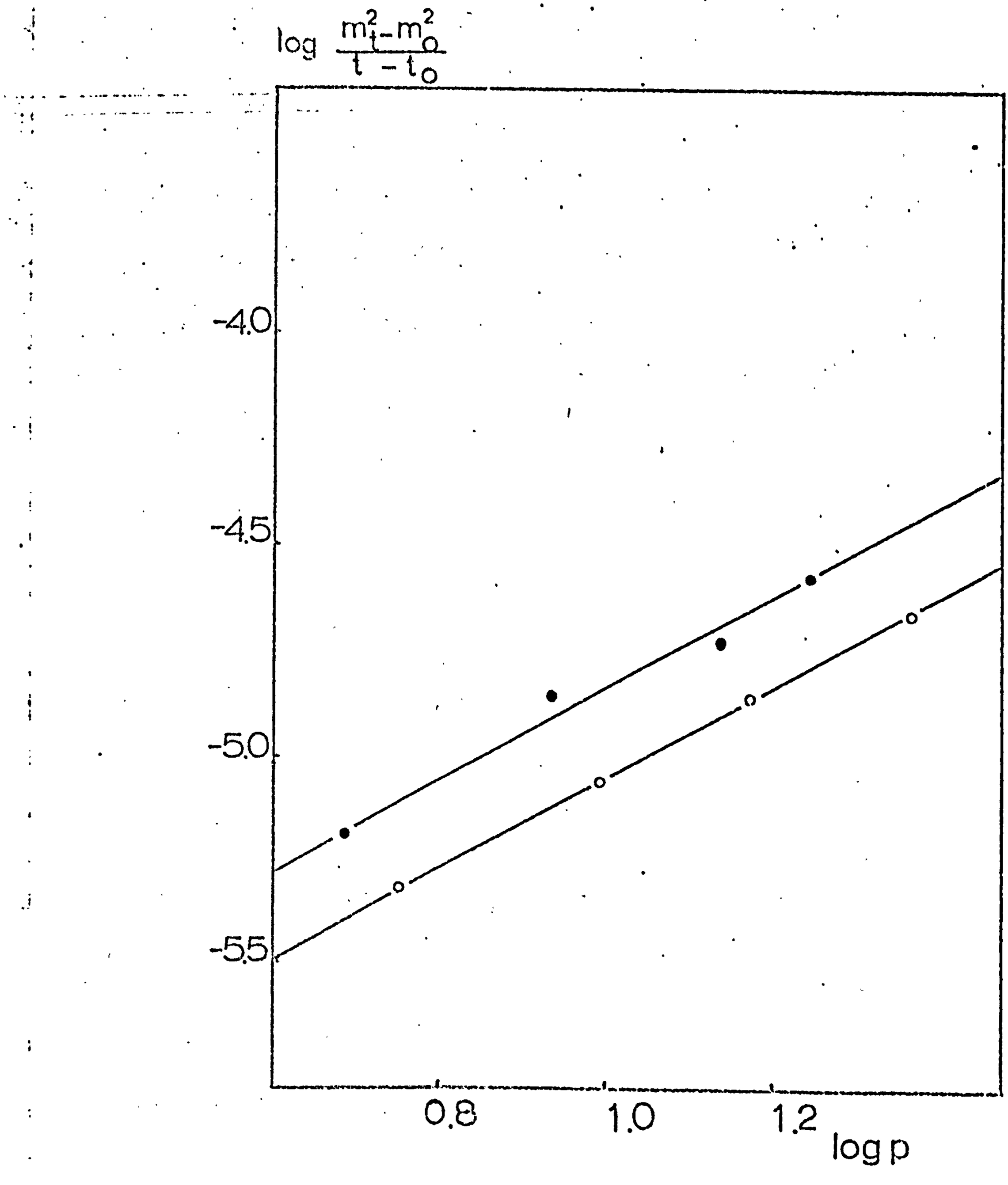

Figure 3.19. C_3H_6 polymerisation. Pressure dependence of the polymerisation rate (o run 7E; • run 8E; table 3.5).

over a range of monomer pressures is shown in figures 3.17 and 3.18 respectively. The gradients of the linear portions are listed in table 3.5. (n), the pressure dependence of the reaction was determined for each run (table 3.4) from the plots of $\log_{10} \frac{m_t^2 - m_o^2}{t - t_o}$ $\log_{10} p$ (figure 3.19). The mean value of n was found to be 1.1.

Table 3.5. The pressure dependence of propylene polymerisation. ($T = 308K$). The units of (Kp^n) are $(m.moles.C_3H_6/mg.Ti)^2.min^{-1}$. (runs 7E, 8E; figure 3.19).

Run No.	pressure (p) / $kN.m^{-2}$	$\log_{10}$ p / $kN.m^{-2}$	$Kp^n \times 10^6$	$\log_{10} Kp^n$
7E	22.58	1.354	21.5	-4.668
	14.67	1.167	13.8	-4.862
	9.76	0.990	8.5	-5.073
	5.58	0.748	4.8	-5.320
8E	17.20	1.236	26.6	-4.576
	10.12	1.130	18.3	-4.738
	8.53	0.932	13.9	-4.855
	4.81	0.683	6.4	-5.192

These results indicated a first order pressure dependence for the polymerisation of C_2H_4 and C_3H_6. Equation 3.7 can thus be written:

$$C_o = k' p \qquad (3.11)$$

This is identical with the Henry's law equation governing dilute solutions of permanent gases. Equation 3.8 can now be written:

$$(m^2_t - m_o^2) = Kp(t - t_o) \qquad (3.12)$$

3.D.4) Temperature dependence of the polymerisation rate.

a) C_2H_4 polymerisation. The polymerisation of ethylene as a function of time at ten different temperatures is shown in figure 3.20 (run 9E). Application of equation 3.8 to each of the temperature regions yielded the plots shown in figures 3.21 and 3.22. Below 320K a linear relationship between $(m_t^2 - m_o^2)$ and $(t - t_o)$ was observed and the gradient increased with temperature. Above 320K departures from linearity were observed and the initial slopes decreased with increasing temperature. The temperature dependent constant, K, was found to obey an Arrhenius law at temperatures between 273 and 320K. (table 3.6; figure 3.23):

$$K = K_o \exp\left(-\frac{E_{act}}{RT}\right) \qquad (3.13)$$

Table 3.6. Temperature dependence of C_2H_4 polymerisation. (figure 3.23; run 9E). $p = 7.60\ kN.m^{-2}$. The units of K are $(m.moles\ C_2H_4/mg.Ti)^2.min.^{-1}.(kN.m^{-2})^{-1}$.

$T/^oK$	$1/T \times 10^3$	$K \times 10^4$	$\log_{10}K$
273.0	3.66	0.65	-4.187
285.0	3.51	2.94	-3.531
296.0	3.38	5.43	-3.265
302.0	3.31	5.30	-3.275
307.0	3.26	8.25	-3.084

Continued/....

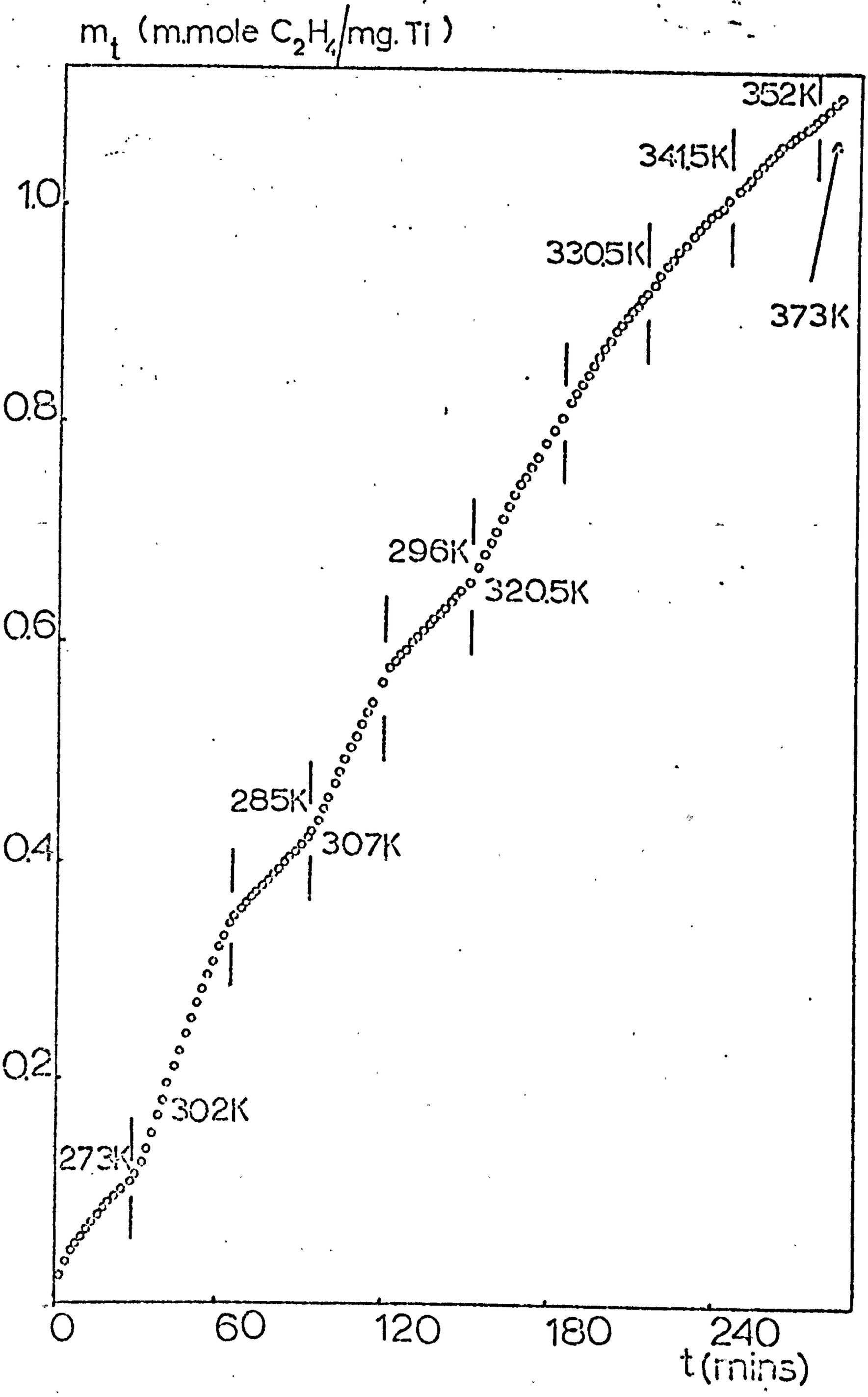

Figure 3.20. C_2H_4 polymerisation. The effect of changing the temperature on the polymerisation rate. p = 7.60 kN.m^{-2}. (run 9E).

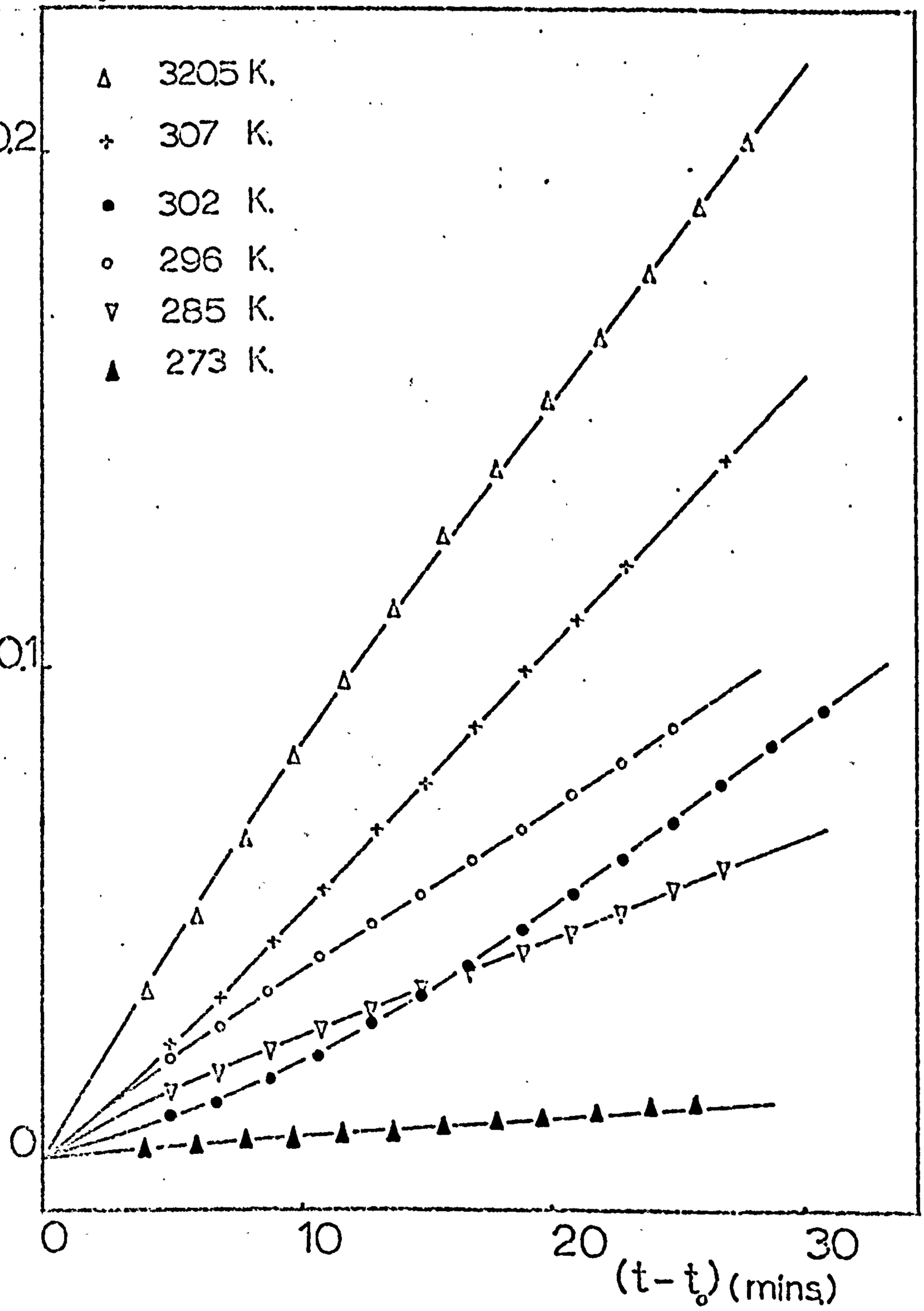

Figure 3.21. C_2H_4 polymerisation. Variation of rate with temperature below the catalyst decomposition temperature.
$p = 7.0\ kN.m^{-2}$. (run 9E).

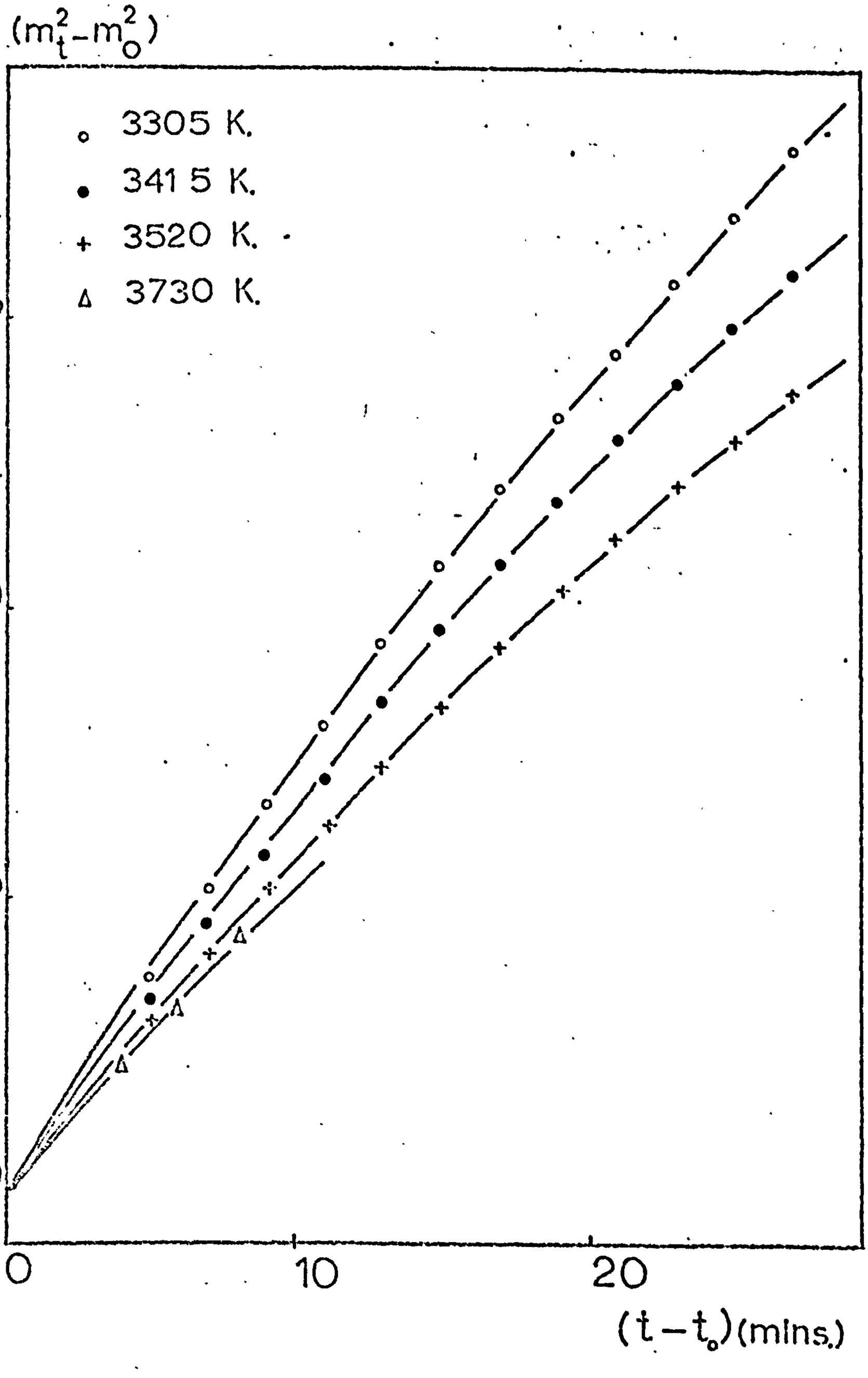

Figure 3.22. C_2H_4 polymerisation. Variation in polymerisation rate with temperature above the catalyst decomposition temperature. $p = 7.6\ kN.m^{-2}$. (run 9E)

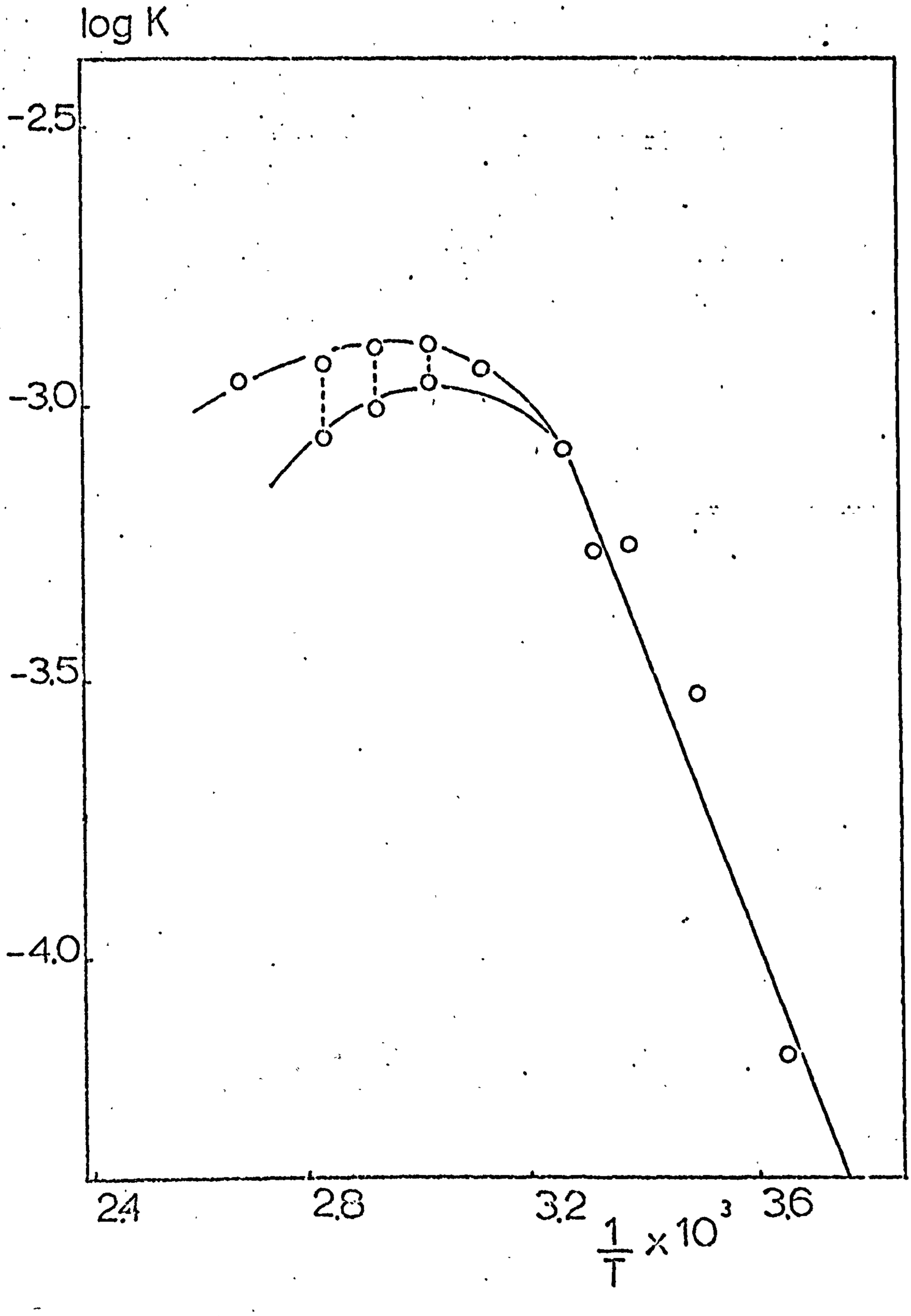

Figure 3.23. C_2H_4 polymerisation. Temperature dependence of the polymerisation rate (Arrhenius law). (Run 9E; table 3.6).

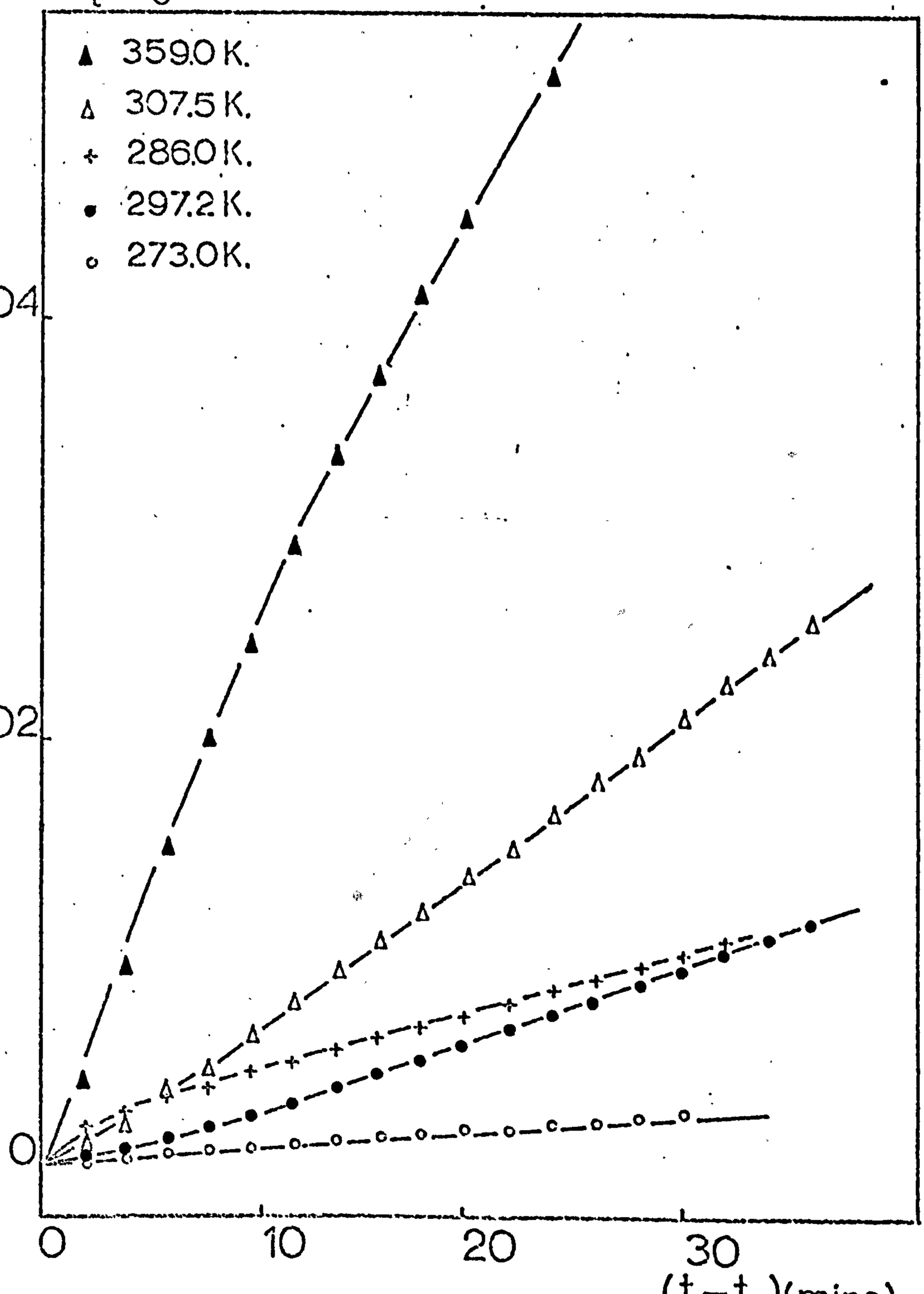

Figure 3.24. C_2H_4 polymerisation. Variation of polymerisation rate with temperature for a catalyst sample prior to high temperature ageing (359 K) p = 7.6 kN.m^{-2} (run 10E).

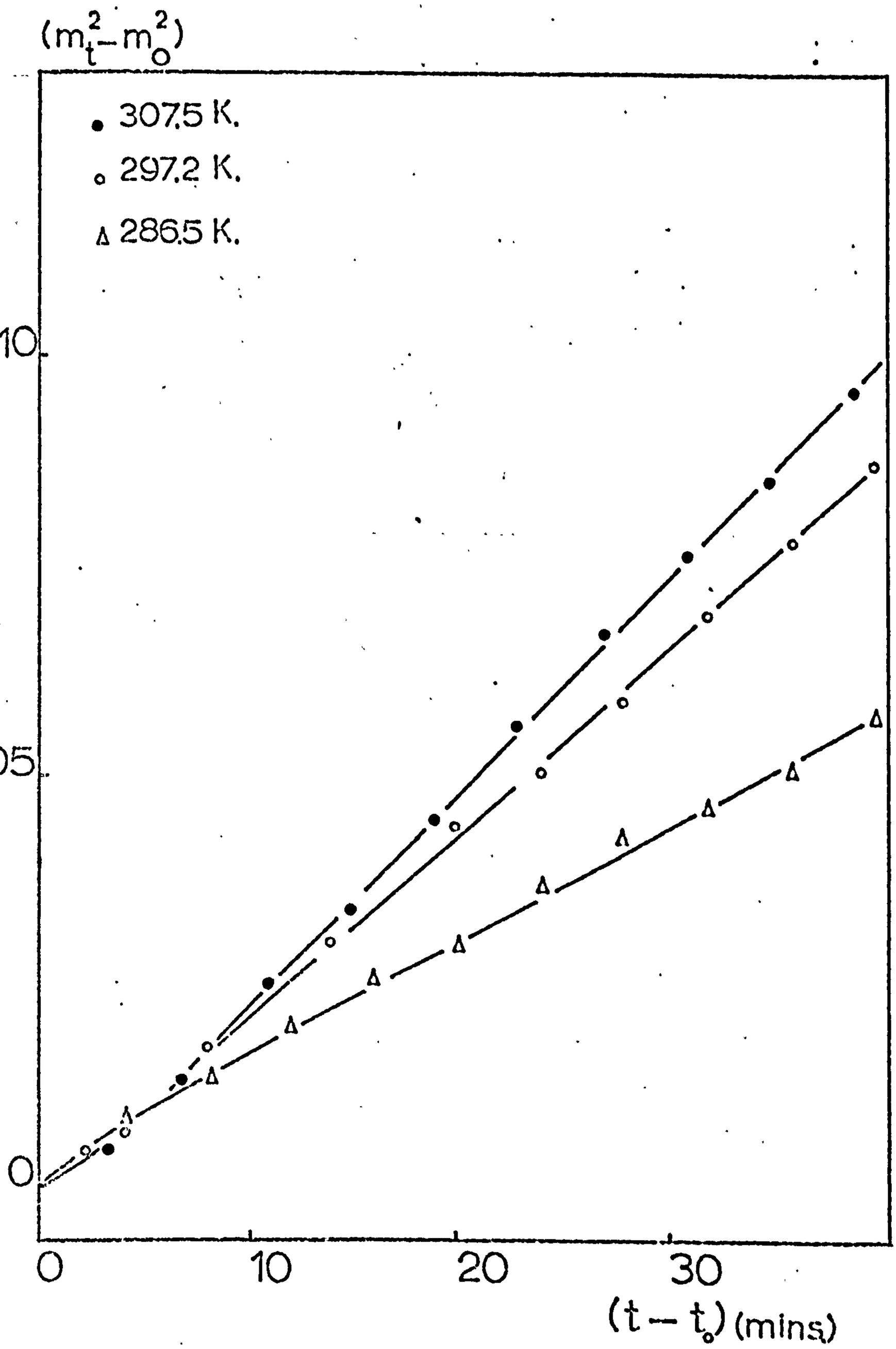

Figure 3.25. C_2H_4 polymerisation. Variation of polymerisation rate with temperature following catalyst ageing at 359 K. $p = 7.6\ kN.m^{-2}$. (run 10E).

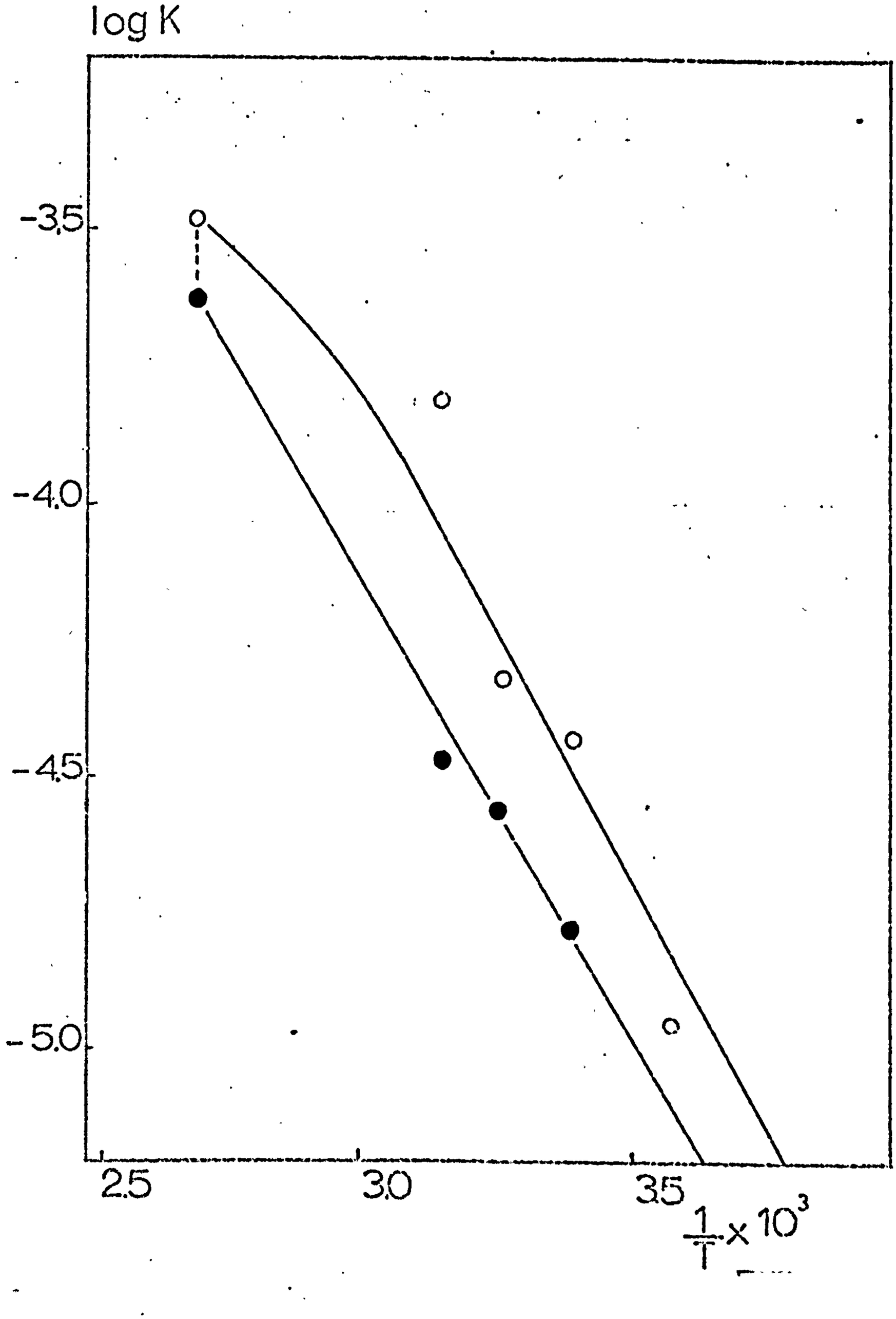

Figure 3.26. C_2H_4 polymerisation. Temperature dependence of the polymerisation rate (Arrhenius law) prior to (o), and after (•) ageing at 359 K. p= 7.6 kN.m^{-2}. (run 10E; table 3.7).

Table 3.6 continued.

$T/^oK$		$1/T \times 10^3$	$K \times 10^4$	$\log_{10}K$
320.5		3.12	11.75	-2.939
330.5	i	3.03	12.60	-2.899
330.5	f	3.03	10.78	-2.937
341.5	i	2.93	12.31	-2.909
341.5	f	2.93	9.70	-3.013
352.0	i	2.84	11.63	-2.934
352.0	f	2.84	8.75	-3.058
373.0		2.68	10.84	-2.964

i = initial value.

f = final value.

At higher temperatures this relationship did not hold and K became time dependent. It was believed that the progressive decrease in the value of K at temperatures above 320K resulted from deactivation of the polymerisation sites. This was confirmed by ageing an active catalyst sample at 359K and comparing the pre-ageing (fig. 3.24) and post-ageing (fig. 3.25) polymerisation activities (run 10E). Figure 3.26 (table 3.7) illustrates that while heat treatment above 320K led to a decay of catalyst activity, the slope of the Arrhenius plot remained effectively unchanged. In view of this catalyst deactivation at elevated temperatures, subsequent studies of the temperature dependence of the polymerisation system were carried out below 320K.

Table 3.7. Temperature dependence of ethylene polymerisation before and after high temperature (359K) treatment of the sample. (fig.3.26; run 10E) $p = 7.6\ kN.m^{-2}$. The units of K are $(\text{m.moles } C_2H_4/\text{mg.Ti})^2.\ min.^{-1}(kN.m^{-2})^{-1}$

$T/^oK$		$1/T \times 10^3$	$K \times 10^4$	$\log_{10}K$
273.0		3.66	0.111	-4.953
286.0		3.50	0.374	-4.427
297.2		3.36	0.480	-4.319
307.5		3.25	1.154	-3.818
359.0	i	2.79	3.320	-3.478
359.0	f	2.79	2.440	-3.612
286.5		3.48	0.170	-4.770
297.2		3.36	0.180	-4.552
307.5		3.25	0.341	-4.467

i = initial value

f = final value

Three determinations of the activation energy for the polymerisation of ethylene were made over the temperature range 273 to 320 K. Catalyst activity, as a function of temperature for each of the three polymerisations (runs 11E, 12E, 13E) is shown in figures 3.27, 3.28 and 3.29. The corresponding Arrhenius plots are illustrated in figure 3.30 (table 3.8). The values of the constants K_o and E_{act} (equation 3.13) are given in table 3.9 and the mean value of the activation energy was found to be $36.0 \pm 4.2\ kJ.mole^{-1}$.

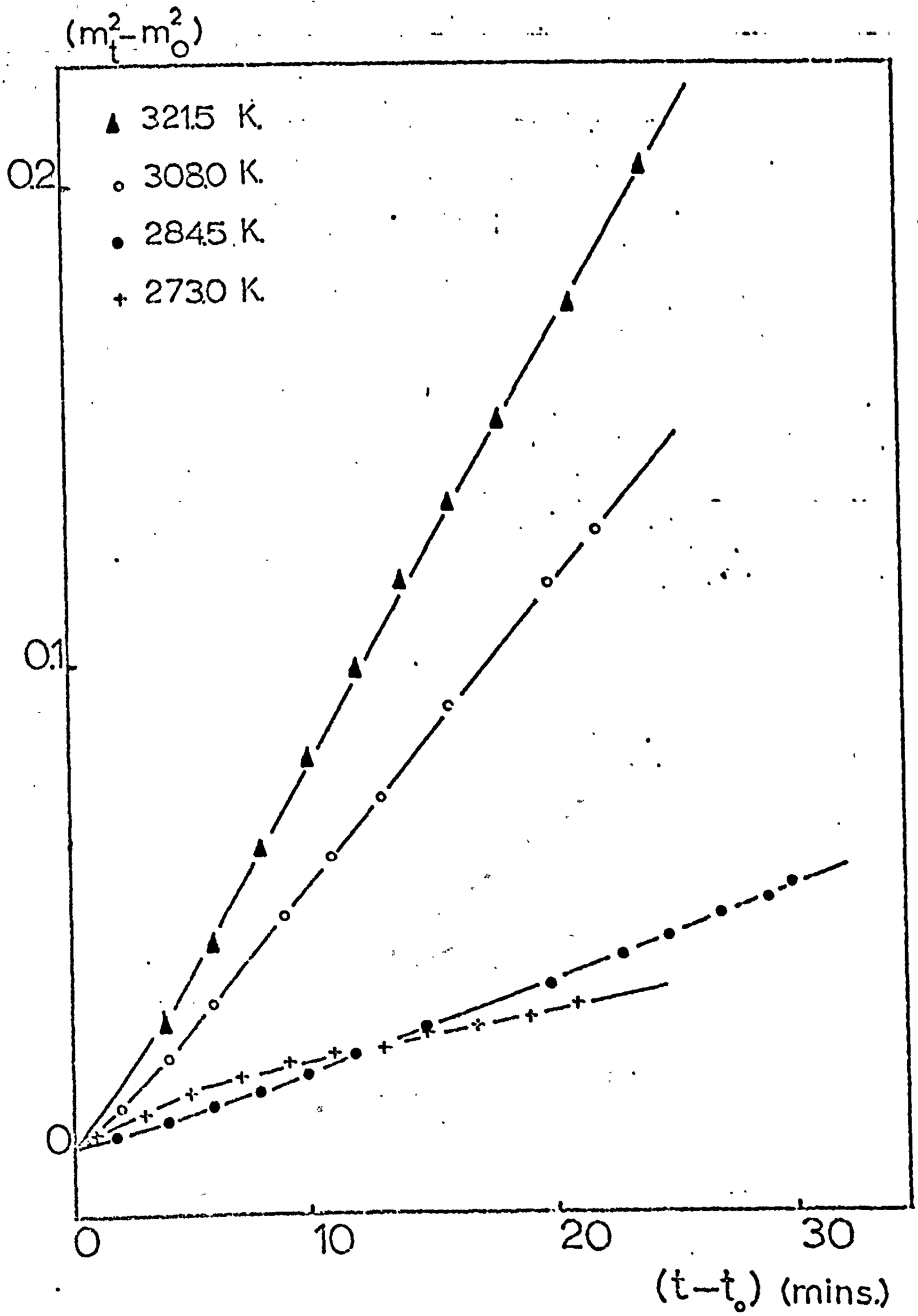

Figure 3.27. C_2H_4 polymerisation. Variation of polymerisation rate with temperature below the catalyst decomposition temperature. $p = 7.4\ kN.m^{-2}$. (run 11E).

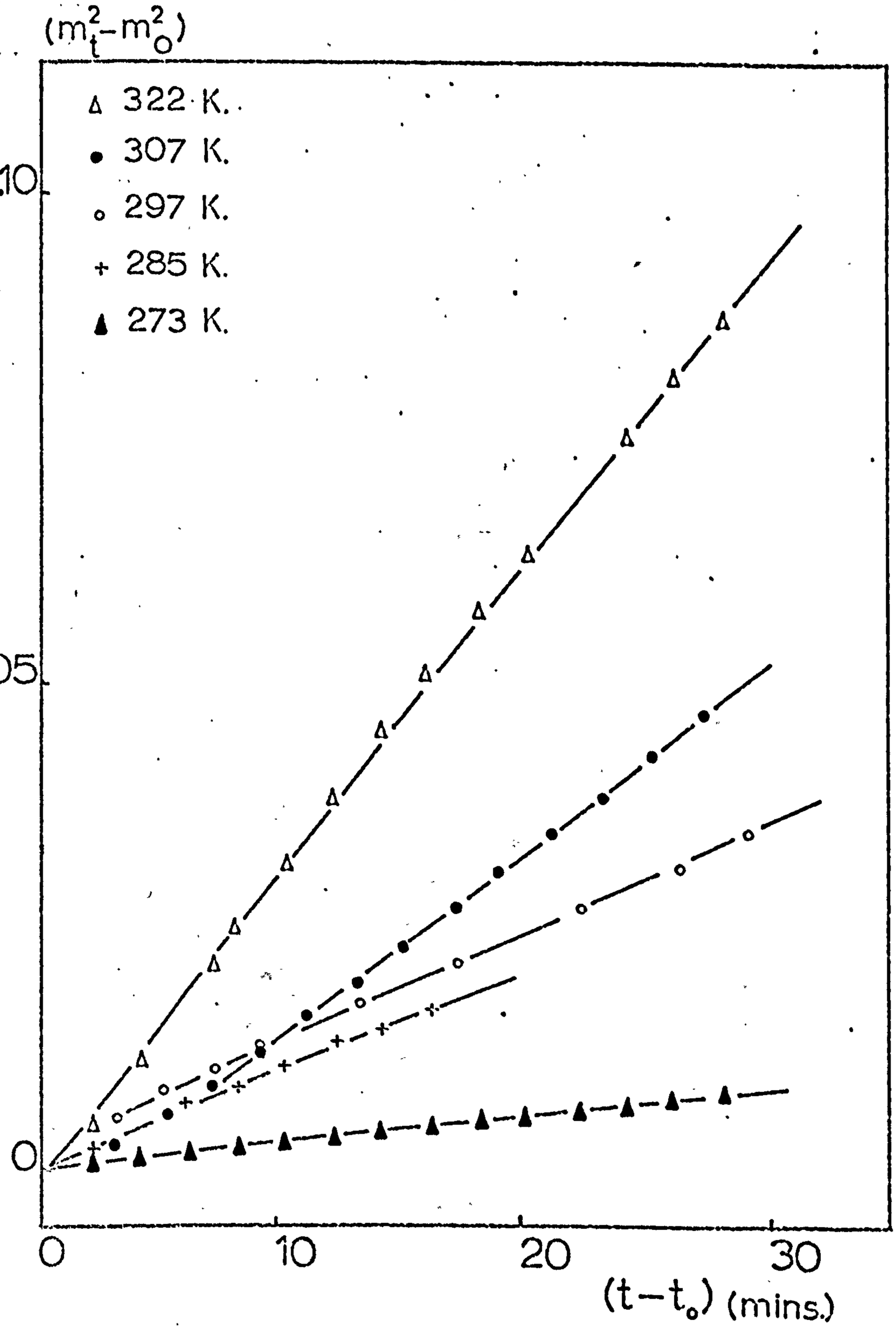

Figure 3.23. C_2H_4 polymerisation. Variation of polymerisation rate with temperature below the catalyst decomposition temperature $p = 7.4\ kN.m^{-2}$ (Run 12E).

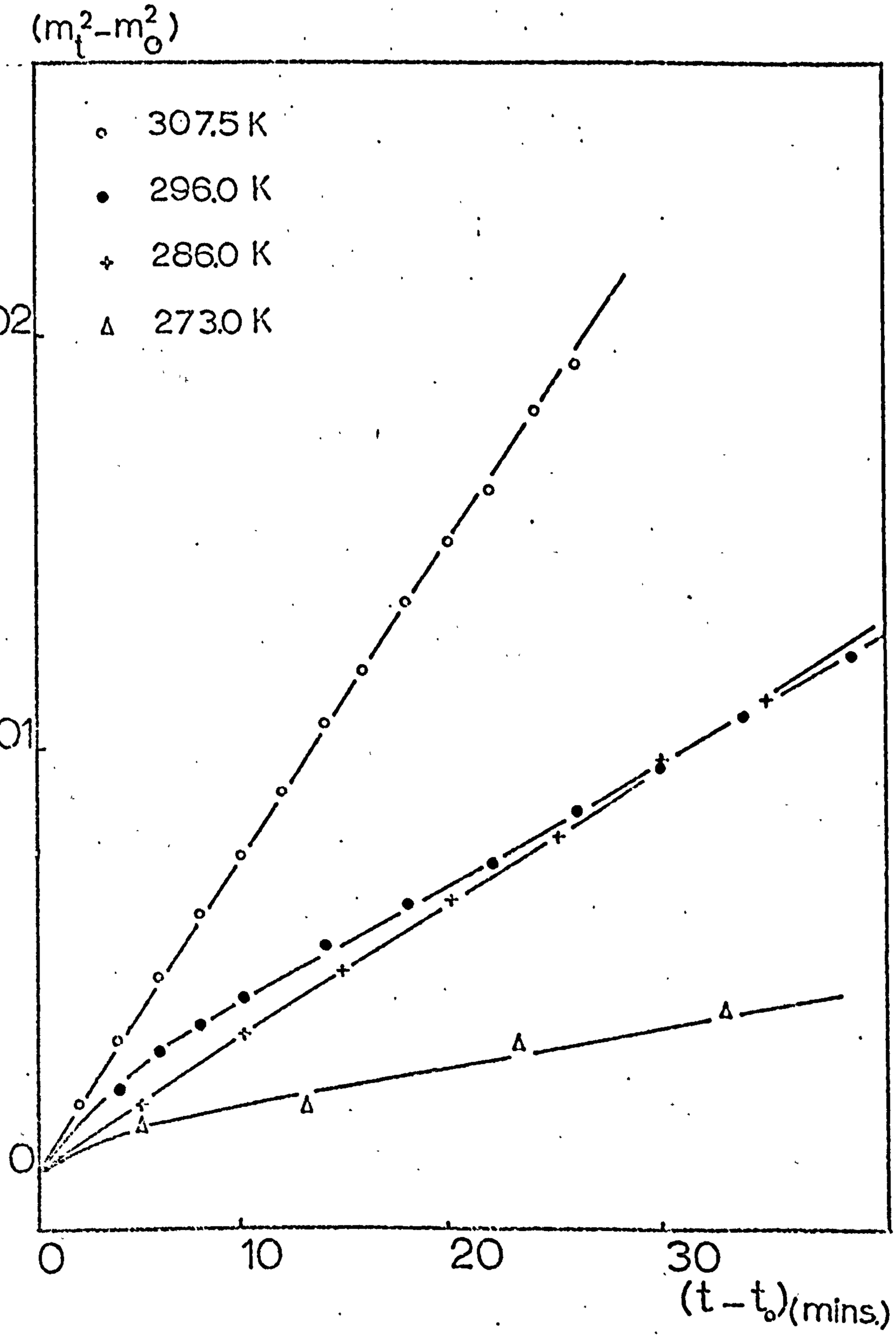

Figure 3.29. C_2H_4 polymerisation. Variation of polymerisation rate with temperature below the catalyst decomposition temperature. $p = 7.4$ kN.m^{-2}. (run 13E).

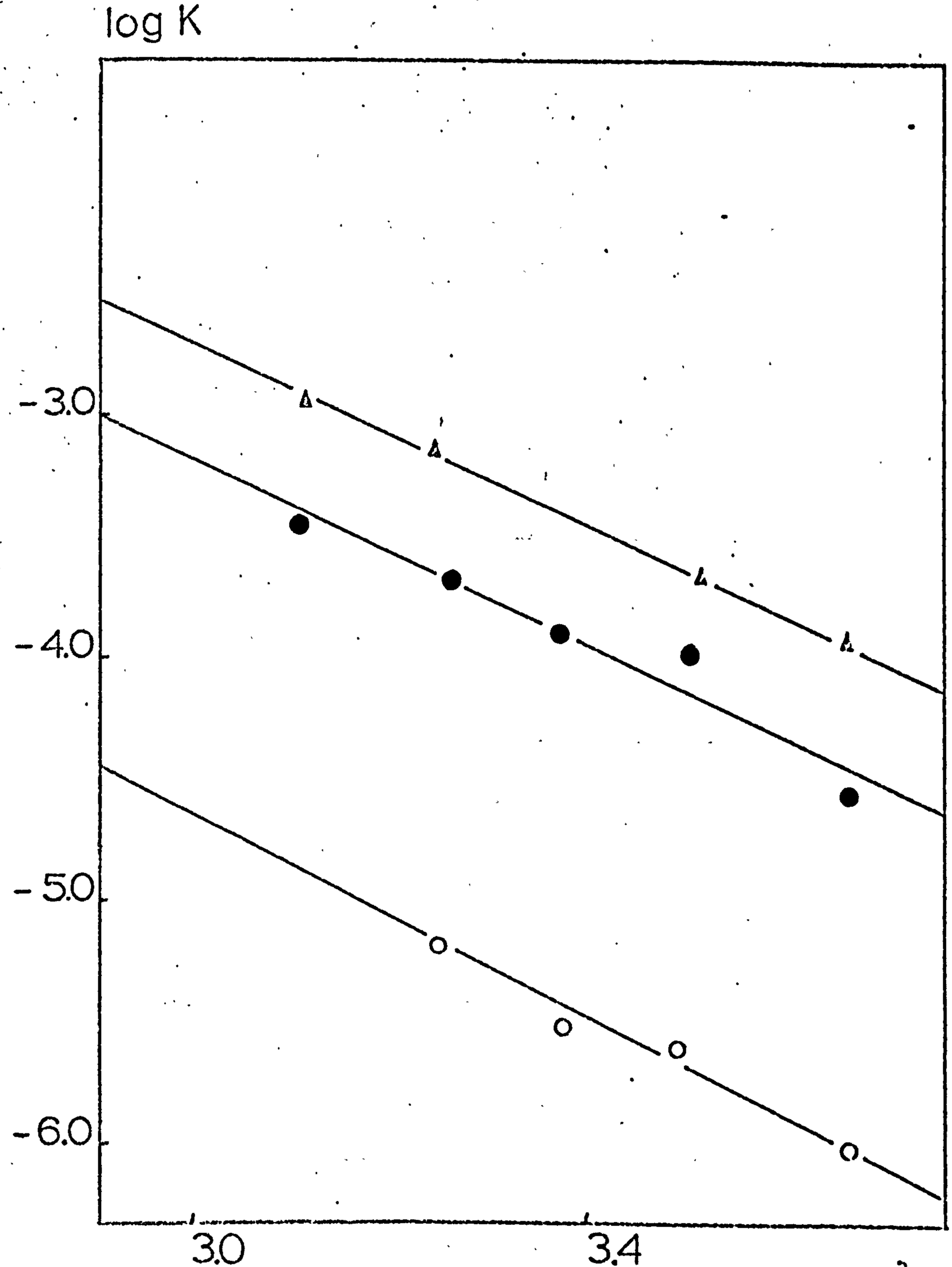

Figure 3.30. C_2H_4 polymerisation. Temperature dependence of the polymerisation. rate (Arrhenius law) (▲ run 11E; ● 12E; o run 13E; table 3.8).

Table 3.8. Arrhenius plots for the polymerisation of ethylene (fig. 3.30; runs 11E, 12E, 13E.) p = 7.40 $kN.m^{-2}$. The units of Kare $(m.moles\ C_2H_4/mg.Ti)^2.min.^{-1}\ (kN.m^{-2})^{-1}$.

Run No.	$T/^oK$	$1/T \times 10^3$	$K \times 10^4$	$\log_{10}K$
11E	273.0	3.66	1.50	-3.823
	284.5	3.51	2.66	-3.574
	308.0	3.24	9.00	-3.046
	321.5	3.12	14.95	-2.854
12E	273.0	3.66	0.37	-4.427
	285.0	3.53	1.37	-3.864
	297.0	3.37	1.69	-3.772
	307.0	3.26	2.75	-3.561
	322.0	3.11	4.38	-3.358
13E	273.0	3.66	0.013	-5.903
	286.0	3.50	0.033	-5.480
	296.0	3.38	0.039	-5.407
	307.5	3.25	0.087	-5.061

Table 3.9. Temperature dependence parameters for ethylene polymerisation (fig. 3.30; runs 11E, 12E, 13E), see equation 3.13.

Run No.	$K_o \times 10^{-2}$	E_{act} / $kJ.mole^{-1}$
11E	6.2 ± 2.8	34.9 ± 1.7
12E	2.8 ± 2.6	35.7 ± 6.3
13E	0.3 ± 0.2	38.6 ± 3.4

b) C_3H_6 polymerisation. The temperature dependence of the propylene polymerisation was studied and was found to obey an Arrhenius type law (equation 3.13) over the range 273 to 320K. Figures 3.31, 3.32 and 3.33 show the variations of catalyst activity with temperature for three polymerisations (runs 14E, 15E, 16E). The corresponding

Table 3.10. Arrhenius plots for the polymerisation of propylene (fig. 3.34; runs 14E, 15E, 16E). The units of K are (m.moles C_3H_6/mgTi)^2. min.$^{-1}$ (kN.m^{-2})$^{-1}$.

Run No.	p/kN.m^{-2}	T/^oK	1/T x 10^3	K x 10^4	$\log_{10}$K
14E	16.3	273.0	3.66	2.48	-6.606
		292.0	3.42	4.88	-6.311
		307.5	3.25	7.50	-6.125
		318.5	3.14	13.55	-5.868
15E	11.5	273.0	3.66	0.74	-7.129
		292.0	3.42	1.68	-6.774
		307.5	3.25	2.56	-6.592
		318.5	3.14	3.88	-6.411
16E	18.5	273.0	3.66	0.66	-7.182
		291.5	3.43	1.03	-6.986
		307.0	3.26	2.55	-6.593
		318.5	3.14	3.56	-6.448

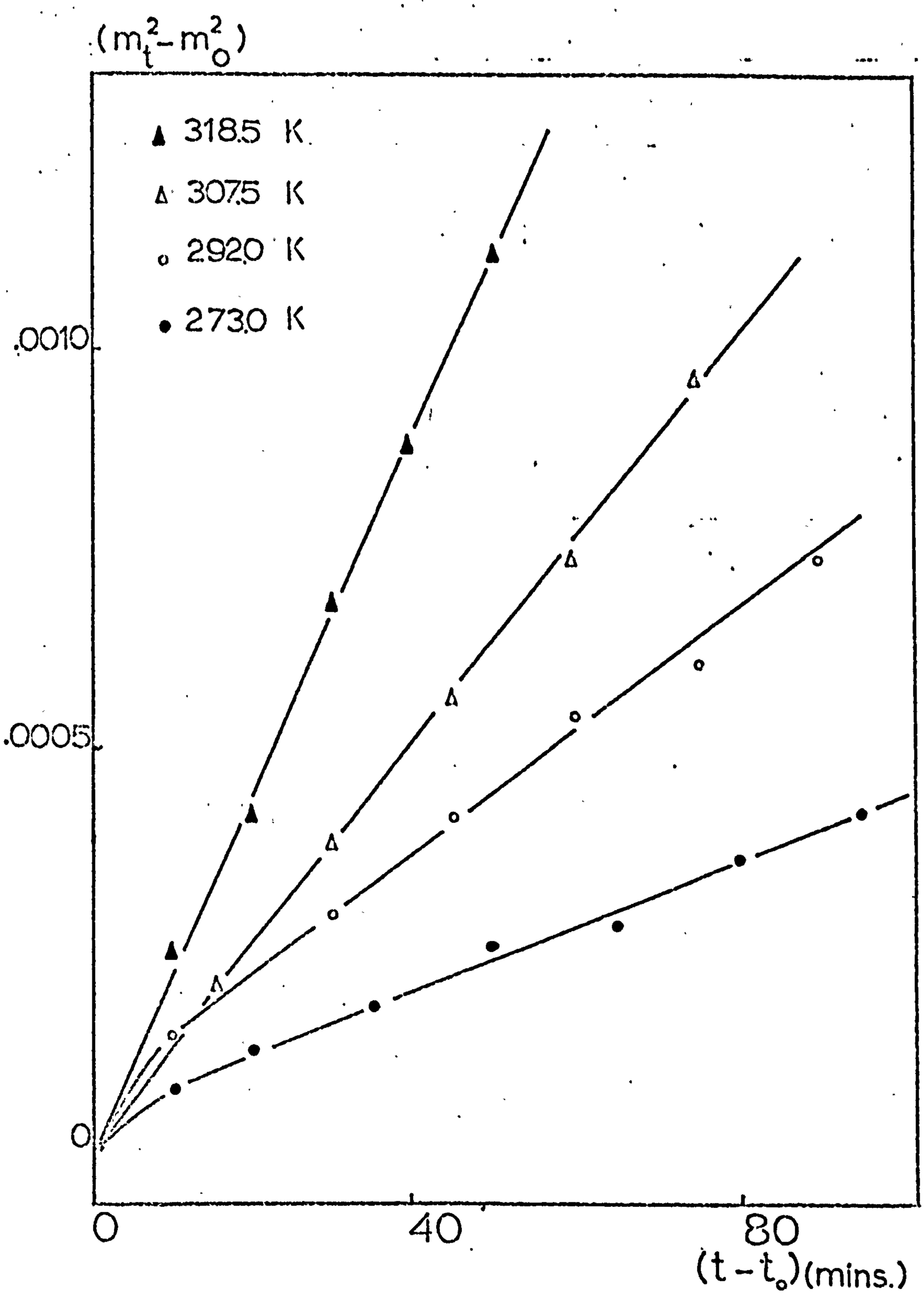

Figure 3.31. C_3H_6 polymerisation. Variation of polymerisation rate with temperature. $p = 16.3\ kN.m^{-2}$ (Run 14E).

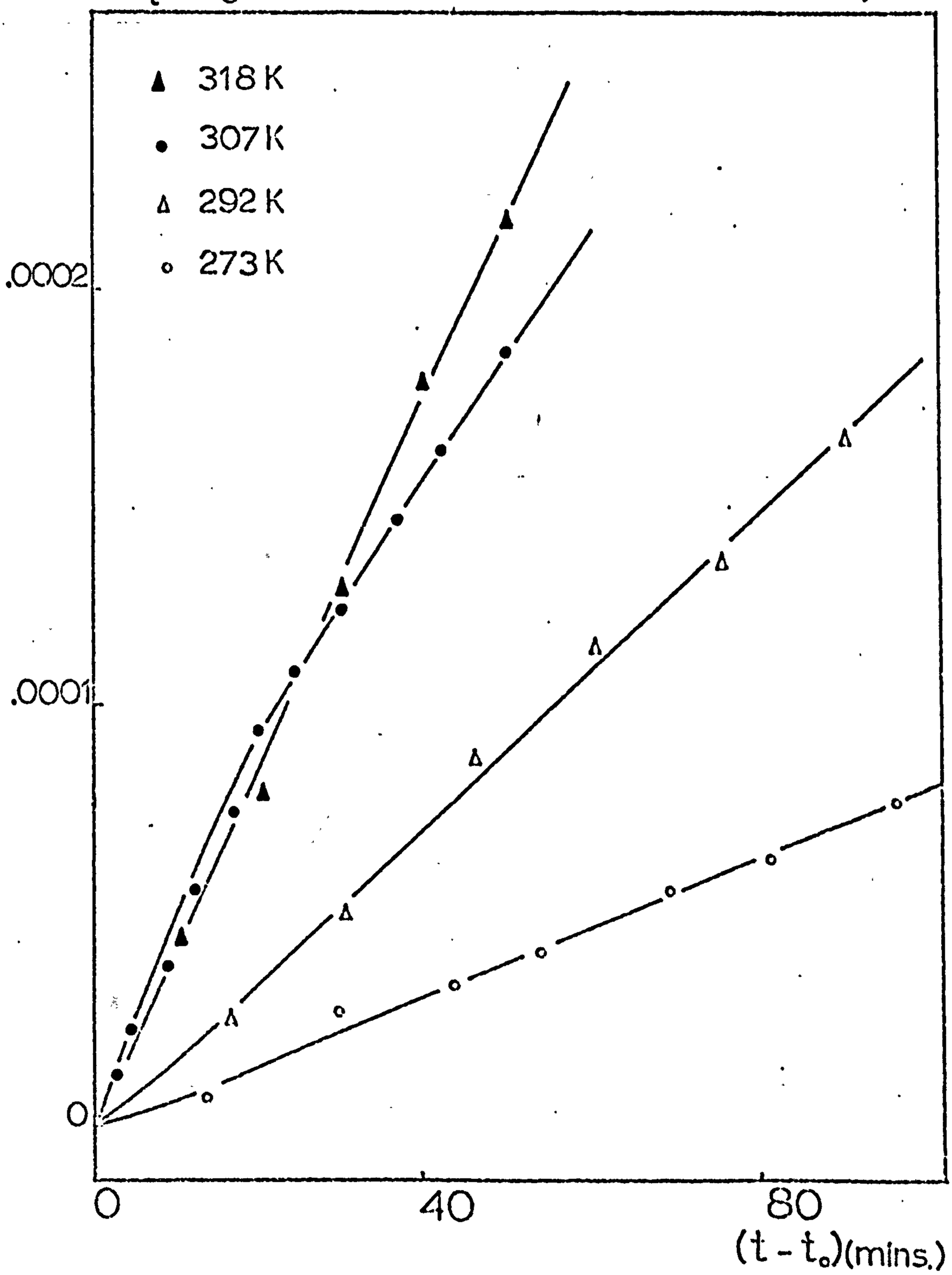

Figure 3.32. C_3H_6 polymerisation. Variation of polymerisation rato with temperature. $p = 11.5\ kN.m^{-2}$. (run 15B).

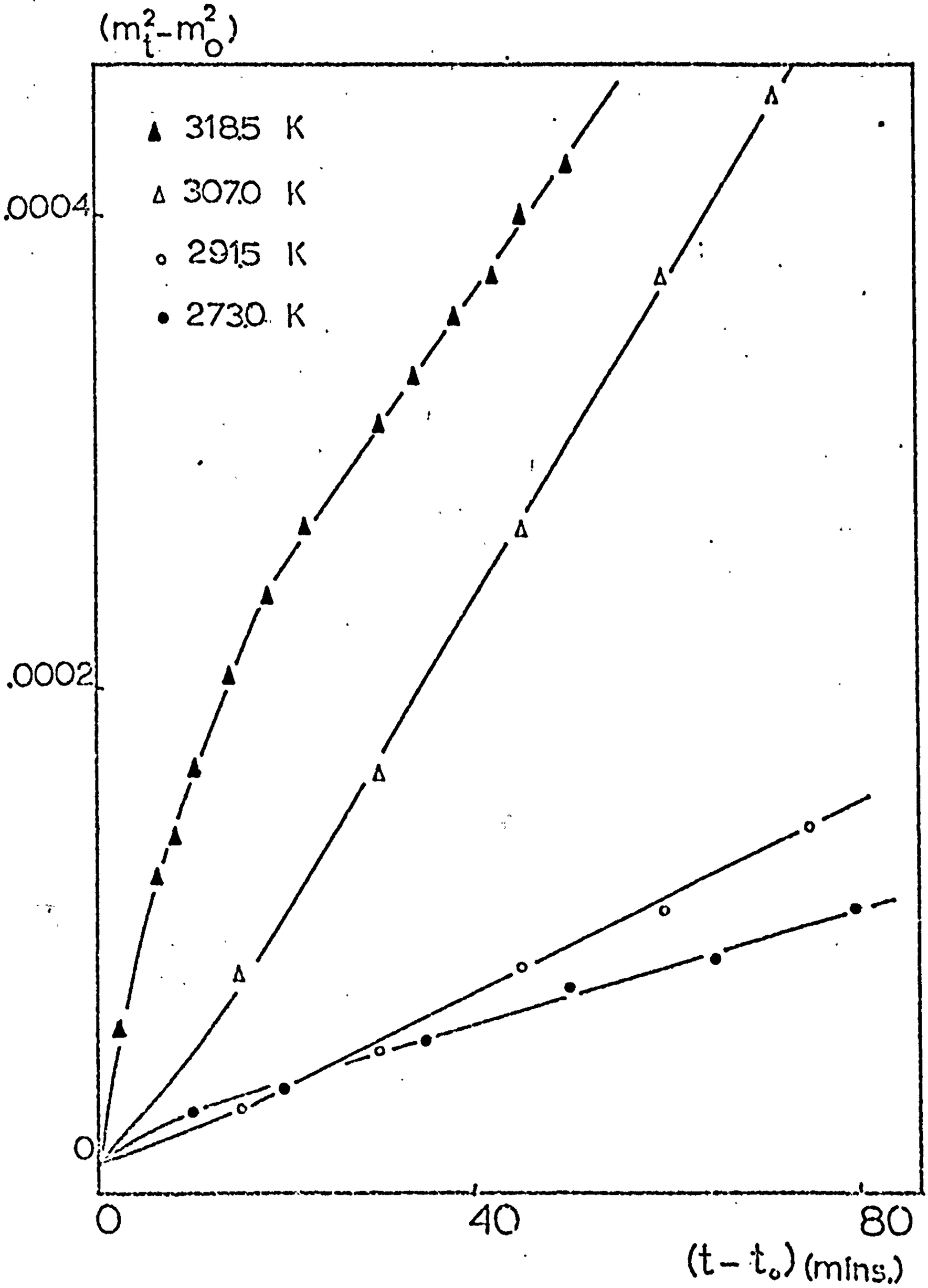

Figure 3.33. C_3H_6 polymerisation. Variation of polymerisation rate with temperature. $p = 18.5\ kN.m^{-2}$. (run 16E).

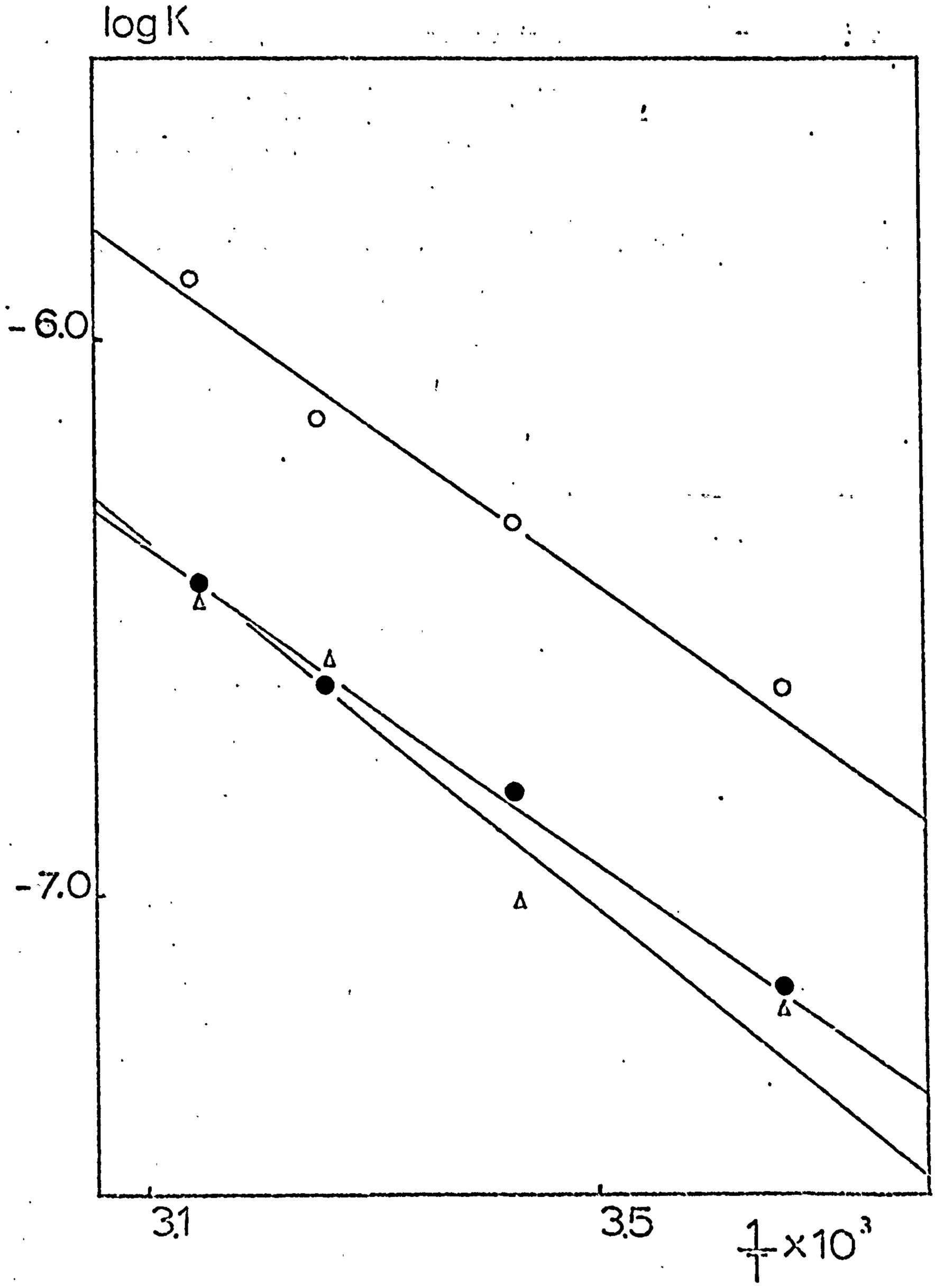

Figure 3.34. C_3H_6 polymerisation. Temperature dependence of the polymerisation rate (Arrhenius law) (o run 14E; ● run 15E; Δ run 16E; table 3.10).

Table 3.11. Temperature dependence parameters for propylene polymerisation (fig. 3.34; runs 14E, 15E, 16E), see equation 3.13.

Run No.	$K_o \times 10^2$	E_{act}/kJ.mole^{-1}
14E	4.3 ± 29.7	27.3 ± 1.7
15E	1.2 ± 0.6	27.3 ± 1.7
16E	3.6 ± 1.8	30.7 ± 5.0

Arrhenius plots are shown in fig. 3.34 (table 3.10) and the values of the constants K_o and E_{act} (equation 3.13) are given in table 3.11. The mean activation energy for propylene polymerisation was found to be 28.6 ± 2.9 kJ.mole^{-1}.

3.D.5) The effect of gaseous impurities on the polymerisation rate of ethylene (figure 3.35).

a) Hydrogen. The effect of adding hydrogen gas to an established ethylene polymerisation run at 308K is shown in figure 3.35. Hydrogen (1.06 kN.m^{-2}) was added after 40 minutes of polymerisation and the ratio of C_2H_4 to H_2 above the catalyst was 7.5:1.0. The rate of polymerisation was not affected by the addition of hydrogen.

b) Oxygen. The sensitivity of the polymerisation catalyst to gaseous oxygen is shown in figure 3.35. An ethylene polymerisation

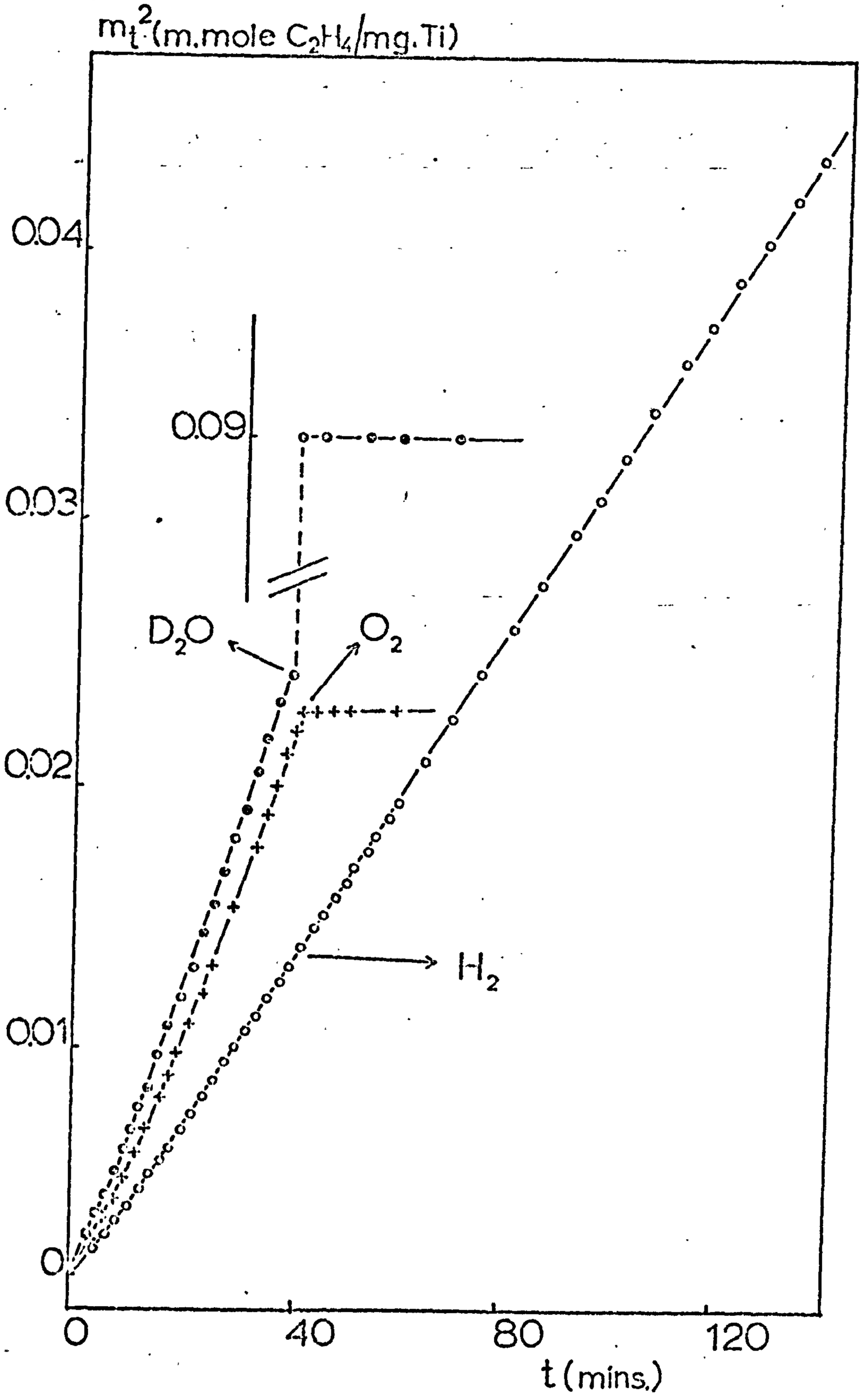

Figure 3.35. C_2H_4 polymerisation. The effect of gaseous additives on the polymerisation rate. $P_{C_2H_4}$ = 7.50 kN.m^{-2}; P_{H_2} = 1.06 kN.m^{-2}; T = 308 K.

run at 308K was followed for 40 minutes and then the monomer was withdrawn from the system. Oxygen (0.40 $kN.m^{-2}$) was admitted to the reaction vessel for 3 minutes and then removed by pumping for 15 minutes. The colour of the catalyst sample changed from grey to white during the oxygen treatment. Following the re-admission of ethylene to the system, no polymerisation could be detected, even after twelve hours.

c) $\underline{D_2O}$. After 40 minutes reaction, the C_2H_4 was withdrawn from the reaction vessel and the active catalyst was exposed to D_2O vapour at 308K for three minutes. A large weight increase was recorded over this three minute period. After pumping away excess reagent, the sample was re-exposed to ethylene gas. No polymerisation activity was detected.

PART E Studies of the nature of the surface of the active catalyst.

3.E.1) Catalyst solubility.

The active catalyst was readily wetted by aqueous media and was completely soluble in dilute mineral acids. Following olefin polymerisation, the catalyst particles exhibited hydrophobic character and became insoluble in hot or cold, dilute or concentrated hydrochloric and nitric acids. Addition of a surface active agent (Sunlight Lemon Liquid) led to wetting of the catalyst but did not affect the solubility of the particles in aqueous acid media (less than 4% by weight after stirring with warm dilute hydrochloric acid for 18 hours). Treatment

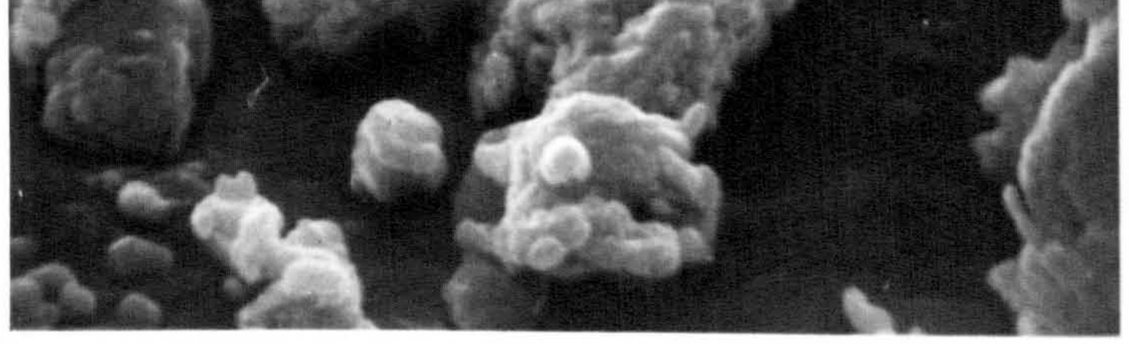

10μ.

Figure 3.36a. Scanning electron micrograph of the catalyst surface.

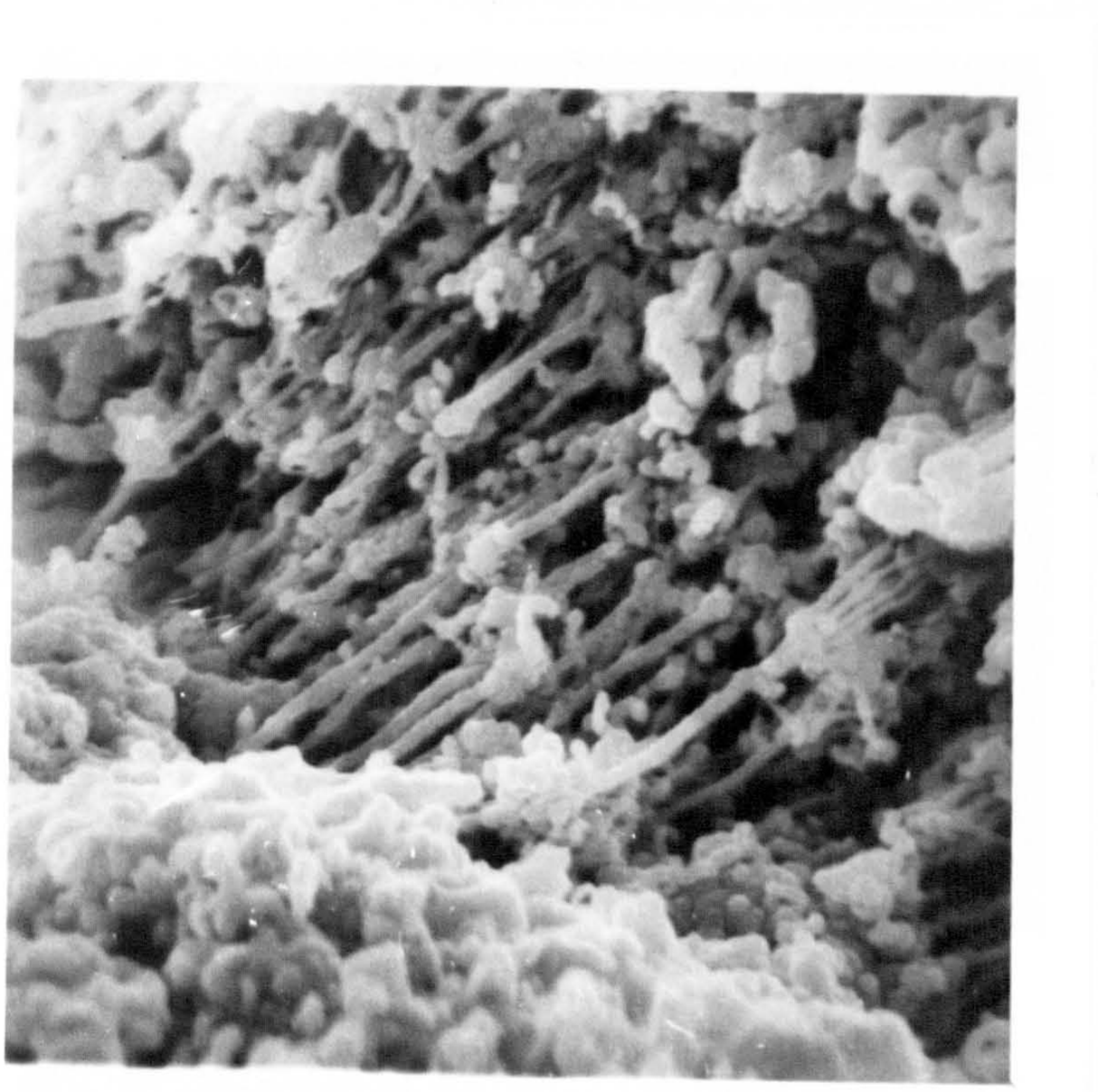

Figure 3.36b. Scanning electron micrograph of the catalyst surface after ethylene polymerisation. ($T = 308K$, $P = 8.0\ kN.m^{-2}$.)

of the polymerised samples with boiling tetralin prior to the solubility test resulted in the restoration of almost complete solubility in cold hydrochloric acid.

3.E.2). Scanning electron microscopy (S.E.M.)

S.E.M. was used to investigate the surface features of the catalyst powder prior to and after ethylene polymerisation. The fresh catalyst surface is shown in figure 3.36a. Ethylene polymerisation did not substantially alter the appearance of the surface. The polymer (which imparted hydrophobic properties to the catalyst particles) appeared as a continuous film except for small sporadic areas of fibrous growths (figure 3.36b).

PART F. Permeation Studies.

3.F.1) Permeation of ethylene gas in a polyethylene film.

Monomer transfer through a polymer film was studied by following the rate of pressure increase of the low pressure side of the film.

Two different polyethylenes were investigated over the temperature range 289 to 322 K. and the pressure/time plots are shown in figures 3.37 and 3.38. All of the curves followed the same pattern, exhibiting a non-linear induction period succeeded by a constant rate of monomer transfer. The linear portion of the curve, which yielded the permeability constant (P), was extrapolated to give the time lag (θ secs). For both samples the values of θ were too small to be determined with any accuracy, although in each case the value of θ decreased with increasing temperature. The value of P at each temperature was calculated (table 3.10) using the relationship:-

$$P = \frac{V \times 273 \times l}{a \times T \times p \times 101.23 \times 22.414} \times \frac{dp}{dt} \qquad (3.14)$$

P = Permeability constant $\left[\text{moles.}\ m^{-1}.sec^{-1}.(kN.m^{-2})^{-1} \right]$

V = volume of the low pressure side of the permeation cell (0.153 l.)

T = room temperature

l = film thickness (m)

a = film area = $2.03 \times 10^{-3}\ m^2$

$\frac{dp}{dt}$ = gradient of the linear portion of the pressure/time plot ($kN.m^{-2}.sec^{-1}$)

p = pressure on high pressure side of cell ($kN.m^{-2}$)

The permeability of additive-free polyethylene was found to be greater than that of Marlex, a commercial polymer. Over the temperature range studied, P obeyed an Arrhenius type law (figure 3.39; table 3.12).

$$P = P_o \exp.\left(\frac{-E_p}{RT} \right) \qquad (3.15)$$

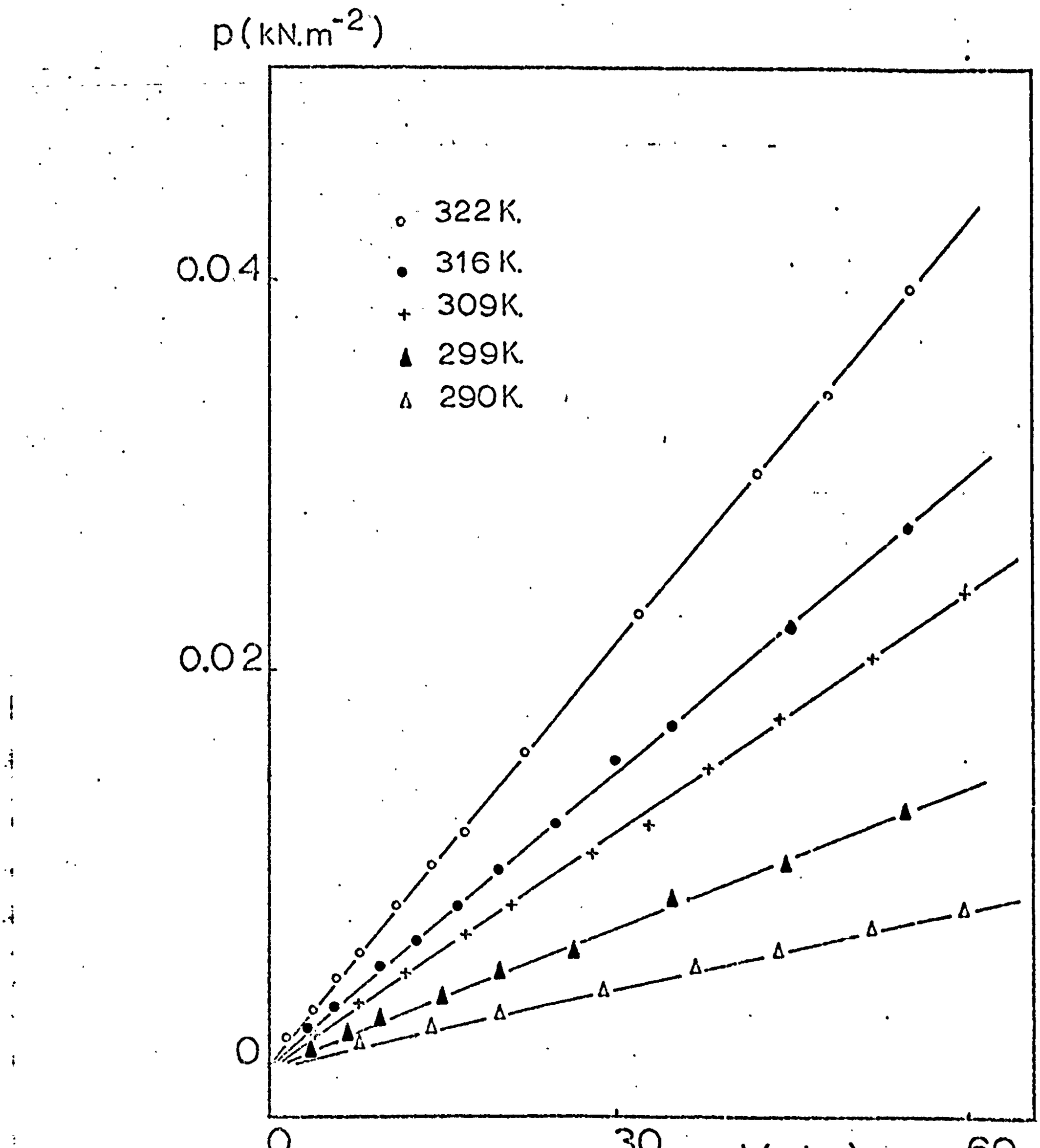

Figure 3.37. The permeation of C_2H_4 gas through a Marlex polyethylene film. $l = 7.0 \times 10^{-5}$m; $P_{C_2H_4} = 85.3$ kN.m^{-2}.

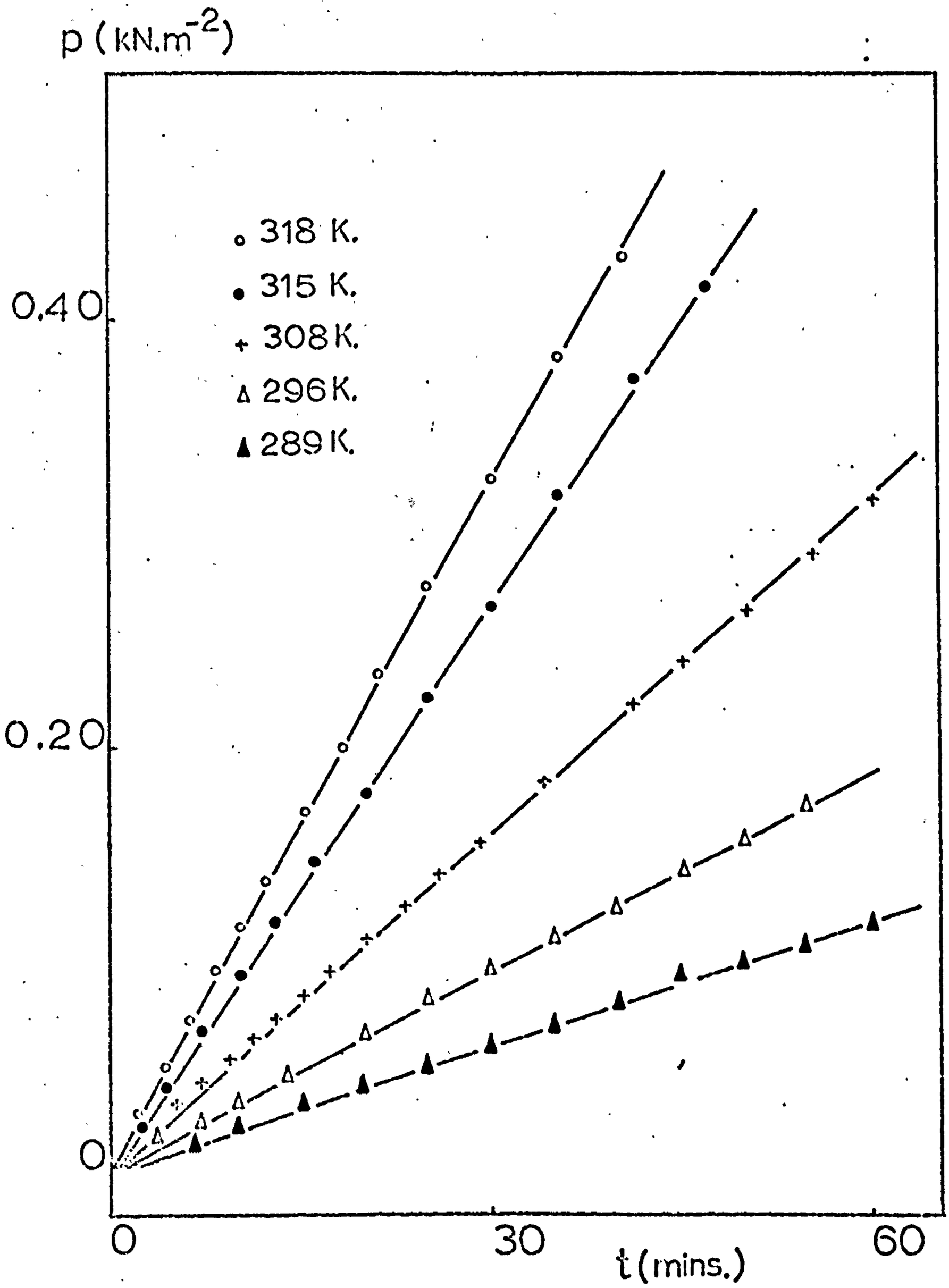

Figure 3.38. The permeation of C_2H_4 gas through an additive-free polyethylene film. $l = 4.0 \times 10^{-5}$ m.; $P_{C_2H_4} = 86.0$ kN.m^{-2}.

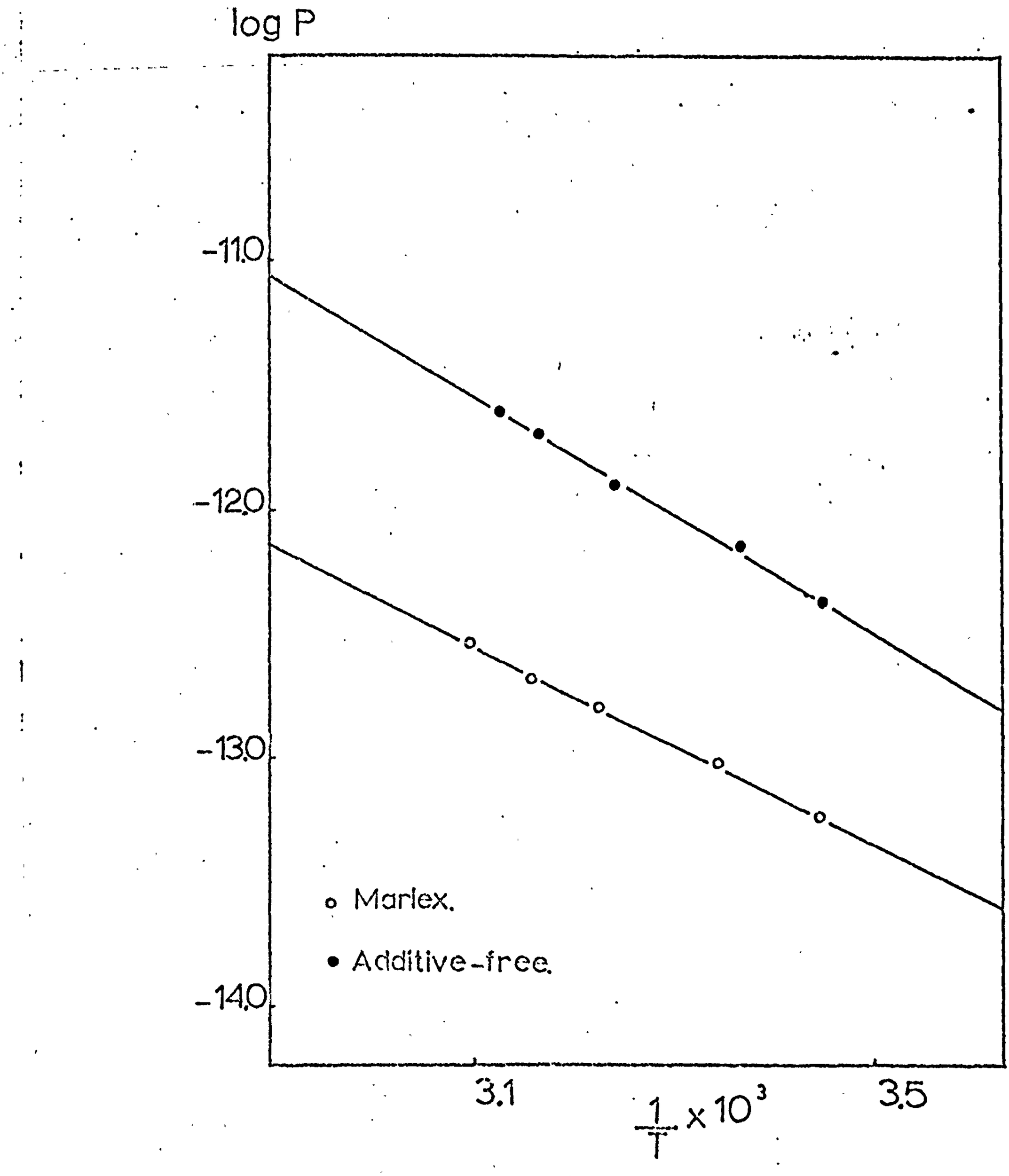

Figure 3.39. The temperature dependence of the permeability coefficient (P) for the system C_2H_4/polyethylene. (equation 3.15; table 3.12).

The values of P_o and E_p for the two polyethylenes are given in table 3.13. The mean value of the activation energy for permeation (E_p) of ethylene in polyethylene was found to be 41.5 (± 2.1) $kJ.mole^{-1}$.

Table 3.12. Permeation of C_2H_4 through $(C_2H_4)_n$ - the temperature dependence of P (figure 3.39; equation 3.15). The units of P are moles. m^{-1}. $sec.^{-1}$ $(kN.m^{-2})^{-1}$.

$T/^oK$	$1/T \times 10^3$	$P \times 10^{13}$	$\log_{10}P$
Marlex polyethylene	$p = 85.3$	$kN.m^{-2}$;	$l = 7.0 \times 10^{-5}$ m.
290	3.45	0.60	-13.22
299	3.35	1.03	-12.99
309	3.23	1.73	-12.76
316	3.17	2.20	-12.66
322	3.11	3.09	-12.51
Additive-free polyethylene	$p = 86.0$ $kN.m^{-2}$;	$l = 4.0 \times 10^{-5}$ m.	
289	3.45	4.35	-12.36
296	3.38	7.54	-12.12
308	3.25	12.67	-11.90
315	3.18	21.26	-11.67
318	3.14	25.99	-11.59

Table 3.13. Permeation of C_2H_4 through $(C_2H_4)_n$ - the values of P_o and E_p for two polyethylenes (equation 3.15).

$(C_2H_4)_n$	P_o	$E_p/kJ.mole^{-1}$
Marlex	$3.9(\pm 2.3) \times 10^{-7}$	37.8(± 2.5)
additive-free	$8.7(\pm 5.0) \times 10^{-5}$	45.4(± 1.3)

3.F.2) Permeation of propylene in a polypropylene film.

The mass transfer curves for the permeation of propylene through a high purity polypropylene film are shown in figure 3.40. Values of θ were sufficiently large to permit the determination of the diffusion coefficient (D) and the solubility coefficient (S) using equations 1.12 and 1.6 respectively (table 3.14).

Table 3.14. Permeation of C_3H_6 through $(C_3H_6)_n$ - the variation of P, D and S with temperature. Pressure = 86.0 $kN.m^{-2}$; l = 1.3 x 10^{-4}m.

T / °K	P x 10^{13} / moles.sec.$^{-1}$m^{-2}(kN.m^{-2})$^{-1}$	D x 10^{13} / m^2.sec^{-1}	S / moles.m^{-3}.(kN.m^{-2})$^{-1}$
289	1.73	5.16	0.335
298	2.33	10.10	0.231
310	3.94	18.28	0.216
315	5.23	25.65	0.204

Over the temperature range 289 to 315K, relationships 3.15, 3.16 and 3.17 were obeyed (table 3.15; figure 3.41) and the values of P_o, D_o, S_o, E_p, E_D and ΔH_S are given in table 3.16.

$$D = D_o \exp\left(\frac{-E_D}{RT}\right) \qquad (3.16)$$

$$S = S_o \exp\left(\frac{-\Delta H_S}{RT}\right) \qquad (3.17)$$

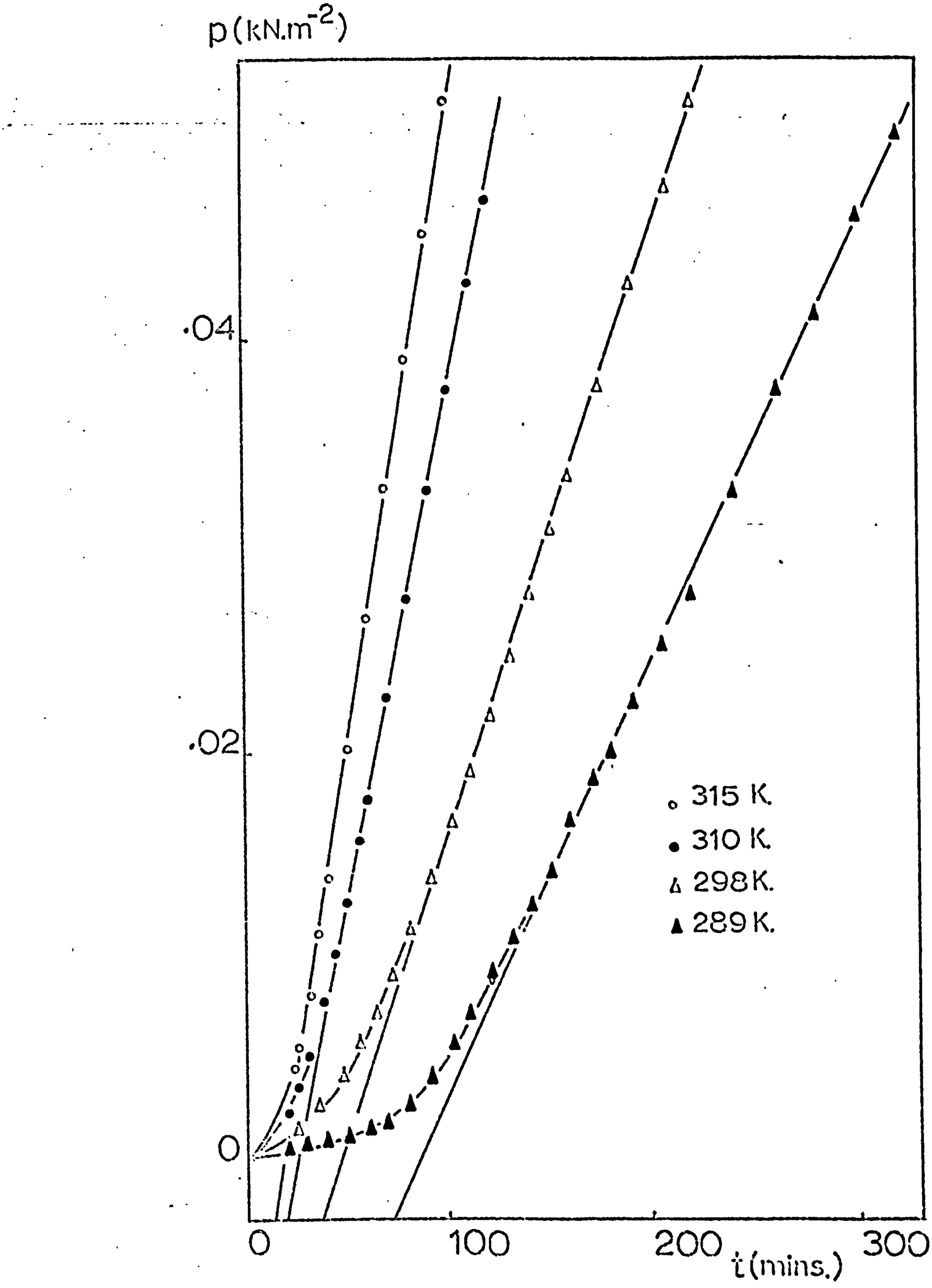

Figure 3.40. The permeation of propylene gas through a polypropylene film. $p = 86.0\ kN.m^{-2}$ $l = 1.3 \times 10^{-4} m$.

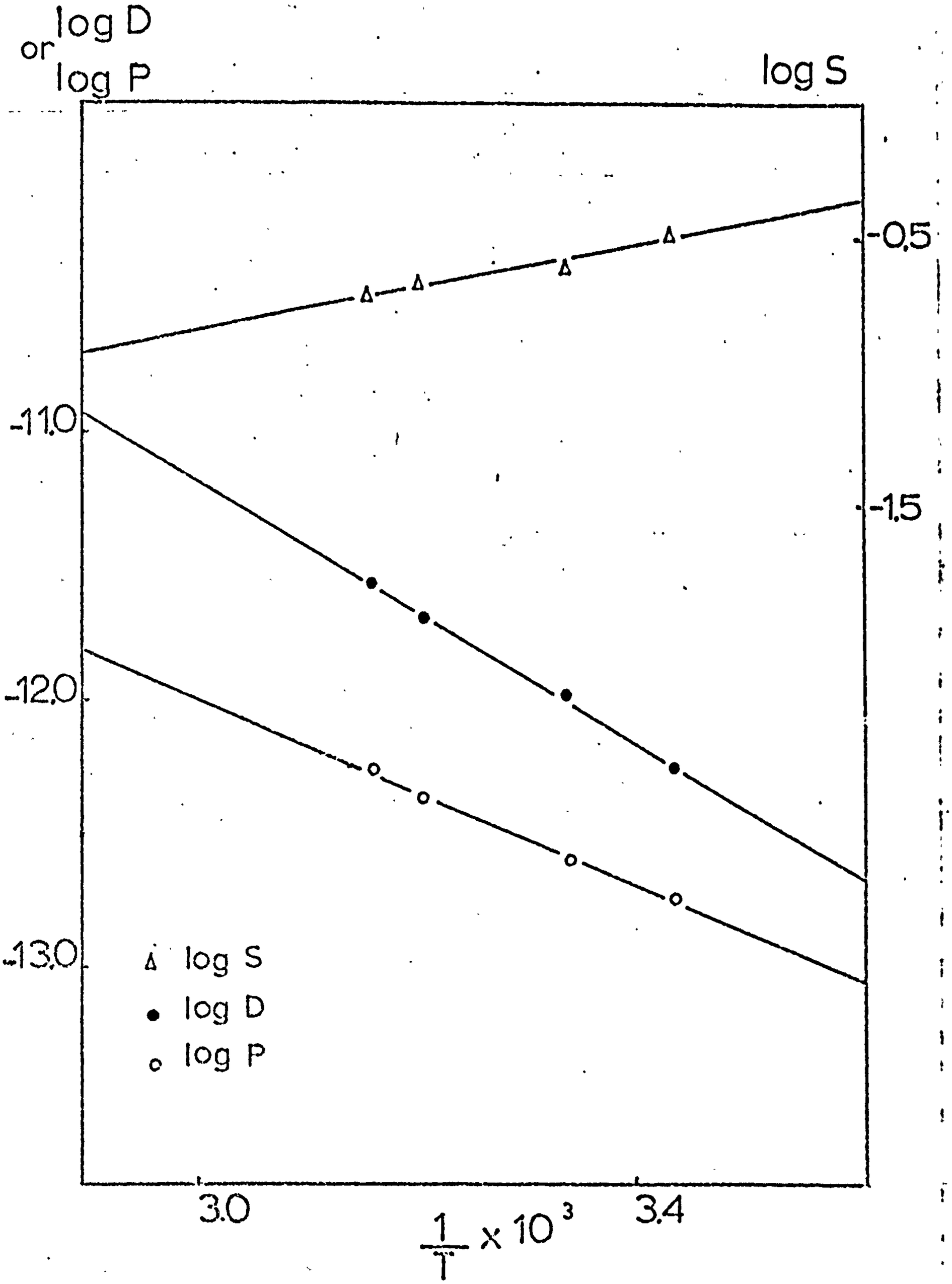

Figure 3.41. The temperature dependences of P, D and S for the system C_3H_6/polypropylene (equations 3.15, 3.16, 3.17; table 3.15).

Table 3.15. Permeation of C_3H_6 through $(C_3H_6)_n$ - temperature dependence of P, D and S. Pressure 86.0 $kN.m^{-2}$; 1 = 1.3×10^{-4}m. (figure 3.41).

$\frac{1}{T} \times 10^3$	$\log_{10}P$	$\log_{10}D$	$\log_{10}S$
3.46	-12.76	-12.29	-0.47
3.35	-12.63	-12.00	-0.63
3.22	-12.40	-11.74	-0.66
3.18	-12.28	-11.59	-0.69

Table 3.16. Permeation of C_3H_6 through $(C_3H_6)_n$ - values of the temperature dependence parameters (equations 3.15, 3.16, 3.17)

$$P_o = 1.3\ (\pm 5.0) \times 10^{-7}$$

$$D_o = 10.5(\pm 6.7) \times 10^{-5}$$

$$S_o = 6.9(\pm 8.3) \times 10^{-4}$$

$$E_p = 32.8\ (\pm 3.8)\ kJ.mole^{-1}$$

$$E_D = 46.5(\pm 1.7)\ kJ.\ mole^{-1}$$

$$\Delta H_S = -14.7(\pm 2.1)\ kJ.\ mole^{-1}$$

The results tabulated in table 3.16 are in good agreement with equation 1.10:-

$$E_p = E_D + \Delta H_S \qquad (1.10)$$

CHAPTER FOUR

DISCUSSION OF RESULTS

PART A Catalyst activation.

4.A.1) Studies on a magnesium oxide carrier.

a) Infrared studies

i) MgO. The two bands in the infrared spectrum of the calcined magnesia surface (fig. 3.1a) have been assigned to the two different hydroxyl environments. Characteristically sharp free-hydroxyl stretching vibrations (3770 cm^{-1}) and perturbed H-bonded hydroxyl absorptions (3640 cm^{-1}) are in agreement with the model proposed by Anderson[76] for the hydroxylated magnesia surface.

ii) $MgO/TiCl_4$. The reaction of $TiCl_4$ vapour at such a magnesia surface is undoubtedly complicated by the formation of HCl as a product of the initial reactions:

$$TiCl_4 + MgOH \longrightarrow Cl_3.Ti\text{-}O\text{-}Mg + HCl \qquad (4.1)$$

$$TiCl_4 + 2MgOH \longrightarrow Cl_2.Ti\begin{matrix}O\text{-}Mg\\O\text{-}Mg\end{matrix} + 2HCl \qquad (4.2)$$

Interaction of this HCl with the basic magnesia surface is likely:

$$HCl + 2MgO \longrightarrow MgOCl + MgOH \qquad (4.3)$$

$$HCl + MgOH \longrightarrow MgCl + H_2O \qquad (4.4)$$

The resultant H_2O can itself participate in a further reaction:

$$MgOTiCl_3 + H_2O \longrightarrow MgOTi(OH)Cl_2 + HCl \qquad (4.5)$$

The complex nature of the ultimate surface is reflected in its broad hydroxyl spectrum (fig. 3.1b). Direct interaction of gaseous HCl with the magnesia surface was studied using a deuteroxylated sample (fig.3.4b) having free and hydrogen-bonded deuteroxyl groups at 2680 and 2500 cm^{-1} respectively (shifted downfield by a factor of 0.74 from their hydroxyl equivalents, fig. 3.4a). The formation of H_2O (1620 cm^{-1}) and DOH (1430 cm^{-1}) was observed and attributed to equations 4.3, 4.4 and 4.6.

$$MgOD + HCl \longrightarrow MgCl + DHO \qquad (4.6)$$

A small amount of D_2O (1190 cm^{-1}) was also formed, presumably due to isotopic exchange between the aqueous species. Again the complexity of the resultant surface is demonstrated by the perturbed hydroxyl (3500 cm^{-1}) and deuteroxyl (2625 cm^{-1}) stretching vibrations. The shoulder at 2350 cm^{-1} has not been assigned although it must signify an interacting deuteroxyl environment.

(Ti-OH) groups, proposed in reaction 4.5, would be expected to absorb in the infrared between 3500 and 3600 cm^{-1}. In this region they would be masked by the very strong magnesia hydroxyl absorptions. Accordingly $SiCl_4$ was chosen as a compound closely analagous to $TiCl_4$ in both geometry and reactivity, except that (Si-OH) groups absorb above 3700 cm^{-1} and can be readily distinguished from (Mg-OH) absorptions. The infra absorption band (3740 cm^{-1}) produced by the reaction of $SiCl_4$ with the magnesia surface is characteristic of the (Si-OH) stretching vibration (fig. 3.5b). The interaction was interpreted in terms of reactions 4.7, 4.4 and 4.8, forming strong evidence for the incidence of reaction 4.5.

$$SiCl_4 + MgOH \longrightarrow SiCl_3\text{-}O\text{-}Mg + HCl \qquad (4.7)$$

$$HCl + MgOH \longrightarrow Mg\text{-}Cl + H_2O \qquad (4.4)$$

$$SiCl_3\text{-}O\text{-}Mg + H_2O \longrightarrow Si(OH)Cl_2.OMg + HCl \qquad (4.8)$$

In figure 3.1b, the shoulder at 3450 cm^{-1} is rather low for the $TiCl_2(OH)$ species and is attributed to a hydroxyl species in a very polar environment.

Thus the reaction of $TiCl_4$ with the basic magnesia surface proceeds through a complicated sequence of reactions. This is in contrast to the silica/$TiCl_4$ system[36,41], in which the HCl produced in the initial reaction does not react further with the acidic surface of the silica.

iii) <u>$MgO/TiCl_4/Al(C_2H_5)_3$</u>. Reaction of $Al(C_2H_5)_3$ with the titanium modified surface produced the spectrum shown in fig. 3.1a. The absorption peaks were assigned to symmetric (ν_s) and asymmetrical (ν_a) C-H vibrations as follows:

2955 cm^{-1}	ν_a	CH_3 stretch
2800 cm^{-1}	ν_s	CH_3 stretch
2920 cm^{-1}	ν_a	CH_2 stretch
2860 cm^{-1}	ν_s	CH_2 stretch

These bands indicate the fixation of an ethyl species (C_2H_5) on the catalyst surface.

An identical C-H stretching spectrum was produced by the direct action of $Al(C_2H_5)_3$ on the hydroxylated magnesia surface (fig. 3.6b). The fixation of the hydrocarbon species did not perturb the surface hydroxyl environments (fig. 3.6a and b), such that fixation occurred on bare oxide sites. This reflects the basic nature of the Hydroxyls, in direct contrast to those of silica which reacted readily with aluminium alkyls[36]. Subsequent exposure of the magnesia surface to $TiCl_4$ led to the removal of the ethyl species and resulted in an inactive catalyst sample. This is once again at variance with the analagous system based on silica, in which the appended alkyl reacts readily with $TiCl_4$ to yield an active polymerisation catalyst.

iv) Olefin polymerisation. The activity of catalyst samples for olefin polymerisation was demonstrated by exposure to ethylene and propylene gases. Polymer formation was evidenced by the growth of a transparent film on the surface of the catalyst disc. Infrared spectra of the (C-H) stretching region were characteristic of polyethylene and polypropylene respectively[13] (fig. 3.2 and 3.3). The spectra were not well resolved and peaks below 1200 cm^{-1}, normally used in estimating crystalline content, were not observed due to the absorptions of the oxide carrier.

Assignments

Polyethylene	2955 cm^{-1}	ν_a	CH_3 stretch
	2880 cm^{-1}	ν_s	CH_3 stretch
	2920 cm^{-1}	ν_a	CH_2 stretch
	2860 cm^{-1}	ν_s	CH_2 stretch
Polypropylene	2955 cm^{-1}	ν_a	CH_3 stretch
	2880 cm^{-1}	ν_s	CH_3 stretch
	2920 cm^{-1}	ν_a	CH_2 stretch

b) Gravimetric and analytical studies.

i) $TiCl_4$ reaction. The reagent reacted in a reproducible manner with the oxide surface, exhibiting a constant weight increase and taking up a definite amount of Ti (25.5% of the total weight gain). This corresponded to the fixation of 2.8×10^{19} titanium atoms on the magnesia surface. A model for the magnesia surface has been discussed by Anderson[76]. He assumed that the surface consisted predominantly of the (100) crystallographic plane and estimated that after equilibrating in vacuo at 673K, the surface hydroxyl coverage was 0.5 monolayer (0.1

OH groups/$Å^2$). Thus a magnesia sample typically used in the present investigation (50 mg. S.S.A. 170 $m^2 . g^{-1}$.) would have 8.5×10^{20} surface hydroxyl groups. The ratio of appended titanium atoms to available surface hydroxyl groups would be 1:3. Since not all the appended titanium atoms could be constrained in triple or even double coordination with the oxide surface, the surfeit of hydroxyl groups would be as required for reaction 4.4. Thus it is envisaged that HCl produced by the initial reaction of $TiCl_4$ with a surface hydroxyl reacts immediately with an adjacent hydroxyl forming water and precluding the further fixation of titanium species. At this stage the appended titanium was in its +4 state, imparting a faint yellow colouration to the sample.

ii) $\underline{Al(C_2H_5)_3}$ reaction. Upon exposure of the Ti modified magnesia surface to the metal alkyl, an initial weight increase was accompanied by a colour change from faint yellow to grey. This colour change is indicative of the reduction of the surface Ti^{4+} species at least as far as the Ti^{3+} state. Subsequent exposure of this sample to oxygen resulted in oxidation back to Ti^{4+}, evidenced by the sample changing colour to white. Evacuation of the reduced sample led to a loss of weight although this was irreproducible and in several instances resulted in a nett decrease in sample weight. The nature of the overall weight change did not correlate with the ultimate polymerisation activity.

Ligand exchange between the surface and an absorbed metal alkyl, as proposed by several workers,[15,31] is presumably the initial step:

$$Mg\text{-}O\text{-}TiCl_3 + Al(C_2H_5)_3 \longrightarrow Mg\text{-}O\text{-}TiCl_2.C_2H_5 + Al(C_2H_5)_2.Cl. \quad (4.9)$$

$(Ti^{4+} - C_2H_5)$ bonds are unstable at ambient temperatures and decompose by either a free-radical or bimolecular mechanism, leading

to reduction of the transition metal[40]. Realkylation of the Ti^{3+} species is now possible, forming the relatively stable (Ti^{3+} - C_2H_5) bond:

$$Mg\text{-}O\text{-}Ti^{3+}Cl_2 + Al(C_2H_5)_3 \longrightarrow Mg\text{-}O\text{-}Ti^{3+}Cl.C_2H_5. + Al(C_2H_5)Cl \quad (4.10)$$

Excess $Al(C_2H_5)_3$ can be easily removed by evacuation of the samples. However the reaction products $Al(C_2H_5)_2Cl.$ and $Al(C_2H_5)Cl_2.$ are more strongly adsorbed on the surface and their complete removal is dependent upon the vacuum achieved in the vicinity of the sample. Complete removal would be reflected in an overall weight loss arising out of the exchange of two chloride atoms for one ethyl group on each reacting Ti atom. If all the Ti reacted in the above fashion, then the expected weight loss on atypical sample containing 2.8×10^{19} Ti atoms would be 2 mg. However some of the Ti is initially in the form 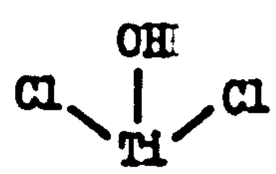 (equation 4.5) and may not react in the prescribed fashion. The theoretical weight loss would thus be reduced below 2 mg. A weight change of this order would be easily masked by the presence of $Al(C_2H_5)_2Cl$ and/or $Al(C_2H_5)Cl_2$ on the surface. However, analysis failed to reveal the presence of aluminium in active catalyst samples. Infrared spectroscopy indicated that $Al(C_2H_5)_3$ was adsorbed on the magnesia surface. Since the surface hydroxyls remained unperturbed, thispresumably occurred by adsorption of the metal alkyl onto oxide sites. The failure to detect aluminium in any of these samples is quite likely an artifact, attributable to the low concentrations, comparable with the lower detection limit of the analytical technique. It has been suggested that a prerequisite for polymerisation activity is the existence of accessible, alkylated Ti^{3+} atoms[31]. In this investigation, the available evidence certainly does not argue against this proposition. The irreproducible nature of the

alkylation reaction does not permit elucidation of the role of aluminium atoms in the polymerisation mechanism.

4.A.2) Infrared studies on a rutile carrier.

The fine structure normally associated with infrared studies of the rutile surface[71] was subjugated to the requirement of the increased sample size necessary for the catalyst study. Four hydroxyl environments were initially discerned in the spectrum of the freshly prepared rutile surface (fig. 3.9, 3.10). The small shoulder at 3730 cm^{-1} has been attributed to the presence of silica impurities introduced during preparation of the rutile and concentrated in the surface[115]. Peaks at 3700 cm^{-1} and 3665 cm^{-1} have been assigned to free hydroxyl groups and hydrogen bonded hydroxyl groups on the rutile surface respectively. A broad absorption at 1640 cm^{-1} in conjunction with theband at 3400 cm^{-1} indicated the retention of physisorbed water on the surface. The action of $TiCl_4$ vapour removed all four of these hydroxyl bands, revealing the presence of a hitherto unobserved hydroxyl absorption (3350 cm^{-1}; fig. 3.9b) which did not react with the metal halide. This was attributed to intraparticulate hydroxyl groups whose escape at 493K was retarded by the thickness of the oxide disc employed. The fixation of Ti to the rutile surface can occur by one of the reactions:

$$Ti\text{-}OH \xrightarrow{TiCl_4} Ti\text{-}O\text{-}TiCl_3 + HCl \qquad (4.11)$$

$$\begin{matrix} Ti\text{-}OH \\ \\ Ti\text{-}OH \end{matrix} \xrightarrow{TiCl_4} \begin{matrix} Ti\text{-}O \\ \diagdown \\ Ti \\ \diagup \\ Ti\text{-}O \end{matrix} \begin{matrix} \diagup Cl \\ \\ \diagdown Cl \end{matrix} + 2HCl \qquad (4.12)$$

The HCl produced during these reactions does not react chemically with the rutile surface.

Subsequent reaction with $Al(C_2H_5)_3$ introduced C-H stretching vibrations characteristic of an ethyl species:

2955 cm^{-1}	ν_a	CH_3	stretch
2880 cm^{-1}	ν_s	CH_3	stretch
2920 cm^{-1}	ν_a	CH_2	stretch
2860 cm^{-1}	ν_s	CH_2	stretch

The appearance of these absorptions was accompanied by the emergence of a dark grey colouration on the oxide surface, a condition reversed by exposure to oxygen and attributed to the reduction of Ti^{4+} by the metal alkyl:

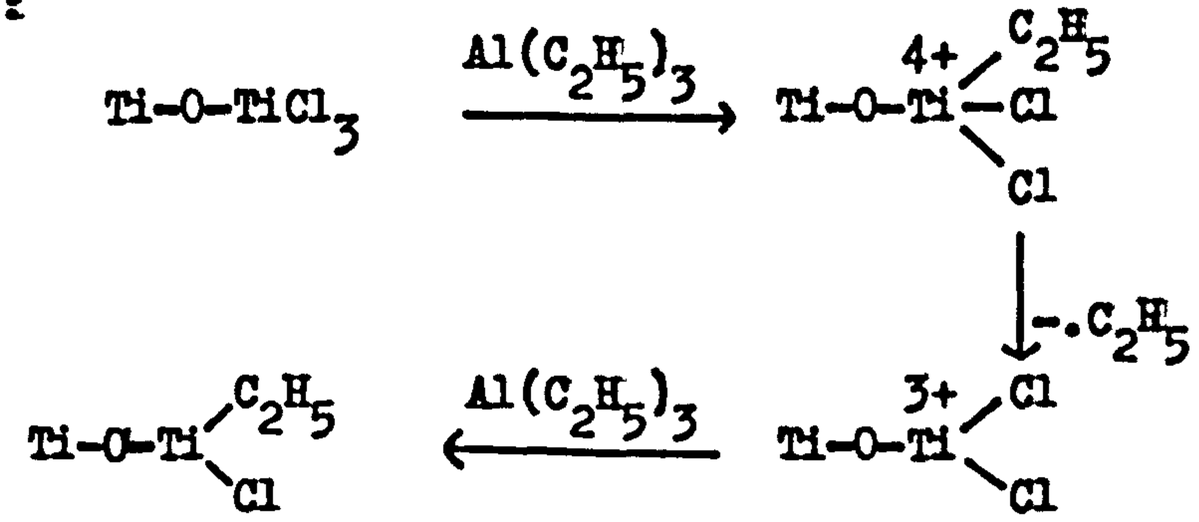

(4.13)

The spectra produced during the growth of polyethylene and polypropylene on the rutile supported catalyst (fig. 3.9, 3.10) are very similar to those obtained from the magnesia based catalyst. Unfortunately the very nature of the studies does not permit a quantitative comparison of the two carrier materials to be made.

PART B Olefin Polymerisation on a Magnesia Supported Catalyst.

4.B.1) Kinetic behaviour.

a) General introduction.

Polymerisation was followed gravimetrically, yielding reaction

profiles of the general form shown in fig. 4.1.

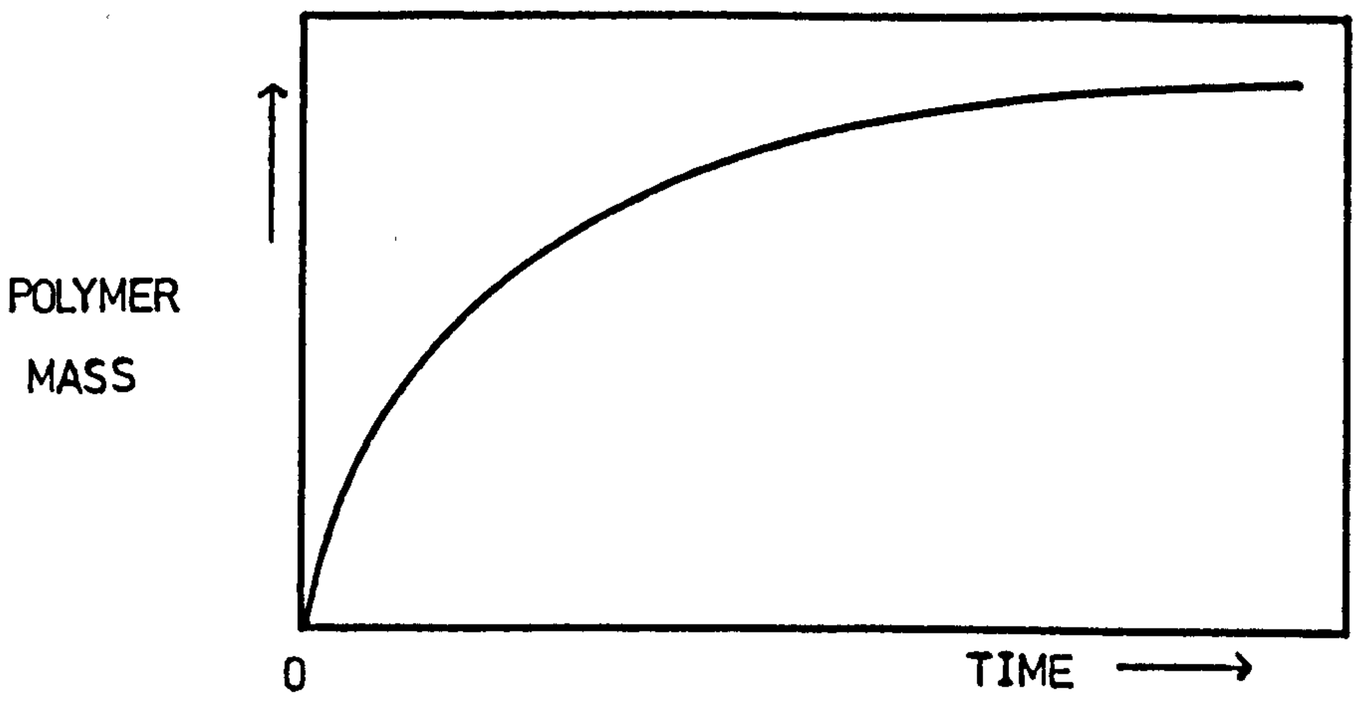

Figure 4.1. General form of the polymerisation curve.

The initial rate of reaction fell off rapidly but after three days polymerisation activity was still discernible for both propylene and ethylene monomers. It was not found possible to repeat a given polymerisation curve (section 2.C.1), precluding quantitative comparison of the activities of different catalyst samples. This was partially overcome by the use of split-temperature and split-pressure techniques but it has not been possible to quantify the relative reactivities of the two monomers studied.

Encapsulation of particulate polymerisation catalysts by growing polymer may occur when a high density of surface growth sites exists and there is no facility for removing the polymer formed. In such systems, if the reaction at the active centre is fast, then the rate determining step becomes the transfer of monomer through the growing polymer film to the active centre. The kinetic principles of a mass transfer controlled reaction are classically embodied in the law which

describes tarnishing reactions at metal surfaces - in essence the rate of reaction varies inversely as the extent of reaction, which on integration gives an extent of reaction having a square root/time dependence. Gas-phase olefin polymerisation with the magnesia supported Ziegler catalyst was found to obey such a rate law. Subsequent studies were formulated within a framework designed to add credance to the concept of diffusion controlled polymerisation.

b) Pressure dependence of the polymerisation.

Both ethylene and propylene polymerisations were found to be first order with respect to monomer pressure, underlining the similarities of the two olefinic reactions (fig. 3.16; 3.19., tables 3.3; 3.5). Thus with n = 1, equation 3.7 becomes:

$$C_o = k'p \qquad (3.11)$$

essentially Henry's law governing dilute solutions of the monomer in its corresponding polymer. Such a relationship is implicit in the permeation theory developed by Barrer[90]. However Ziegler polymerisations in slurry, or in solution, invariably display a first order pressure dependence[15], so that neither mass transfer nor kinetic control may be distinguished at this stage.

c) Temperature dependence of the polymerisation.

i) Ethylene polymerisation. The gradient of the $(m_t^2-m_o^2)/(t-t_o)$ plot (equation 3.8) at constant pressure is given by:

$$K_p = 2k.k' (a\rho)^2 p. \qquad (3.9)$$

If the active catalyst surface (a) and the polymer density (ρ) are

effectively temperature independent over the range considered, then K contains two temperature sensitive terms, the rate constant (k) and the Henry's law constant (ḱ). The composite temperature dependence for the polymerisation is embodied in the Arrhenius equation:

$$K = K_o.\exp\left(\frac{-E_{act}}{RT}\right) \qquad (3.13)$$

where E_{act} is the apparent activation energy for polymerisation. For ethylene polymerisation, equation 3.13 was not obeyed at temperatures above 320K. Decrease in polymerisation activity upon ageing the catalyst above 320K was observed and found to be a function of both the ageing time and the temperature employed (fig. 3.23). The Arrhenius plots prior to, and following, ageing above 320K (fig.3.26) were parallel but vertically displaced, illustrating that the high temperature affected only the concentration of active centres and not their fundamental nature. Subscribing to the widely held view that the active centre is essentially a (Ti-C) bond[15,45] then the loss of activity must be attributed to rupture of this bond at elevated temperatures. However many Ziegler systems have been reported stable at temperatures exceeding 370K. It would appear therefore that the facile deactivation experienced with the magnesia supported catalyst is a feature of either:-

a) steric constraint of the active structure facilitating rupture by the mechanical action of the entangled polymer chains,

b) chemical interference by the support or by species in the catalyst surface.

It is not possible to quantify these factors and it seems probable that both contribute to the overall picture. Subsequent studies were carried

out below the decomposition temperature of 320K.

The apparent activation energy for ethylene polymerisation over the temperature range 273 to 320K was found to be 36.0 ± 4.2 kJ./mole. Values reported in the literature for other Ziegler systems are commonly between 11.0 and 42.0 kJ/mole[116]. For the combination $TiCl_3/Al(C_2H_5)_3$ in hydrocarbon slurry, Schnecko[117] reported an activation energy of 40.7 kJ/mole for ethylene polymerisation, a figure similar to those obtained by Keii[17] and Lanovskaya[118]. Recently published work by Korobova[119] on a magnesia supported titanium catalyst in hydrocarbon suspension with an $Al(i\text{-}Bu)_2H$ co-catalyst gave a value of 37.8 kJ/mole for ethylene polymerisation. However the kinetic control of these polymerisations is not disputed, whereas in the present work there are indications of diffusion control. The close agreement between literature values and the present work must therefore be subject to reservations. This point is discussed fully in section 4.D.

ii) Propylene polymerisation. The reaction obeyed the Arrhenius law (equation 3.13) over the temperature range 273 to 320K - below the decomposition temperature of the catalyst. The value determined for the apparent energy of activation of the polymerisation (28.6 ± 2.9 kJ/mole) falls within the range reported for propylene polymerisations in Ziegler systems[116]. Once again, precise parallels with the literature are not possible due to the novel system studied in this work.

d) The effect of gaseous impurities on the polymerisation of ethylene.

i) Hydrogen. In commercial Ziegler polymerisations hydrogen has been employed as a chain terminator for molecular weight control, acting according to reaction 4.14. The residual Ti-H group may itself form

an active centre (reaction 4.15) or be activated by the organometal co-catalyst (reaction 4.16).

$$\text{Ti-polymer} + H_2 \longrightarrow \text{Ti-H} + \text{H-polymer} \qquad (4.14)$$

$$\text{Ti-H} + C_2H_4 \longrightarrow \text{Ti-}C_2H_5 \qquad (4.15)$$

$$\text{Ti-H} + AlR_3 \longrightarrow \text{Ti-R} + AlHR_2 \qquad (4.16)$$

In the present work, the presence of hydrogen gas in the reaction vessel had no effect on the rate of ethylene polymerisation at 308K. It seems likely that the activation energy of the termination step is sufficiently high to prevent the insertion of the hydrogen molecule into the Ti-polymer bond at the temperature concerned. Since catalyst decomposition became important above 320K, the study of hydrogen termination at elevated temperatures was not pursued.

ii) Oxygen. When an active catalyst sample was treated with oxygen, the polymerisation activity was destroyed. Simultaneously the grey colour of the catalyst surface, produced during activation and characteristic of a reduced oxide surface, was removed. These observations are in accord with the sensitivity exhibited by Ziegler combinations (and their separate components) towards oxygen. The oxygen readily attacks the organo-titanium bonds which form the active centres. Oxidation is heightened when strongly reducing, low valent titanium species are present, generating the stable Ti^{4+} state.

The consequences of this oxygen sensitivity in kinetic studies are such that the presence of small amounts of oxygen in feedstocks can seriously distort the kinetic picture. The irreproducibility of the kinetic data in the present work was attributed to oxygen contamination. That this interference was important only during the catalyst preparation stage was evidenced by the adherence of the polymerisation reaction to

equation 3.8 for the first eight hours of reaction. The source of contamination during catalyst activation appeared to be associated with polymer growth on the walls of the reaction vessel. It was concluded that oxygen desorption from this spongy material during catalyst activation resulted in catalyst poisoning.

iii) $\underline{D_2O}$. The susceptibility of the catalyst to hydrolysis was evidenced by complete destruction of polymerisation activity, accompanied by a large weight increase and removal of the surface grey colouration. Ti-Cl, Ti-C and Al-C bonds are especially sensitive to moisture, and the reduced titanium species would be oxidised through to the Ti^{4+} state.

Such reactions further underline the importance of impurity levels if meaningfull kinetic data are sought. Particularly with the present catalyst system, the lack of a co-catalyst reservoir to scavange impurities and regenerate poisoned sites is significant in the context of kinetic reproducibility.

4.B.2) The nature of the polymer material.

a) Introduction.

Ethylene and propylene polymerisation on the supported catalyst resulted in the formation of a transparent polymer film, clearly visible on the catalyst surface. The relevance of the macroscopic structure of the polymer film to the elucidation of a kinetic model was recognised Encapsulation of the catalyst particles by a regular polymer film would not contravene the hypothesis of diffusion control. Conversely,

dendritic growth of the polymer would argue against mass transfer control.

b) Solubility studies.

The catalyst particles, readily wetted and dissolved by dilute aqueous acids, became hydrophobic and insoluble after polymerisation. They remained insoluble even after wetting in the presence of a surface active agent. This behaviour is indicative of a continuous and impervious polymer film on the catalyst surface. Removal of the polymer by an organic solvent (boiling tetralin) restored the original catalyst solubility properties. Olefin monomer transfer through such a polymer film would of course be relatively facile in view of the favourable Flory/Huggins interaction parameters.[91.]

c) Scanning electron microscopy

The polymer appeared as a continuous surface film, except for a few isolated patches where dendritic growth was observed (figure 3.36b).[31] This contrasts with the work of Rodriguez and Guttman[120.] who reported fibrous polymer growths when polymerisation occurred on $TiCl_3$ crystals activated by $Al(CH_3)_3$. Guttman proposed the growth of surface fibrils from clusters of active sites, as shown in figure 4.2. Rodriguez clearly showed the occurrence of such isolated fibrils along the growth spirals of α-$TiCl_3$ crystals. He proposed that atomic disorder in these growth spirals satisfied the prerequisites of active site formation

i.e. accessible titanium atoms. In the present work the isolated surface titanium species present a comparatively open structure to the

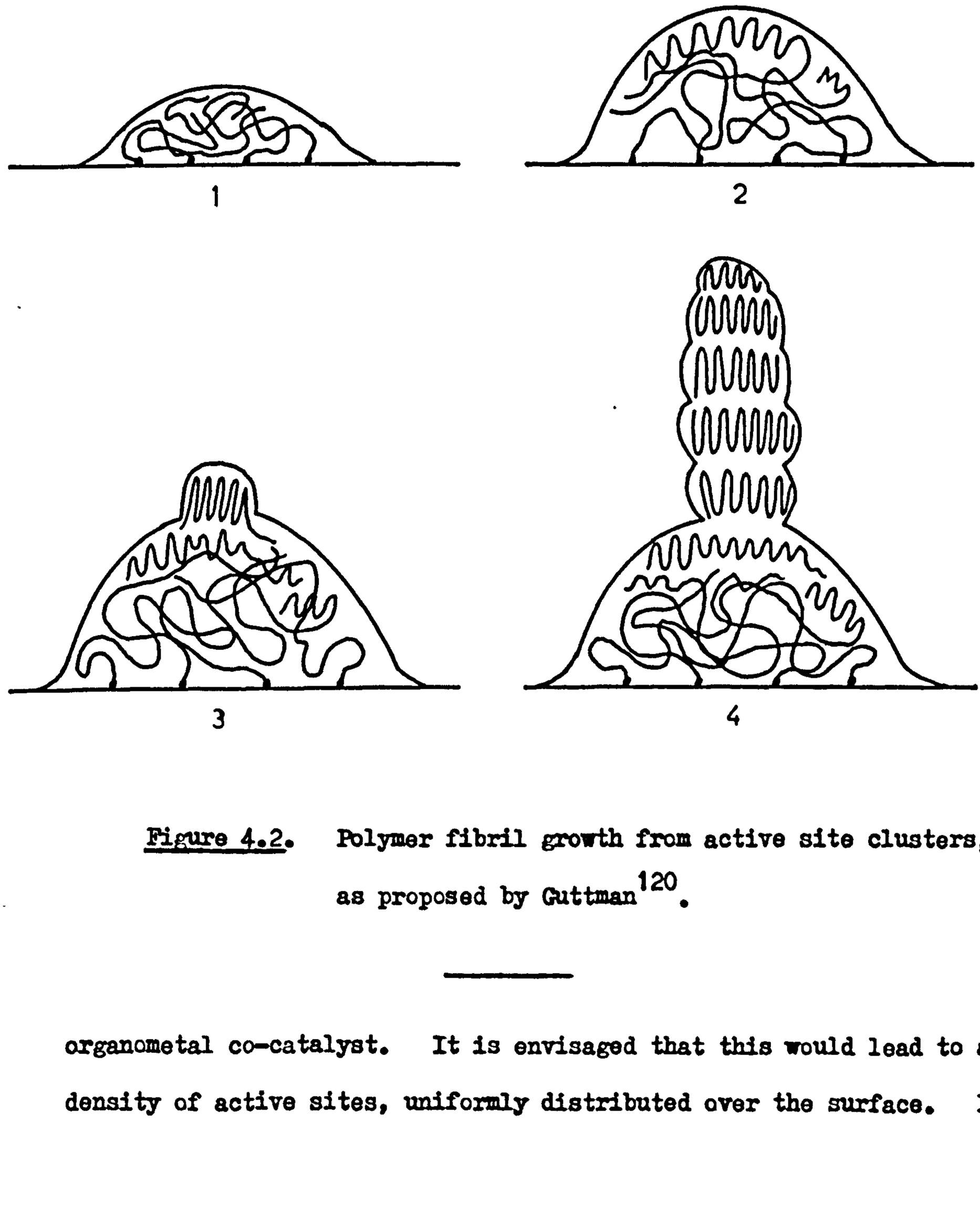

Figure 4.2. Polymer fibril growth from active site clusters, as proposed by Guttman[120].

organometal co-catalyst. It is envisaged that this would lead to a high density of active sites, uniformly distributed over the surface. Polymer

growth on this model would then occur as shown in figure 4.3, appearing as a coherent film.

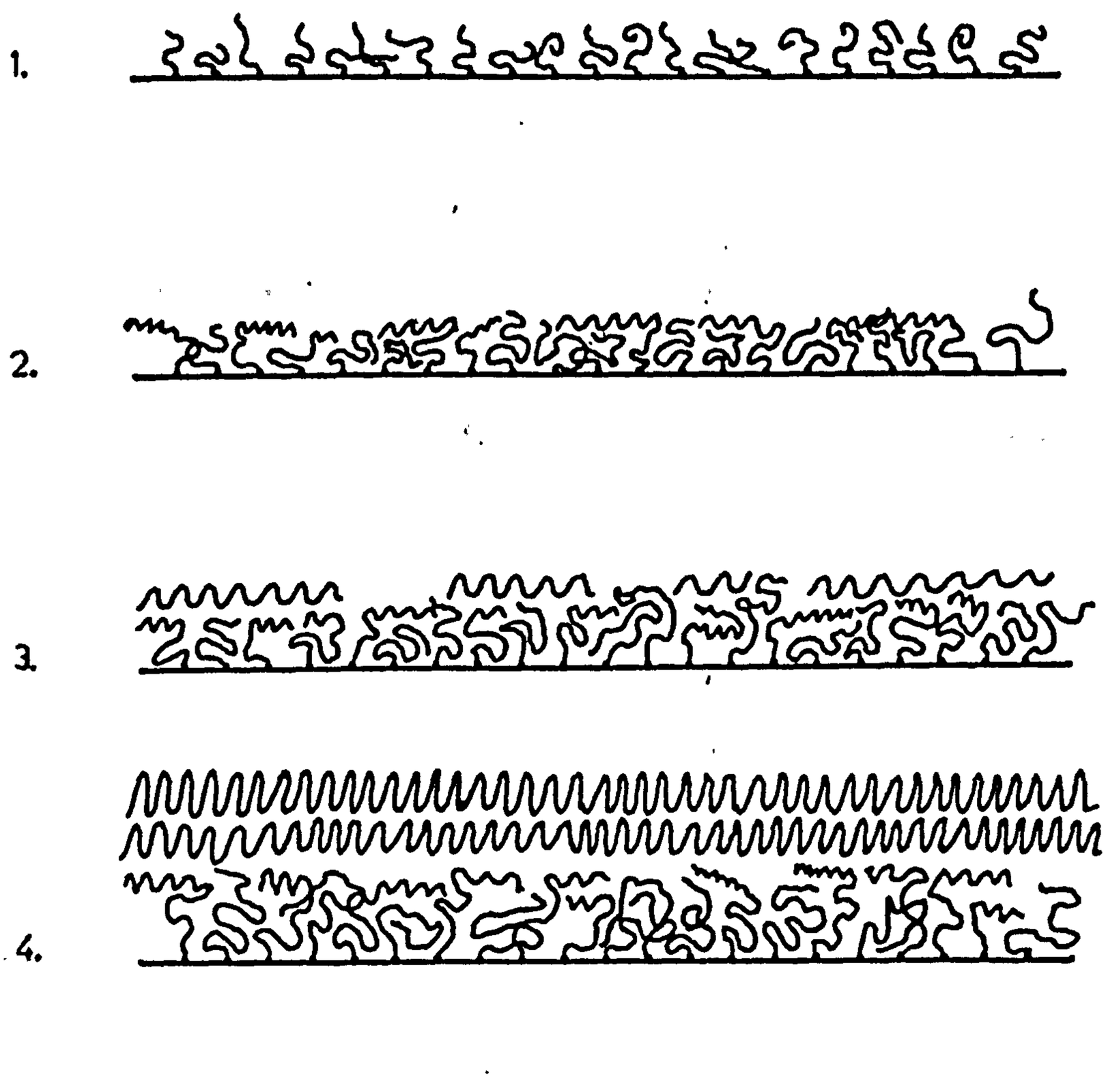

Figure 4.3. The growth of polymer as a continuous film from a uniform distribution of sites.

4.B.3) Summary of polymerisation data.

Consideration of the available evidence suggests a novel kinetic

approach to this system. Once polymerisation is established, the catalyst surface presents a continuous polymer film through which the monomer must pass before being incorporated into the growing chains. The rate of polymerisation obeys a law (equation 3.8) derived on the assumption that the controlling factor is the rate of monomer transfer from the gas phase, through the polymer film to the growth centre.

The apparent activation energies (E_{act}) for the polymerisation of ethylene and propylene are comparable with those reported for conventional Ziegler catalysts where the rate is under kinetic control. However, in the event of diffusion control, the value of E_{act} would simply reflect the activation energy for permeation of the monomer through its associated polymer. No such permeation data were available in the literature. The dichotomy was resolved by experimental determination of the relevant permeation data, discussed in the next section.

PART C Permeation Studies.

4.C.1) The $C_2H_4/(C_2H_4)_n$ system.

Those parameters characterising gas permeation in polymers can be substantially altered as the temperature increases and passes through the glass transition temperature (T_g) of the polymer[97]. This reflects the changes in polymer molecule mobility occurring in the region of T_g. For linear polyethylene the glass transition temperature occurs around 148K[121], sufficiently far removed from the temperature range with which the present work is associated.

The permeation curves for the two polyethylenes studied show the same features (fig. 3.37; 3.38). The initial curved portion of the plot gives way to the linear relationship signifying the onset of steady-state mass transfer. For both materials, the intercepts of the linear portions on the time axis (θ) are too small for accurate determination. This precludes evaluation of the diffusion coefficient (D) and the solubility (S) of ethylene in the polymers, although determination of the permeability (P), and hence E_p, is sufficient for the present investigation. P, obtained from the slope of the linear portion, obeys an Arrhenius type law (equation 3.15). The values of the activation energy for permeation (E_p) are very similar for Marlex (37.8 kJ./mole) and Additive-free (45.4 kJ./mole) polyethylenes. This indicates that the mechanism of transfer is identical in the two solids. The permeability of a material reflects both the presence of extraneous materials (additives such as plasticisers) and the thermal history of the sample[91,92]. The polymer films used in this work were pressed from polyethylene powders under standardised conditions. Thus the lower value of P recorded for Marlex polyethylene (cf. Additive-free polymer) is probably a consequence of the 'impurity' level of the commercial polymer.

There are many reports in the literature of permeation studies with the $C_2H_4/(C_2H_4)_n$ system. However, in view of the wide spectrum of materials and conditions employed in such studies, meaningful comparisons with the present work are not possible. Michaels[122] found that the activation energies for diffusion (E_D) of semi-permanent gases in linear polyethylenes were given by the empirical relationship:-

$$E_D = 2.2\ (d_g - \tfrac{1}{2}\phi^{\frac{1}{2}}) + 2.6 \qquad (4.1)$$

where d_g is the diameter of the gas molecule (in Å; assumed spherical) and $\frac{1}{2}\phi^{\frac{1}{2}}$ is the approximate mean unoccupied distance between two chain segments in Å. Lipman[32] used this equation to estimate a value for E_D of 48.7 kJ/mole for ethylene in polyethylene. E_D differs from E_p by the heat of solution of the monomer in the polymer (ΔH_S). This was estimated at around 12.6 kJ/mole and the calculated value of E_p (35 kJ/mole) compares favourably with the experimental values of 37.8 and 45.3 kJ/mole for the two polyethylenes studied here.

4.C.2) The $C_3H_6/(C_3H_6)_n$ system.

The glass transition temperature for polypropylene is around 250K, well below the range of temperature studied in this work[121]. The initial, cufved parts of the permeation graphs (fig. 3.40) are more pronounced than for polyethylene. Thus it was possible to accurately determine the time lag θ, and through equation 1.12 to study the temperature dependence of D and S as well as that of P.

$$D = \frac{l^2}{6\theta} \qquad (1.12)$$

$$P = DS \qquad (1.6)$$

The variables P, D and S are related by equation 1.6, their pre-exponential factors (equations 1.7, 1.8, 1.9) by equation 1.11,

$$P_o = D_o S_o \qquad (1.11)$$

and their activation energies by equation 1.10,

$$E_p = E_D + \Delta H_S. \qquad (1.10)$$

The inherent errors of the extrapolation employed in determining P_o, D_o

and S_o (fig. 3.41; table 3.16). are reflected in the rather tenuous obedience to equation 1.11. However, equation 1.10 is obeyed:

$$E_D + \Delta H_S = (46.6 - 14.7) = 31.9 \text{ kJ/mole.}$$

$$E_p = 32.8 \text{ kJ/mole.}$$

The solution of propylene in polypropylene is an exothermic process, evidenced by the negative sign of ΔH_S. Now ΔH_S is a compound term comprising the algebraic sum of the molar enthalpy of condensation (ΔH_{cond}) and the partial molar enthalpy of mixing (ΔH_1) of the monomer in the polymer (equation 4.2).

$$H_S = \Delta H_{cond} + \Delta H_1 \qquad (4.2)$$

For C_3H_6 at ambient temperatures, ΔH_{cond} can be estimated from the Clapeyron/Clausius equation. This calculation yields a value of 19 kJ/mole for ΔH_{cond}, indicating that for the propylene/polypropylene system, ΔH_1, is positive (i.e. endothermic).

E_D has more theoretical significance than E_p, representing the activation energy of the process by which the penetrant molecule moves through the polymer. It can be subdivided into the energy required for the formation of holes within the polymer, and the energy necessary for the penetrant molecule to move from hole to hole[123]. Increase in temperature has two effects. Firstly the increased molecular activity of the polymer results in a larger number of holes available for the propagation process. And secondly it produces a larger proportion of penetrant moleculeswith the requisite 'hopping' energy. These factors are of course additive and are reflected in the positive sign of E_D.

PART D The Overall Reaction Scheme.

4.D.1) The role of the carrier in the polymerisation catalyst.

Few supported Ziegler catalysts have been reported in the literature and none in sufficient detail to quantify the role of the carrier in the mechanistic scheme. McInnich[35] reported that additions of metal oxides to hydrocarbon slurries of Ziegler catalysts resulted in rate enhancement in direct proportion to the oxide basicity. In dry form, SiO_2[36], TiO_2 and MgO can be used to support an active catalyst. However, variations in the ultimate performance of these supports are inherent, due to the different chemical responses of the oxide surfaces to the catalyst components. Reaction of $TiCl_4$ at the silica surface is less complex than for magnesia, where side reactions involving HCl lead ultimately to the formation of water and subsequent partial hydrolysis of adsorbed titanium species. It is unclear to what extent this latter reaction occurs and it is difficult to assessits importance in catalyst activity. The acidic hydroxyls of the silica surface react readily with organo-aluminium vapours[36]. In contrast, the basic magnesia hydroxyls remain unperturbed in the presence of aluminium triethyl. Thus the surfaces of supported catalysts prepared in identical fashion may vary considerably and carefully planned experiments must be made to compare carrier efficiencies.

Rodriguez[31] and Cossee[55] contend that exposed titanium atoms are the essential prerequisites for active site formation. The reduced, isolated Ti^{3+} species produced on the surface of the supported catalyst fulfill the above conditions. In this respect the particle-size, porosity and surface roughness each assume significance. Thus it is to be expected that whereas with conventional α-$TiCl_3$ crystals the

growth centres exist only in regions of surface disorder[31], with a suitable supported catalyst a larger and more uniform population of active centres would be created. When such a high density of surface sites exists, decomposition by an intermolecular mechanism (reaction 1.2) becomes more likely. The loss of catalyst activity above 320K observed in the present work may reflect the lability of closely spaced active centres. High site density is also indicated by polymer encapsulation of the catalyst, evident at very short reaction times. Optimisation of site density and stability for the magnesia supported Ziegler catalyst could presumably be achieved by strict control of surface hydroxyl population - the potential active centres.

Even small amounts of catalyst poisons (oxygen, moisture) can drastically affect the catalyst activity and no site regeneration mechanism exists. Informative experiments on progressive poisoning by the introduction of successive aliquots wereprecluded by the apparatus used.

4.D.2) <u>The nature of the active site and the mechanism of polymerisation.</u>

Polymerisation activity was conferred on the magnesia support by the initial reaction of $TiCl_4$ and subsequent exposure to $Al(C_2H_5)_3$. This activity was characterised by the fixation of an ethyl species on the catalyst surface and by a grey colouration, indicative of Ti^{3+} species. The destruction of catalyst activity by oxygen or moisture is further evidence for the importance of reduced titanium species, which are readily oxidised to Ti^{4+}. Identical criteria for polymerisation activity were established for the rutile carrier and similar observations have been reported for the $SiO_2/TiCl_4/Al(CH_3)_3$ system[36]. For the

magnesia support at least, the role of aluminium in the growth centre cannot be unambiguously defined, although gravimetric and analytical studies could not detect the metal in active catalyst samples.

An alkylated Ti^{3+} species on the magnesia surface would possess a vacancy in its coordination sphere, deemed necessary in the most cogent polymerisation mechanism[55]. Coordination of the incoming monomer to the transition metal results in the weakening of the olefinic bond by electron donation to the d-orbitals of the metal. Attempts have been made to detect the elongated (C=C)bond of the coordinated monomer by infrared studies under polymerisation conditions[124]. Failure to do so may be attributed to rapid insertion into the growing polymer chain. In the event of catalyst encapsulation by the growing polymer, this rapid insertion step would place the onus of rate control upon mass transfer processes.

On the evidence presented in the preceding chapters it is possible to formulate a reaction scheme for activation and polymerisation in the magnesia supported Ziegler catalyst (figure 4.4).(overleaf).

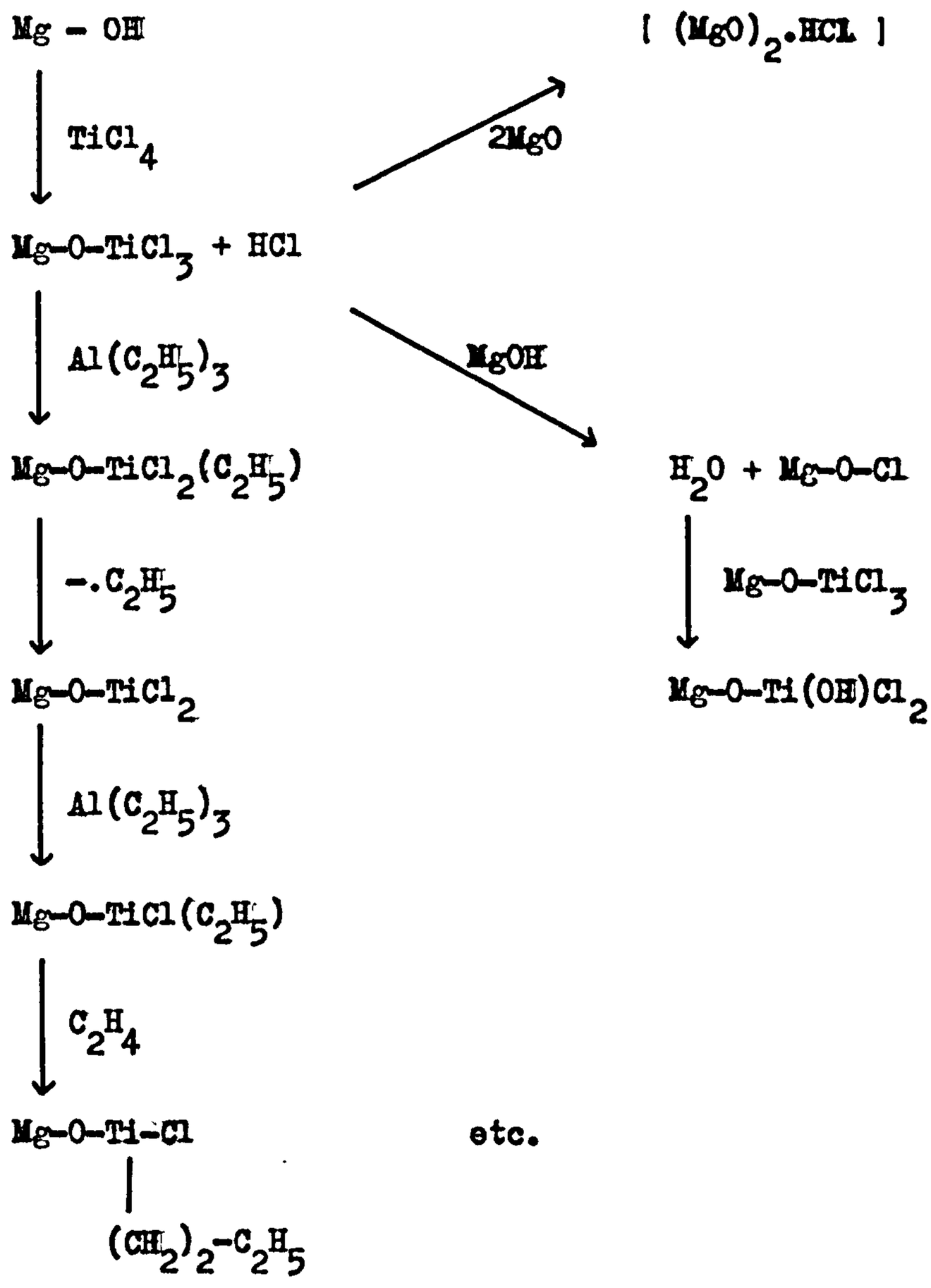

Figure 4.4. Reaction scheme for activation and polymerisation of the magnesia supported Ziegler catalyst.

A similar scheme may be formulated for the rutile supported catalyst (figure 4.5).

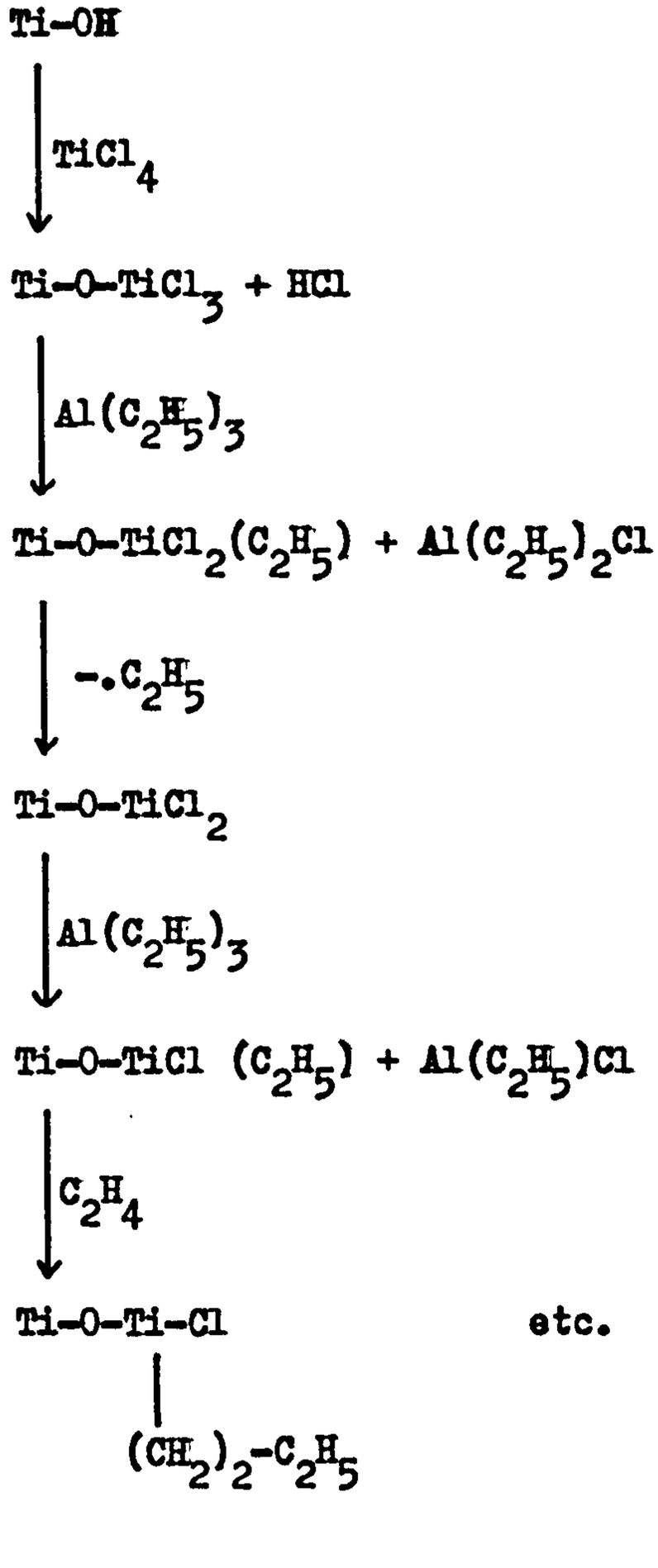

Figure 4.5. Reaction scheme for activation and polymerisation for the rutile supported Ziegler catalyst.

4.D.3) Conclusions from the kinetic studies.

The E_{act} values determined for the polymerisation of ethylene and propylene on the magnesia supported catalyst are compared in table 4.1 with the corresponding values of E_p. For diffusion controlled polymerisation, E_{act} is in fact equivalent to E_p. The close agreement between experimental values of E_{act} and E_p demonstrates their equivalence

System	E_{act} kJ/mole.	E_p kJ/mole.
$C_2H_4/(C_2H_4)_n$	36.0 ± 4.2	37.8 ± 2.5 (a)
		45.4 ± 1.3 (b)
$C_3H_6/(C_3H_6)_n$	28.6 ± 2.9	32.8 ± 3.8

a) Marlex polyethylene

b) Additive free polyethylene.

Table 4.1. Values of E_{act} and E_p for C_2H_4 and C_3H_6 in their corresponding polymers.

and further supports the concept of mass transfer control. In view of the tenuous approximations of the permeation conditions to those obtaining in the polymerisation reaction, the observed agreement is remarkable, reflecting the relative insensitivity of E_p to the thermal history of the polymer sample.

An attempt was made to compare the rate of polymer growth during

reaction with the monomer uptake predicted by the permeation data. Assuming a polymer density of $\simeq$ 0.93 $g.cm^{-3}$ at 308K. for polyethylene on the catalyst surface, the thickness of the polymer film was estimated. The rate of polymer growth at this film thickness (and hence the amount of monomer arriving at the catalyst surface) was deduced from the experimental data. Using this information it was possible to calculate the permeability (P) of the monomer through the polymer film. The value of P obtained in this fashion for the $C_2H_4/(C_2H_4)_n$ system was lower (by a factor of $\simeq 10^2$) than that determined by the conventional permeation studies. The susceptibility of P to the microstructure of the polymer is well documented[91]. Since the polymer samples used in the two different studies are unlikely to bear any resemblance other than on the molecular scale, comparison of the values obtained from the two sources was considered meaningless and was not pursued.

The evidence in favour of a diffusion controlled polymerisation system appears conclusive and may be summarised:-

a) the catalyst rapidly becomes encapsulated by a coherent polymer film,

b) the polymerisation rate obeys a law analogous to that describing classical diffusion controlled reactions,

c) the apparent activation energy for polymerisation is very similar to the activation energy for permeation.

References

1. H. von Pechmann, Ber., 31, 2643, (1898).
2. U.K. Patent 471590, (1937), I.C.I., Ltd.
3. Chem. Eng. News, 34, 1470, (1956).
4. K. Ziegler, E. Holzkamp, H. Breil and H. Martin, Angew. Chem., 67, 426, (1955).
5. K. Ziegler, E. Holzkamp, H. Breil and H. Martin, Angew. Chem., 67, 541, (1955).
6. K. Ziegler and H. Martin, Makro. Chem., 18/19, 186, (1956).
7. G. Natta, P. Pino, P. Corradini, F. Danusso, E. Mantica, G. Mazzanti and G. Moraglio, J.A.C.S. 77, 1708 (1955).
8. Belgium Patent 530,617. (1955), Phillips Chemical.
9. U.S. Patent 2692257, (1954), Standard Oil Co. Ltd., (Indiana).
10. R.A.V. Raff, Ed., Polyethylene, (Interscience, New York, 1956).
11. G. Natta, J. Polymer Sci., 16, 143, (1955).
12. G. Natta and P. Corradini, J. Polymer Sci., 20, 251, (1956).
13. R.A.V. Raff and K.W. Doak, Eds., Crystalline Olefin Polymers I, (Interscience, New York, 1965).
14. M.L. Cooper and J. B. Rose, J. Chem. Soc. 795, (1959).
15. J. Boor, Jr., Macromol. Rev., 2, 115, (1967).
16. M.N. Berger, G. Boocock and R.N. Haward, Adv. in Catalysis, 19, 211, (1969).
17. T. Keii, Kinetics of Ziegler-Natta Polymerisation, (Chapman and Hall, London, 1972).
18. J. Boor. Jr., J. Polymer Sci., (A1), 9, 3075, (1971).
19. E.J. Arlman, Proc. Intern. Cong. Catalysis. 3rd, 2, 957, (1964).
20. F.J. Karol and W.L. Carrick, J.A.C.S., 83, 2654, (1961).

21. F. Danusso and D. Sianesi, Chim. Ind. (Milan), 44, 474, (1962).

22. G. Natta and I. Pasquon, Adv. in Catalysis, 11, 1, (1959).

23. G. Natta, J. Polymer Sci., 34, 151, (1959).

24. D.S. Breslow and N.R. Newbury, J.A.C.S., 81, 81, (1959).

25. G. Natta, P. Pino, G. Mazzanti, R. Lanzo, Chim. Ind. (Milan), 39, 1032, (1957).

26. A.V. Topchiev, B.A. Krentsel, A.I. Perelman and K.G. Miesserov, J. Polymer, Sci., 34, 129, (1959).

27. G. Natta, I. Pasquon and A. Zambelli, J.A.C.S., 84, 1488, (1962).

28. E.A. Youngman and J. Boor, Jr., Macromol. Rev., 2, 33, (1967).

29. I. Okura, A. Kojima, K. Soga and T. Keii, J. Polymer Sci., (A1), 8, 2717, (1970).

30. M.N. Berger and B.M. Grieveson, Die Makro. Chem., 83, 80, (1965).

31. L.A.M. Rodriguez, H.M. van Looy and J.A. Gabant, J. Polymer Sci., (A1), 4, pp. 1905-1989, (1966).

32. R. Lipman and R. Norrish, Proc. Roy. Soc., 257, 310, 1963.

33. R.T.K. Baker, P.S. Harris, R.J. Waite and A.N. Roper, Polymer Letters, 11, 45, (1973).

34. Patents.
a) U.K. 1024336 (1964), Solvay et Cie.
b) S.A. 687223 (1968), Mitsui Petrochemical Industries.
c) U.K. 1085679 (1966), Solvay et Cie.
d) Neth. 6904377 (1969), Solvay et Cie.
e) Neth. 6909140 (1969), Solvay et Cie.
f) Neth. 6908977 (1969), Hoechst A.G.
g) Neth. 6909375 (1969), Hoechst A.G.
h) Neth. 6911791 (1970), Mitsui Petrochemical Industries.
i) Belg. 724691 (1969), Mitsui Petrochemical Industries.
j) Ger. 1950703 (1970), Montecatini-Edison.
k) Ger. 2216357 (1972), Montecatini-Edison.

35. S.E. Tung and E. McIninch, Proc. Intern. Cong. Catalysis 2nd, 1385, (1960).

36. J.A. Hockey, M.J. Sharp and J. Murray, J. Catalysis, 18, 52, (1970).

37. A.S. Matlack and D.S. Breslow, J. Polymer Sci. (A), 3, 2853, (1965).

38. G.D. Bukatov, V.A. Zakharov and Yu. I. Ermakov, Kin. and Cat., 12, 446, (1971).

39. D.G.H. Ballard, Adv. in Catalysis, 23, 263, (1973).

40. H. de Vries, Rec. Trav. Chim., 80, 866, (1961).

41. J. Chien, J. Catalysis, 23, 71, (1971).

42. A.D. Caunt, J. Polymer Sci. C, 4, 49, (1963).

43. J.A. Hockey, P. Jones and J. Kunawicz, Trans. Far. Soc., 67, 848, (1971).

44. T. Keii, J. Polymer Sci. C, 23, 453, (1968).

45. M.N. Berger, G. Boocock and R.N. Haward, Adv. in Catalysis, 19, 211, (1969).

46. H.N. Friedlander and K. Oita, Ind. Eng. Chem., 49, 1885, (1957).

47. G. Natta, P. Pino, G. Mazzanti, U. Giannini, E. Mantica and M. Peraldo, J. Polymer Sci., 26, 120, (1957).

48. G. Natta and G. Mazzanti, Tetrahedron, 8, 86, (1960).

49. F. Patat and H. Sinn, Angew Chem., 70, 496, (1958).

50. M.L. Huggins, J. Polymer Sci., 48, 473, (1960).

51. J. Boor, Jr., J. Polymer Sci.; C, 1, 257, (1963).
B, 3, 7, (1965).
A, 3, 995, (1965).

52. G.L. Karapinka and W.L. Carrick, J. Polymer Sci., 55, 145, (1961).

53. C. Beerman and H. Bestian, Angew. Chem., 71, 618, (1959).

54. W.P. Long and D.S. Breslow, J.A.C.S., 82, 1953, (1960).

55. P. Cossee, J. Catalysis, 3, 80, (1964).

56. E.G. Lovering and W.B. Wright, J. Polymer Sci., (A1), 6, 2221, (1968).

57. W.C. Zeise, Ann. Physik., 9, 632, (1827).

58. J. Chatt and B.L. Shaw, J. Chem. Soc., 705, (1959).

59. J.W. Begley and F. Pennella, J. Catalysis, 8, 203, (1967).

60. U. Giannini, U. Zucchini, E. Albizzati, J. Polymer Sci., B, 8, 405, (1970).

61. J. Boor, Jr., Ind. Eng. Chem. Prod. Res. Dev., 9, 437, (1970).

62. E.J. Arlman and P. Cossee, J. Catalysis, 3, 99, (1964).

63. P. Longi, G. Mazzanti, A. Roggero and A.M. Lachi, Die Makromol. Chem., 61, 63, (1963).

64. A. Schindler and R.B. Strong, Die.Makromol. Chem., 93, 145, (1966).

65. A.S. Hoffman, A. Fries and P.C. Condit, J. Polymer Sci., C, 4, 109, (1964).

66. C.D. Mason and R.J. Schaffhauser, Polymer Letters, 9, 661, (1971).

67. G. Natta, E. Giachetti, I. Pasquon and G. Pajaro, Chim. Ind. (Milan), 42, 1091, (1960).

68. R.P. Eischens and W.A. Pliskin, Adv. in Catalysis, 10, 2, (1958).

69. L.H. Little, Infrared Spectra of Adsorbed Species (Academic Press, London, 1966).

70. M.L. Hair, Infrared Spectroscopy in Surface Chemistry, (Marcel-Dekker, New York, 1967).

71. C.H. Rochester and M.S. Scurrell, Surface and Defect Properties of Solids, Vol. II., Spec. Per. Rep. Chem. Soc., P.114, (1973).

72. N. Takezawa, Bull. Chem. Soc. Japan, 44, 3177, (1971).

73. A. Buckland, J. Ramsbotham, C.H. Rochester and M.S. Scurrell, J. Physics E: Sci. Instruments, 4, 146, (1971).

74. T.H. Nielson and M.H. Leipold, N.A.S.A. Tech. Rep. 32-949.

75. B.J. Linsen, Ed., Physical and Chemical Aspects of Adsorbents and Catalysts, (Academic Press, New York, 1970).

76. P.J. Anderson, R.F. Horlock and J.F. Oliver, Trans. Far. Soc., 61, 2754, (1965); 58, 1993, (1962).

77. R.A. Schoonheydt and J.H. Lunsford, J. Catalysis, 26, 261, (1972).

78. A.A. Lisachenko and V.N. Filimonov, Dokl. Akad. Nauk. S.S.S.R., 177, 391, (1967).

79. M.L. Hair and W. Hertl, J. Phys. Chem. 74, 91, (1970).

80. S.J. Gregg and J.D. Ramsey, J. Chem. Soc. A, 2784, (1970).

81. H. Kogbel, M. Ralek and P. Jiru, Z. Naturforschung, 25, 670, (1970).

82. P. Jackson and G.D. Parfitt, Trans. Far. Soc., 67, 2469, (1971).

83. P. Jones and J.A. Hockey, J. Chem. Soc. (Far.I) 68, 896, (1972).

84. C.G. Armistead, A.J. Tyler, F.H. Hambleton, S.A. Mitchell and J.A. Hockey, J. Phys. Chem., 73, 3947, (1969).

85. J. Kunawicz, P. Jones and J.A. Hockey, Trans. Far. Soc., 67, 848, (1971).

86. G.D. Parfitt, J. Ramsbotham and C.H. Rochester, J. Chem. Soc. (Far.I) 68, 17, (1972).

87. J.R. Nielson and A.H. Woollett, J. Chem. Phys., 26, 1391, (1957).

88. D.D. Eley, C.H. Rochester and M.S. Scurrell, Proc. R. Soc. Lond. A., 329, 375, (1972).

89. R.A.V. Raff and K.W. Doak, Eds., Crystalline Olefin Polymers II, (Interscience, New York, 1965).

90. R.M. Barrer, Trans. Far. Soc., 35, 628, (1939).

35, 644, (1939).

91. C.E. Rogers, Physics and Chemistry of the Organic Solid State, p.510, (Interscience, New York, 1965).

92. V. Stannet, H.B. Hopfenberg and J.H. Petropoulos, M.T.P. Int. Rev. Sci.-Phys. Chem. Series 1, 8, 329, (1973).

93. J. Crank, The Mathematics of Diffusion, (Clarendon Press, Oxford, 1956).

94. T. Graham, Phil. Mag., No. 32, S.4, 401, (1866).

95. A. Fick, Ann. Physik. Leipzig, 170, 59, (1855).

96. G.J. Amerongen, J. App. Phys., 17, 972, (1946).

97. P. Meares, J.A.C.S., 25, 3415, (1954).

98. A. Peterlin, and J.L. Williams, Brit. Poly. J., 4, 271, (1972).

99. S.A. Stern, J.T. Mullhaupt and P.J. Garris, Amer. Inst. Chem. Eng. J., 15, 64, (1969).

100. S.A. Stern, S.M. Fang and R.M. Jobbins, J. Macromolec.Sci., B5, 41, (1971).

101. A.S. Michaels and H.J. Bixler, J. Polymer Sci., 50, 393, (1961).

102. N.N. Li and E.J. Henley, Amer. Inst. Chem. Eng. J., 10, 666, (1964).

103. G.N. Gerasimov, A.D. Abkin and P.M. Khomikovskii, Vysokomol. Soyed., 5, 479, (1963).

104. D.M. Leitao, J. Polymer Sci., A2, 10, 1111, (1972).

105. A.G. Savin, T.K. Shaposhnikova, V.I. Karpov, T.I. Sogolova and V.A. Kargiu, Vysokomol. Soyed., A10, 1584, (1968).

106. Z.P. Kosovova and S.A. Reitlinger, Vysokomol. Soyed., A9, 415, (1967).

107. F. Bozon-Verduraz, J. Catalysis, 18, 12, (1970).

108. T.N. Rhodin and E.A. Gulbransen, Adv. in Catalysis, V, 39, (1953).

109. E.A. Gulbransen, Adv. In Catalysis, V, 119, (1953).

110. D.D. Eley and R.B. Leslie, Trans. Far. Soc., 62, 1002, (1965).

111. St. Malinowski, S. Szczepanska, A. Bielanski and J. Sloczyanski, J. Catalysis, 4, 324, (1965).

112. V. Fic and J. Dvorak, Chem. Prumsyl., 15, 732 (1965).

113. A.I. Vogel, Quantitative Inorganic Analysis (Longmans, London, (1961)), p.788.

114. M.D. Amos and J.B. Willis, Spectrochim. Acta., 22, 1325, (1966).

115. P. Jackson, Thesis, (Nottingham University, 1969).

116. G. Natta, G. Mazzanti, D. de Luca, U. Giannini and F. Bandini, Makromol. Chem., 76, 54, (1964).

117. H. Schnecko, M. Reinmoeller, K. Weirauch, W. Lintz and W. Kern, Makromol. Chem., 69, 105, (1963).

118. L.M. Lanovskaya, N.V. Makletsova, A.R. Gantmakher and S.S. Medverev, Vysokomolekul. Soedin., 7, 741, (1965).

119. N.M. Korobova, M.I. Leitman, E. Ya. Paramonkov, L.G. Stefanovich, A.A. Baulin, N.M. Chirkov and A.S. Semenova, Plast. Massy., 3, 3, (1973).

120. J.Y. Guttman and J.E. Guillet, Amer. Chem. Soc. Div. of Org. Coatings and Plastics Chemistry, 30, 177, (1970).

121. W.A. Lee, Min. Aviation R.A.E., Tech. Rep. 65151, (1965).

122. A.S. Michaels and J.H. Bixler, J. Polymer Sci., 50, 413, (1961).

123. S. Glasstone, K.J. Laidler and H. Eyering, The Theory of Rate Processes, (McGraw-Hill, New York, 1941).

124. M.S. Scurrell, Thesis, (Nottingham University, 1972).